Dissertation

submitted to the

Combined Faculty of Natural Sciences and Mathematics

of the Ruperto Carola University Heidelberg, Germany

for the degree of

Doctor of Natural Sciences

Novel mode of action of the branched-chain amino acid transaminase BCAT1 in glioblastoma

Presented by

M. Sc. Liliana François Martín del Campo

Born in Morelos, México

Oral examination: 9th December 2019

Dissertation

submitted to the

Combined Faculty of Natural Sciences and Mathematics

of the Ruperto Carola University Heidelberg, Germany

for the degree of

Doctor of Natural Sciences

Presented by

M. Sc. Liliana François Martín del Campo

Born in Morelos, México

Oral examination: 9th December 2019

Novel mode of action of the branched-chain amino acid transaminase BCAT1 in glioblastoma

Referees: Prof. Dr. Thomas Höfer

Prof. Dr. Peter Lichter

Declaration

I hereby declare that I have written the submitted dissertation “Novel mode of action of the branched-chain amino acid transaminase BCAT1 in glioblastoma” myself and in this process have not used any other sources than those expressly indicated.

I hereby declare that I have not applied to be examined at any other institution, nor have I used the dissertation in this or any other form at any other institution as an examination paper, nor submitted it to any other faculty as a dissertation.

_____

Liliana François Martín del Campo

Summary

The branched chain amino acid transaminase 1 (BCAT1) catalyzes the first step in the catabolism of the branched chain amino acids (BCAAs), a reaction that utilizes alpha-ketoglutarate (α-KG) as an acceptor of the BCAA alpha-amino group to generate branched-chain ketoacids (BCKAs) and glutamate. In prior work, our work group has identified BCAT1 as a novel pro-tumorigenic metabolic enzyme in glioblastoma. Most recently, we proposed that BCAT1 supports tumor growth by limiting intracellular α-KG levels and thus the activity of chromatin-modifying DNA and histone demethylases and other α-KG-dependent enzymes. In this doctoral thesis, I aimed to elucidate the mode of action of BCAT1 in glioblastoma cells, using the α-KG depletion model as a working hypothesis. I found that BCAT1 localize to the nucleus as well as the cytoplasm of glioblastoma cells, but immunoprecipitation and mass spectrometry analysis did not identify any α-KG-dependent enzymes as potential BCAT1 interaction partners. Instead, BCAT1 was associated with components of the cytoskeleton and proteins involved in cell cycle regulation, mitosis, and endocytic signaling. Knockout of BCAT1 in glioblastoma cell lines reduced cell proliferation and migration, impeded the cells' capacity to buffer reactive oxygen species, suppressed peroxide-dependent epidermal growth factor receptor (EGFR) activation and caused extensive mitotic failures. Using a knockout and rescue approach, I showed that re-expression of wildtype and catalytic-mutant BCAT1 rescued the reactive oxygen species-buffering and proliferation phenotypes of BCAT1 knockout cells, whereas re-expression of BCAT1 in which a redox-active CXXC motif had been mutated did not. In summary, I identified a redox-dependent mode of action underlying BCAT1-driven growth of glioblastoma and provided evidence that this new BCAT1 redox mechanism might be more important for clinically relevant glioblastoma phenotypes than the well-established BCAT1 transaminase activity.

Zusammenfassung

Die Verzweigtkettige Aminosäuren Transaminase 1 (BCAT1) katalysiert den ersten Schritt des Katabolismus der essentiellen verzweigtkettigen Aminosäuren (BCAAs) in einer Reaktion, bei der Alpha-Ketoglutarat (α-KG) als Akzeptor für die BCAA-Alpha-Aminogruppe fungiert, um verzweigtkettige Ketosäuren (BCKAs) und Glutamat zu generieren. In früheren Arbeiten hat unsere Arbeitsgruppe BCAT1 als ein neues pro-tumorigenes metabolisches Enzym in Glioblastomen identifiziert. Kürzlich schlugen wir vor, dass BCAT1 das Tumorwachstum unterstützt, indem es die intrazellulären α-KG-Konzentrationen und damit die Aktivität von Chromatin-modifizierenden DNA- und Histon-Demethylasen und anderen α-KG-abhängigen Enzymen limitiert. In dieser Doktorarbeit war es mein Ziel, den Mechanismus von BCAT1 in Glioblastomzellen unter Annahme des α-KG-Depletionsmodells aufzuklären. Ich konnte herausfinden, dass BCAT1 sowohl im Zellkern als auch im Zytoplasma von Glioblastomzellen lokalisiert ist- Durch Immunpräzipitation und Massenspektroskopieanalyse konnten keine α-KG-abhängigen Enzyme als potenzielle BCAT1-Interaktionspartner identifiziert werden. Stattdessen war BCAT1 mit Komponenten des Zytoskeletts und Proteinen assoziiert, die an der Regulation des Zellzyklus, der Mitose und der endozytischen Kontrolle der Signalübertragung beteiligt sind. Das Ausschalten von BCAT1 in Glioblastom-Zelllinien verringerte deren Zellproliferation und -migration, beeinträchtigte die Fähigkeit der Zellen, reaktive Sauerstoffspezies zu puffern, unterdrückte die peroxidabhängige Aktivierung des Epidermalen Wachstumsfaktorrezeptors (EGFR) und verursachte häufige Mitosefehler. Unter Verwendung eines Knockout- und Rescue-Ansatzes konnte gezeigt werden, dass die Re-Expression von Wildtyp oder katalytisch-inaktivem BCAT1 die Phänotypen der Pufferung reaktiver Sauerstoffspezies und der Proliferation in BCAT1-Knockout-Zellen wiederherstellten, während die Re-Expression von BCAT1 mit einer Mutation des Redox-aktiven CXXC-Aminosäuren-Motivs dies nicht konnte. Zusammenfassend identifizierte ich einen Redox-abhängigen Wirkmechanismus, der dem BCAT1-getriebenen Wachstum von Glioblastomen zugrunde liegt, und lieferte Hinweise darauf, dass dieser neue BCAT1-Redoxmechanismus für klinisch relevante Glioblastomphänotypen relevanterbedeutsamer sein könnte als die bekannte BCAT1-Transaminaseaktivität.

Table of Contents

Figures and tables

Supplementary figures and tables

Abbreviations

4EBP1	eukaryotic initiation factor 4E binding protein 1
5mC	5-methylcytosine
AML	Acute myeloid leukemia
ACRP3	Actin related protein 3
AURKA	Aurora kinase A
BCAA	Branched-chain amino acids
BCAT1	Branched-chain aminotransferase 1
BCAT1^{K222A}	BCAT1 K222A mutant = catabolically dead
BCAT1^{SXXS}	BCAT1 C335S and C338S mutant = redox insensitive
BCAT1^{wt}	BCAT1 wild-type
BCAT2	Branched-chain aminotransferase 2
BCKA	Branched-chain keto acids
BRET	Bioluminescence resonance energy transfer
Cas9	CRISPR associated protein 9
CDK	Cyclin dependent kinase
CFP	Cyan fluorescent protein
CNS	Central nervous system
CRISPR	clustered regularly interspaced short palindromic repeats
Dm-α-KG	Dimethyl-alpha-ketoglutarate
DNA	Deoxyribonucleic acid
DTT	Dithiothreitol
EGF	Epidermal growth factor
EGFR	Epidermal growth factor receptor
EGLN	Egl-9 family hypoxia inducible factor 1
eIF4E	eukaryotic initiation factor 4E
F-actin	Microfilaments, polymerized form of actin
FCS	Fetal calf serum

FRET	Förster (Fluorescence) resonance energy transfer
G-actin	Globular, monomeric form of actin
GFP	Green fluorescent protein
GPX	Glutathione peroxidase
GLRX	Glutaredoxin
GSH	glutathione
H_2O_2	Hydrogen peroxide
hEGF	Human epidermal growth factor
HIF1A	Hypoxia-inducible factor 1-alpha,
HMW	High molecular weight
$IDH^{wt/mut}$	Isocitrate dehydrogenase wild-type/mutant
IgG	Immunoglobulin
IP	Immunoprecipitation
IPA	Ingenuity pathway analysis
IP-MS	Immunoprecipitation and Mass spectrometry
KDM	Lysine demethylases (Fe (II) and α-KG dependent, JmJC family)
MICAL	[F-actin]-monooxygenase
MAP	Microtubule associated protein
MS	Mass spectrometry
mtDNA	Mitochondrial DNA
MTOR	mammalian target of rapamycin
NEM	N-Ethylmaleimide
NO	Nitric oxide
NOX	NADPH oxidase
NSCLC	Non-small cell lung carcinoma
PDC	Pyruvate dehydrogenase complex
PDGF	Platelet derived growth factor
PFKL	Phosphofructokinase, Liver type
PI3K	phosphoinositide 3-kinase

PIP_3	Phosphatidylinositol (3,4,5) trisphosphate
pKa	Acid dissociation constant
PKM	Pyruvate kinase
PLP	pyridoxal 5-phosphate
PRX	Peroxiredoxin
PTEN	Phosphatase and tensin homolog
PTM	Post-translational modification
RNS	Reactive nitrogen species
ROS	Reactive oxygen species
RTK	Receptor tyrosine kinase
S6K1	p70 ribosomal S6 kinase 1
SDS-PAGE	sodium dodecyl sulfate–polyacrylamide gel electrophoresis
SOD	superoxide dismutase
STAT3	Signal Transducer And Activator Of Transcription 3
TET	Tet-eleven translocation
TGF-β1	Transforming growth factor beta-1
TR	Thioredoxin reductase
TRX	Thioredoxin
TSC	tuberous sclerosis complex
ZF-CXXC	Cysteine rich zinc finger domain
α-KG	Alpha-ketoglutarate

1. Introduction

1.1. The Branched chain amino acid transaminase

The human branched chain amino acid transaminase (hBCAT, EC 2.6.1.42) catalyzes the reversible transamination of the essential branched-chain amino acids (BCAAs) leucine, isoleucine and valine into their respective branched chain alpha-keto acids (BCKAs). The reaction utilizes alpha-ketoglutarate (α-KG) as an acceptor of the amino group from the BCAA and produces glutamate as a byproduct. BCKAs (*viz*, α-ketoisocaproate, α-keto-β-methylvalerate and α-ketoisovalerate) are then shuttled to the branched chain α-ketoacid dehydrogenase complex (BCKDC) and are irreversibly converted by oxidative decarboxylation into branched-chain Acyl-CoAs. These last are further metabolized and enter the Krebs cycle to generate energy and macromolecule precursors (Hutson, Sweatt and Lanoue, 2005; Tönjes *et al.*, 2013) .

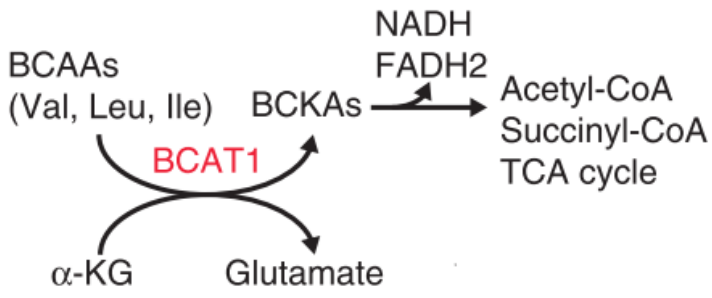

Figure 1. The BCAT1 reaction (taken from Tönjes et al. 2013). BCAT1 catalyzes the first step in the catabolism of branched chain amino acids (BCAA) to form branched-chain keto acids (BCKA) and glutamate. In the reaction, the amino group of the BCAA is transferred to alpha ketoglutarate (α-KG). BCKA can be further metabolized and enter the Krebs cycle.

1.1.1. The BCAT isoforms and their distribution

In mammals, two isoforms of BCAT have been identified, one in the cytosol and one in the mitochondria, that were originally referred to as BCATc and BCATm, respectively (Hutson, Fenstermacher and Mahar, 1988). In this thesis, I will be using the official gene names, *BCAT1* for the cytoplasmic and *BCAT2* for the mitochondrial isoenzyme. In humans and rodents, *BCAT2* is ubiquitously expressed in all tissues, with low activity in the liver and very high activity in the

muscle. BCAT2 has an important role in the metabolism of glutamine and alanine in skeletal muscle, which constitute the main nitrogen carriers to the liver and other tissues (Sweatt *et al.*, 2004). Expression of BCAT1 is limited mostly to the nervous system, ovaries and placenta. In the brain, BCAAs serve as an important donors of nitrogen for the synthesis of the neurotransmitters glutamate and γ-amino butyric acid (Hutson, Sweatt and Lanoue, 2005).

Based on amino acid sequence, BCAT1 and BCAT2 share 58% homology, with a highly conserved C-terminal region and most of the differences at the N-terminus (Yennawar *et al.*, 2001; Goto *et al.*, 2005). For both isoenzymes, the active enzyme is formed by homodimers, which monomers (subunits) are composed, each, of a small and a large domain (Figure 2). The active-site cavity is located between the two domains, facing the interface of the two monomers (Figure 3).

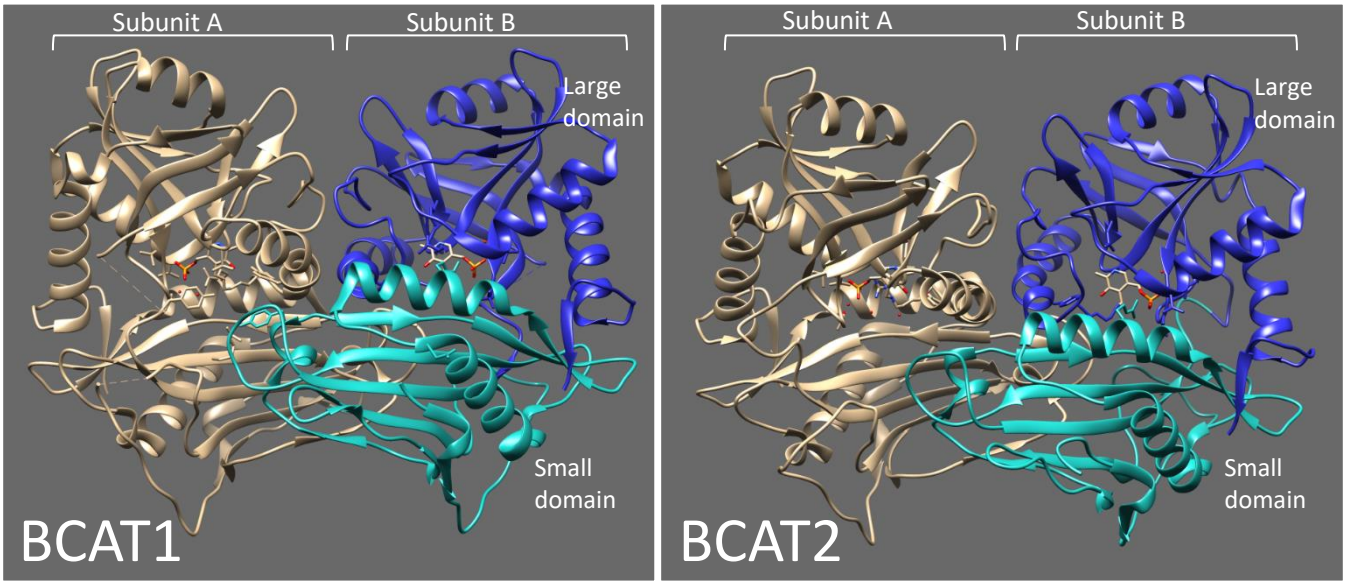

Figure 2. 3D structure of BCAT1 and BCAT2 showing the similarities between both isoforms. Both isoenzymes forms homodimers composed of subunit A and B (colored in white and blue). Each subunit presents a large and a small domain (colored in dark or light blue). The catalytic site is located at the interphase of the two subunits, where the PLP cofactor can be observed (colored in light gray and red). (Adapted from Yennawar et al. 2001 and Goto et al. 2005, BCAT2 PDB: 1EKP, BCAT1 PDB: 2COG, images generated using the software Chimera 1.13.1)

The BCAT proteins are classified as pyridoxal 5-phosphate (PLP)-dependent enzyme, fold-type IV. They require PLP, the active form of Vitamin B_6, as a cofactor, which facilitates the migration of protons during the transamination reaction. Each subunit can bind one PLP molecule, which covalently binds via a Schiff-base link to the amino group of the lysine 222 (K222; or K202 in BCAT2) present at the cavity of the active site (Figure 3) (Yennawar *et al.*, 2001). The PLP is further stabilized by hydrogen bonds with other residues at the active-site cavity (Yennawar *et al.*, 2001). Single mutation of the lysine at the active site of the BCAT1 and BCAT2 homologs in *Saccharomices cereviceae* ($BAT1^{K219R/A}$ and $BAT2^{K202A}$) renders the enzyme catalytically inactive (Kingsbury, Sen and Cardenas, 2015).

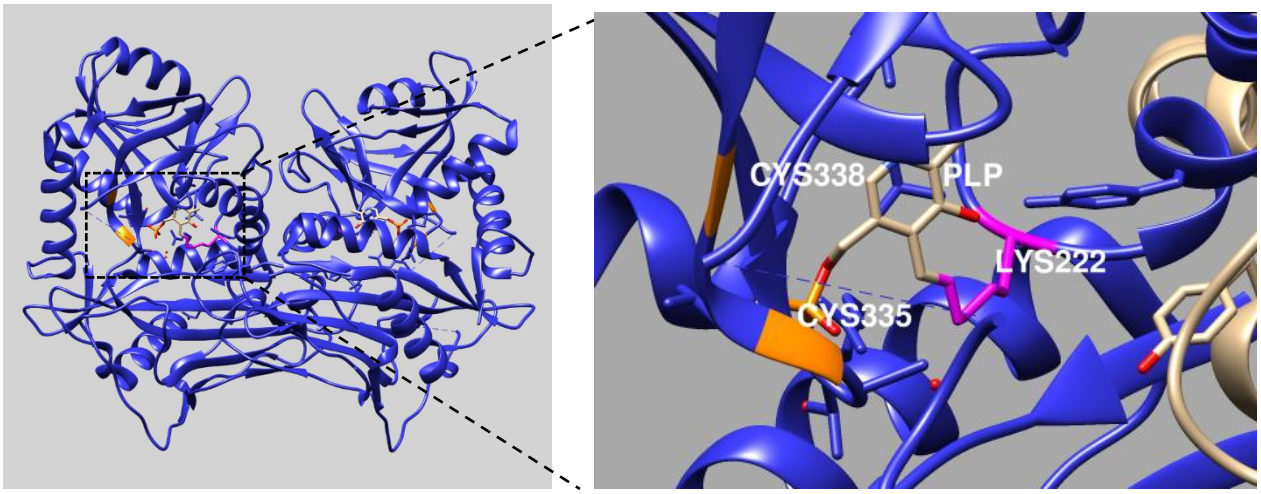

Figure 3. Zoom into the active site of BCAT1, showing the lysine 222 (LYS 222, colored in magenta) bound by the cofactor PLP. At the entrance of the active site, two cysteines (CYS 335 and CYS 338, colored in orange) regulate the catalytic activity of BCAT1 by forming an intra-molecular disulfide bridge under oxidizing conditions. PDB: 2COG, image generated with Chimera 1.13.1

1.1.2. The redox center of BCAT

An additional feature of mammalian BCAT1 and BCAT2 is the presence of a conserved CXXC motif surrounding the active site (Figure 3, colored in orange)(Yennawar *et al.*, 2001, 2006; Goto *et al.*, 2005). CXXC motifs are defined by the consensus sequence Cys-Xaa-Xaa-Cys, where Xaa is any amino acid. These redox-sensitive centers are characteristic of oxidoreductases, such

as thioredoxins (TRX) and glutaredoxins (GLRX), which transfer electrons to molecules and play important roles in maintaining a reduced intracellular environment of the cell (Fomenko and Gladyshev, 2003; López-Grueso *et al.*, 2019). Interestingly, only mammalian BCATs and not those of lower eukaryotes or prokaryotes possess this redox center (Schuldiner *et al.*, 1996; Yennawar *et al.*, 2001; Conway *et al.*, 2002).

In BCAT1, the CXXC center is formed by C335 and C338 with two valines (V) in between: CVVC, whilst in BCAT2, it is formed by the C315 and C318 separated by glutamate and a valine (CQVC). The crystal structure of the PLP-bound form of BCAT2 shows that C315 and C318 (CXXC motif) are only ~10 Å from the active site. However, they do not interfere directly with the substrate or PLP binding, but C315 shares a hydrogen bond with Y173, which is essential for stabilizing the side chain binding pocket and controlling the orientation of the substrate. Under oxidizing conditions, C315 and C318 form an intramolecular disulfide bond causing a reorientation of the binding pocket that weakens the interaction with the substrate and thus the catalysis is impeded (Yennawar *et al.*, 2006).

Most of the current understanding about the redox-regulation of the catalytic activity of BCATs has been gathered by biochemistry methods using recombinant human BCAT (hBCAT) overexpressed and purified from *Escherichia coli* (*E.coli*). These studies have shown that BCAT1 and BCAT2 exhibit distinct sensibility to oxidation that is determined by the local environment given by the amino acids surrounding the active site (Davoodi *et al.*, 1998). In contrast to BCAT2, which enzymatic activity is completely inhibited by oxidation of the CXXC-motif, BCAT1 still retains ~ 70 % of its residual activity when only these two cysteines are oxidized. In the case of BCAT1, four additional cysteines have been reported to be solvent accessible. Oxidation of the CXXC-motif and two more cysteines results in loss of ~ 80% of BCAT1 metabolic activity. However, complete inactivation of the enzyme, was reported to be only possible when the six cysteines are oxidized, which was only achieved with supra-physiological concentrations (> 5 mM) of H_2O_2 (Davoodi *et al.*, 1998; Conway, Poole and Hutson, 2004; Conway *et al.*, 2008). The last suggests that under physiological conditions, BCAT1 most likely retains its metabolic activity by at least 60 percent.

The above described mechanism of reversible disulfide bond formation between the thiols of the CXXC-motif of the BCAT enzymes has been proposed to act as a redox-switch to regulate the transaminase activity of the enzyme in response to physiological reducing or oxidizing conditions (Yennawar *et al.*, 2006; Coles, Hancock and Conway, 2012). However, more evidence showing the functional role of the CXXC-motif in a physiological context is needed to understand the implications of this redox-center of BCAT1 in health and disease.

1.2. BCAT1 and cancer

The first associations of BCAT1 and cancer dates to 1977, when this isoenzyme was observed to be highly expressed in tumors of the liver, kidney, stomach and other tissues where in the normal adult was not expressed (Goto, Shinno and Ichihara, 1977). It was not until the 90's that the mouse *Bcat1* gene, called by then *Eca39*, was discovered in a screen aiming to detect immediate targets of the proto-oncogene *c-myc* (Benvenisty *et al.*, 1992). The strategy used was based on the hypothesis that a direct target of c-Myc would be highly up-regulated in two different tumor cell lines derived from *c-myc* overexpressing transgenic mice. cDNA libraries were made from a *c-myc* transgenic brain tumor cell line, and by a subtraction/coexpression method, a gene was found to be massively upregulated compared to normal brain tissue. This same cDNA had been identified previously as highly expressed in teratocarcinoma cell lines and was thereafter called *Eca39* (Niwa *et al.*, 1990). Although its function was still elusive, the overexpression of *BCAT1* in c-MYC driven human tumors was later on evidenced in increasing numbers of cancer entities, including colorectal cancer, breast cancer and Burkitt's lymphomas (Ben-Yosef *et al.*, 1998; Yoshikawa *et al.*, 2006).

Interestingly, the mouse and human *BCAT1* coding sequence shares high similarity with the nematode and yeast homologues. However the MYC regulatory sequence upstream of the *BCAT1* transcription start site is not present in these lower organisms. Nevertheless, yeast deficient of *Bat1* and *Bat2* (corresponding to the human *BCAT2* and *BCAT1,* respectively) exhibit growth defects and altered cell cycle, suggesting that the pro-proliferative function of these proteins is conserved in evolution (Kispal *et al.*, 1996; Schuldiner *et al.*, 1996).

1.2.1. Glioblastoma

Among malignant tumors originating in the central nervous system (CNS), glioblastoma, classified by the World Health Organization (WHO) classification as grade IV, is the most common and aggressive type of tumors in adults (Weller *et al.*, 2017). Glioblastoma is diagnosed by histological evaluation, being characterized by nuclear atypia, mitotic activity, proliferation of the microvasculature and necrosis. About 90-95% of glioblastoma develop *de novo,* and manifest as grade IV tumors at the time of diagnosis. These "primary glioblastoma" have a particularly poor prognosis, with a median survival after diagnosis of less than 2 years. This makes glioblastoma the third-highest cancer-related cause of death for patients under the age of 35. The remaining ~ 5% of glioblastoma are referred to as "secondary glioblastoma" since they initially manifest as lower grade lesions and progress to WHO IV glioblastoma in only few years (Parker *et al.*, 2015).

The current standard therapy for glioblastoma consists of surgery, radio- and chemotherapy, which can expand the patient´s lifetime for up to 5 years. However, the maximum beneficial effect only evolves in less than 5% of the cases. This poor outcome of glioblastoma patients is due to the high cellular and molecular heterogeneity of the tumors (Sturm, Bender, D. T. W. W. Jones, *et al.*, 2014; Parker *et al.*, 2015). With the objective of developing strategic therapies specific to individual tumor's characteristics, extensive work has been put to characterize and categorize glioblastoma tumors based on their genomic and epigenomic abnormalities (Sturm, Bender, D. T. W. W. Jones, *et al.*, 2014; Weller *et al.*, 2017).

According to the latest WHO classification (Louis *et al.*, 2016) the presence of mutated forms of isocitrate dehydrogenase (IDH) 1 is the most important molecular diagnostic parameter to distinguish primary and secondary glioblastoma (Parsons *et al.*, 2008; Toedt *et al.*, 2011; Parker *et al.*, 2015). The IDH isoenzymes IDH1 and IDH2 convert isocitrate into α-KG, which is further catabolized in the Krebs cycle and used by several transaminases including BCAT1. α-KG also acts as a co-substrate for histone lysine demethylases (KDMs) and ten-eleven translocation (TET) family of 5-methylcytosine (5mC) hydroxylases (Cascella and Mirica, 2012; Yun *et al.*, 2012). Mutated forms of IDH1 (commonly R132H, IDH^{mut}) have acquired the ability to catalyze

the conversion of α-KG into R(-)-2-hydroxyglutarate (2HG), which acts as a competitive inhibitor of α-KG dependent dioxygenases (Dang *et al.*, 2009). Accumulation of 2HG in IDH^{mut} gliomas inhibits the DNA-demethylase activity of TET1 and TET2, resulting in genome-wide promoter-associated hypermethylation and silencing of metabolic genes (Turcan *et al.*, 2012; Chesnelong *et al.*, 2014; Izquierdo-Garcia *et al.*, 2015). IDH^{mut} is considered a hallmark feature of secondary glioblastoma, which are likely to be derived from undiagnosed lower-grade astrocytomas (Sturm, Bender, D. T. W. Jones, *et al.*, 2014).

1.2.2. BCAT1 and glioblastoma

In 2013, our group discovered BCAA catabolism as an essential driver of glioblastoma growth (Tönjes *et al.*, 2013). It was found that, relative to normal brain, BCAT1 was overexpressed in glioblastoma carrying wild-type IDH (IDH^{wt}) but was silenced by promoter hypermethylation in IDH^{mut} gliomas. Experiments with glioblastoma cell lines and glioblastoma-xenograft mouse models suggested a functional role of BCAT1 in IDH^{wt} cell proliferation and disease progression. In conclusion, the malignant phenotype of IDH^{wt} glioblastomas, compared to the slow growing IDH^{mut}, seemed to be tightly linked with increased catabolism of BCAAs (Tönjes *et al.*, 2013). In the following years, these findings were confirmed for a number of additional tumor entities by ourselves and others (Wang *et al.*, 2015a; Mayers *et al.*, 2016; Zheng *et al.*, 2016; Raffel *et al.*, 2017; Thewes *et al.*, 2017). Following studies in our group showed that the carbons of the BCKA derived from BCAT1 activity were not directed to the Krebs cycle and thus were not used for macromolecule and ATP synthesis. Instead BCKA were shown to be excreted by the tumor cells and exhibit immunosuppressive functions in tumor-associated macrophages (Silva *et al.*, 2017).

More recently, in collaboration with the group of Andreas Trumpp (Hi-Stem, DKFZ), we showed that in addition to controlling BCAA catabolism, BCAT1 activity also strongly affects cellular α-KG concentrations (Raffel *et al.*, 2017). This was evidenced in acute myeloid leukemia (AML), which also exhibits a correlation of BCAT1 overexpression in IDH^{wt} and suppression in IDH^{mut} patients. Depletion of α-KG by BCAT1 overexpression compromised the activity αKG-dependent dioxygenases including the TET family of DNA demethylases and the Egl-9 family hypoxia

inducible factor 1 (EGLN1) that controls the stability of the transcription factor hypoxia inducible factor 1A (HIF1A).

Overall, the current view on the mode of action of BCAT1 in glioblastoma is largely linked to its central role in BCAA metabolism. On one hand, by controlling α-KG levels BCAT1 regulates metabolic and epigenetic programs and on the other hand affects the tumor microenvironment by producing BCKAs (Figure 4).

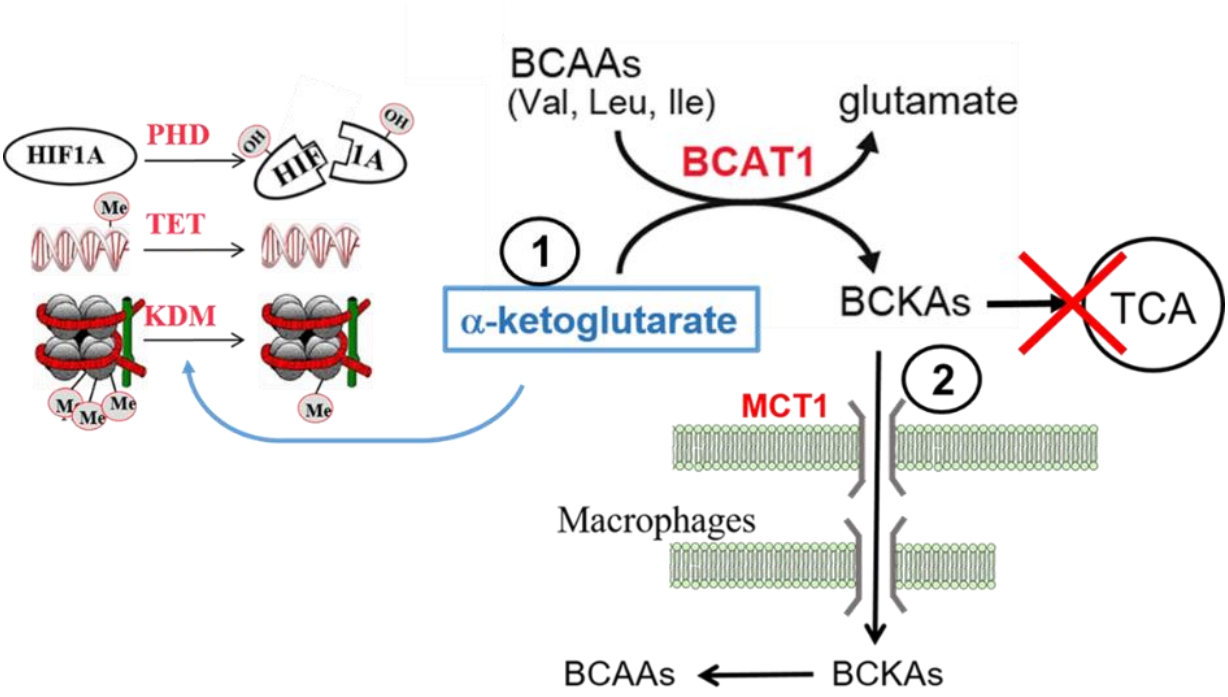

Figure 4. Current view on the mode of action of BCAT1 in glioblastoma. Overexpression of BCAT1 and high metabolic activity of BCAT1 affects levels of α-KG (co-substrate) and BCKAs (product). (1) Changes in α-KG affects the activity of α-KG-dependent dioxygenases such as PHD (EGLN), TET, and KDM, affecting in turn the stability of HIF1A and epigenetics. (2) The produced BCKAs are not directed to the TCA cycle and are excreted and taken up by the tumor-associated macrophages. (adapted from: https://www.dkfz.de/en/genetics/pages/projects/Tumor-metabolism/Tumor_metabolism.html, accessed: 30th September 2019).

1.3. Reactive oxygen species and redox signaling

Reactive oxygen species (ROS) were first discovered as a cell's defense mechanism to destroy exogenous pathogens. For long, ROS were thought to be cytotoxic agents due to their high reactivity and oxidative damage they can cause in proteins, lipids and nucleic acids. At high concentrations, ROS cause misfolding, inactivation and degradation of essential proteins, which eventually can lead to dysfunction of the cell and lead to disease. However, it is now recognized that ROS are not only damaging products but are important mediators in cell signaling of pathways controlling cell growth, proliferation, differentiation and apoptosis (Sarsour *et al.*, 2009; Zhang *et al.*, 2016).

ROS include a number of chemical species that contain at least one single oxygen and display stronger reactivity than molecular oxygen (O_2). Examples of ROS are the superoxide anion radical (O_2^-), hydrogen peroxide (H_2O_2) and the hydroxyl radical (•OH). Another group of reactive species contains a nitrogen group, and thus is termed reactive nitrogen species (RNS). These includes nitric oxide (NO) and peroxynitrite ($ONOO^-$) (Bae *et al.*, 1997; Zhang *et al.*, 2016).

Sources of ROS can be endogenous or exogenous. The former are those generated as byproduct of cellular reactions, to which the mitochondrial oxidative metabolism contributes to a large extent. The activity of NADPH oxidases (NOX) constitutes another important source of ROS. Exogenous stimuli such as growth factors, cytokines and bacterial invasion induce superoxide production via activation of NOX (Bae *et al.*, 2011; Zhang *et al.*, 2016). Examples of cytokines that activate NOX after stimulation of membrane receptors are transforming growth factor-β1 (TGF-β1) (Jiang *et al.*, 2014), platelet-derived growth factor (PDGF) (Catarzi *et al.*, 2005) and epidermal growth factor (EGF) (Paulsen *et al.*, 2012; Truong and Carroll, 2012)

1.3.1. Hydrogen peroxide as redox signaling molecule

Redox signaling refers to changes in oxidant levels that can trigger different cellular responses (Rudyk et al. 2014, Zhang *et al.*, 2016). Of all ROS, H_2O_2 has the most characteristics of a second

messenger: it is small, ubiquitous, rapidly produced and degraded, and is selective for target proteins (Sies, 2017). H_2O_2 is generated from superoxide by the activities of superoxide dismutases (SOD) present in the mitochondrial matrix, the cytoplasm and the extracellular environment and is transported across membranes via aquaporins. H_2O_2 can only oxidize thiols with particularly low *pKa* and its effect on proteins depends on its concentrations near its target and the duration of exposure. However, cells are packed with ubiquitous peroxiredoxins (PRX) that due to the low *pKa* of their thiols, scavenge most of the intracellular H_2O_2. PRXs, thus prevent oxidation of signaling molecules, but can rapidly become inactivated by overoxidation or phosphorylation allowing fast, localized increases of H_2O_2, which trigger redox-signaling events (Woo *et al.*, 2010; Truong and Carroll, 2012). It is now also accepted that the two-cysteine PRXs, PRX1 and PRX2, can directly transmit redox modifications via the formation of transient mixed-disulfide exchange reactions and therefore constitute an important component of redox-signaling (Neumann, Cao and Manevich, 2009; Sobotta *et al.*, 2014; Stöcker *et al.*, 2017).

1.3.2. Redox modifications

Most redox modifications happen at the so-called thiol (-SH) side chain of cysteine, also known as sulfhydryl or mercaptan. Cysteine is the second last more abundant amino acid forming part of only around 2-3% of the human proteome and yet the one with highest susceptibility to be modified by posttranslational modification (PTM). The susceptibility of cysteines to oxidation is determined by the acid dissociation constant "p*K*a" of their thiols. At physiological pH, most thiols are protonated, with a p*K*a between 8 and 9 and thus not susceptible to oxidation. Thiols with deprotonated (-S-), named thiolate anion, have a low p*K*a and are more prone to be targets of oxidants (Groitl and Jakob, 2014). Redox-sensitive proteins, possessing either reactive thiols (with low pKa) and/or CXXC motifs, are susceptible to modification by ROS or RNS present in the cellular environment. These modifications confer higher oxidation states which leads to a gain or loss of function (Cumming *et al.*, 2004; Cremers and Jakob, 2013).

Oxidation of a thiol by H_2O_2, a reaction termed sulfenylation, produces a sulfenic acid modification (R-SOH). This state is reversible and normally of short duration. Further oxidation can lead to formation of irreversible sulfinic acid (R-SO_2H) and sulfonic acid (R-SO_3H) (Figure 5). Sulfenic acids can react with other protein's thiols to form intra- or inter-molecular disulfide bonds (Cremers and Jakob, 2013; Groitl and Jakob, 2014). Transient disulfide bonds can also be formed with glutathione (GSH), the most abundant non-protein thiol. This modification, termed S-glutathionylation, induces functional protein changes and is suggested as a protective mechanism preventing protein over-oxidation during redox-stress (Dalle-Donne *et al.*, 2007; Singh *et al.*, 2018). Cysteines can also react with NO and other RNS, a reaction called S-nitrosylation, forming the chemical intermediate S-nitrosothiol (R-SNO). Although less frequently happening than sulfenylation, S-nitrosylation have also important roles in redox signaling (López-Grueso *et al.*, 2019).

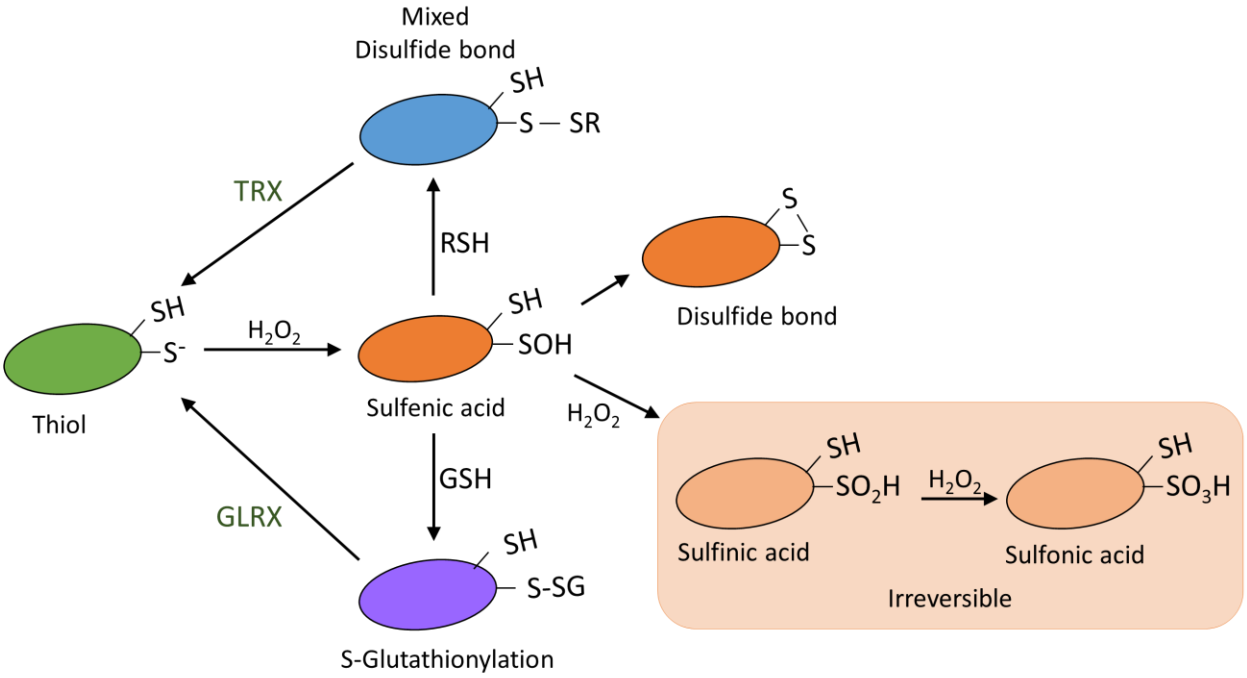

Figure 5. Redox modification of cysteines. Protein thiols (S-) can be oxidize by H_2O_2 to sulfenic acid, which can a react with other thiols in the same protein, to form intramolecular disulfide bonds (S-S), or can react to other protein thiol (RSH) to form an intermolecular mixed disulfide bond (RS-SR). A sulfenic acid can also form disulfides with glutathione (GSH), a modification called S-glutathionylation. Under excessive concentrations of H_2O_2, irreversible sulfinic or sulfonic acids could be formed. Reduction of S-glutathionylation is performed by glutaredoxins (GLRX) and sulfenic acids are commonly reduced by

thioredoxins (TRX) (adapted from: Cremers and Jakob, 2013; Thruong and Carroll 2013; Jarvis, Hughes and Ledgerwood, 2012)

Redox modifications can be reversed by the activity of the thioredoxins (TRX) and glutaredoxins (GLRX). These oxidoreductases possess a CXXC-motif responsible for recycling oxidized thiols to their initial reduced state. The reaction starts with the attack of the first cysteine (that has lower *pKa*, known as "sensor") to form a mixed-disulfide bond with the oxidized cysteine of the "client" protein. The second cysteine (known as the "resolving" cysteine) then attacks the mixed disulfide bond by forming an intramolecular disulfide bond, releasing in turn the reduced client protein. Reduction of TRX is mediated by thioredoxin reductase (TR), which utilizes NADPH for its own reduction (Pastore and Piemonte, 2012; Groitl and Jakob, 2014).

1.3.3. Oxidative stress and cancer

In a healthy cell, ROS levels are kept in homeostasis, meaning that there is a balance between ROS production and removal. However, a shift towards increased synthesis of oxidants or a poor scavenging capacity cause overoxidation, and thus damaging of proteins, lipids and DNA. Sustained exposure to ROS, results in oxidative stress, causing cellular dysfunction, cell cycle arrest and induction of apoptosis. Oxidative stress has been implicated in aging and numerous pathologies, including neurodegenerative and cardiovascular diseases, diabetes, fibrosis and cancer (Sarsour *et al.*, 2009; Liou and Storz, 2010; Ghezzi, 2013; Parker, Kavallaris and McCarroll, 2014; Salazar-Ramiro *et al.*, 2016).

In cancer, sustained high levels of ROS are fed by a vicious feedback circle. ROS are produced in a larger extent during high metabolic activities and mitochondria dysfunction. Additionally, NOX-derived ROS production is stimulated by overactive cytokine and growth factor receptors. High ROS in turn activates redox-dependent signaling pathways promoting growth, proliferation and survival (Liou and Storz, 2010; Sullivan and Chandel, 2014). To cope with consistent high levels of ROS, cancer cells activate adaptative stress responses to resist cell cycle arrest or

apoptosis that would otherwise be induced by redox stress. Master switches, such as Nrf2/Keap1, upregulate antioxidant mechanisms (e.g. TRX/TR, GLRX/GR systems, PRXs) that help preventing overoxidation of biomolecules, while contributing at the same time (Figure 6) (DeNicola *et al.*, 2011; Sullivan and Chandel, 2014; Lennicke *et al.*, 2015).

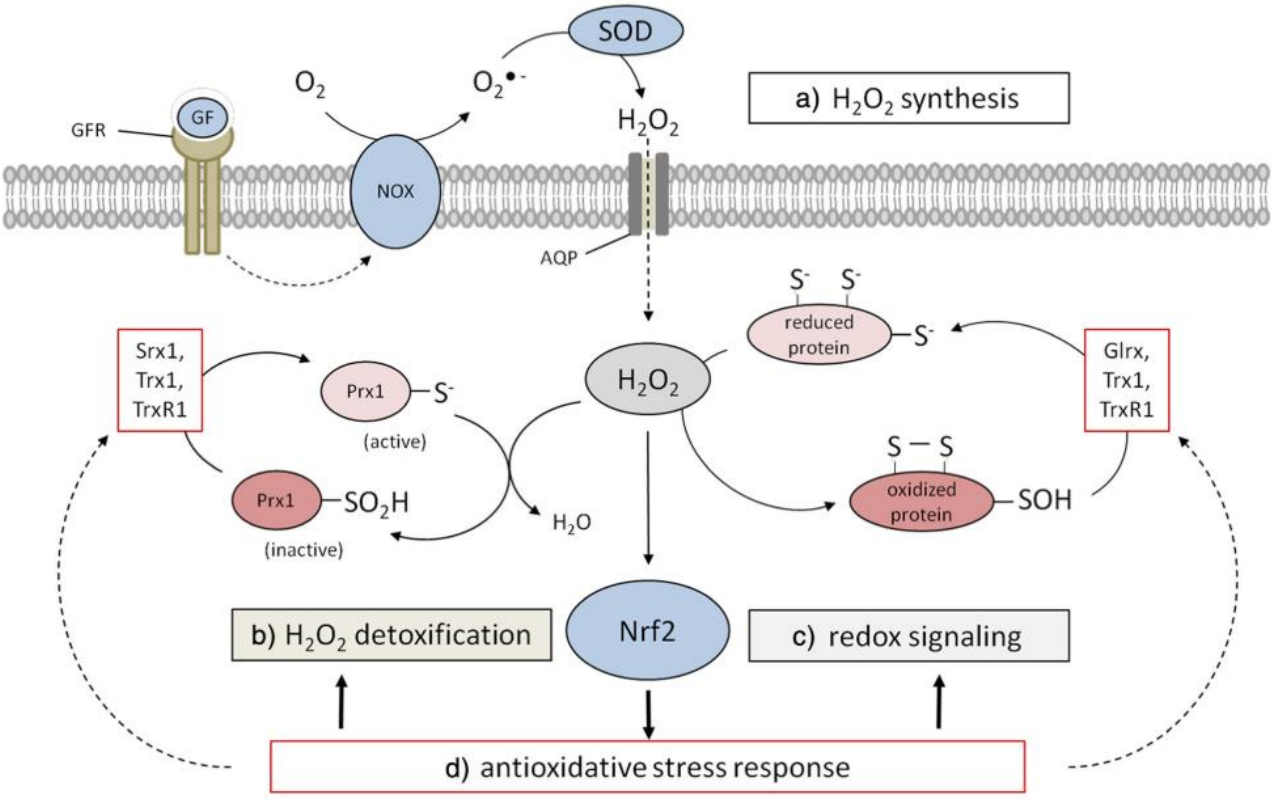

Figure 6. Mechanisms of generation and detoxification of ROS (taken from Lennicke et al. 2015). Activation of growth factor (GF) receptors (GFR) induce ROS production through activation of NADPH oxidases (NOX). Superoxide (O2•−) radicals are converted to H_2O_2 by the superoxide dismutase (SOD) enzymes. ROS contribute to cellular signaling by oxidizing thiols of redox sensitive proteins, which is controlled by cytosolic antioxidant systems, such as thioredoxin/thioreductases (Trx, TrxR1), glutaredoxin (Glrx) and peroxiredoxins (Prx1). High levels of ROS can activate Nrf2 leading to upregulation of antioxidant stress response elements. Cancer cells exhibit increased production of ROS by dysregulated metabolism and GF signaling. To cope with high ROS, cancer cells upregulate the antioxidative stress response (red squares).

1.4. The cytoskeleton

The cytoskeleton is an organized network of fibers essential in cellular processes such as migration, resistance to stress, cell division, movement of organelles and vesicles, and cell signaling. There are three main types of filaments: microtubules, intermediate filaments and microfilaments. Each type is built out of small soluble subunits that can diffuse rapidly from one site of the cell to another enabling fast response to incoming signals. In addition to the building blocks, a large variety of cytoskeleton-associated accessory proteins regulate the dynamics and spatial distribution of the filaments. Accessory proteins play important roles in the transduction of extra- and intracellular signals for specific cellular functions. Although each type of filament is more important for a specific task, thigh coordination between all the cytoskeletal elements is necessary for cellular function (Alberts *et al.*, 2002; Schatten, 2015).

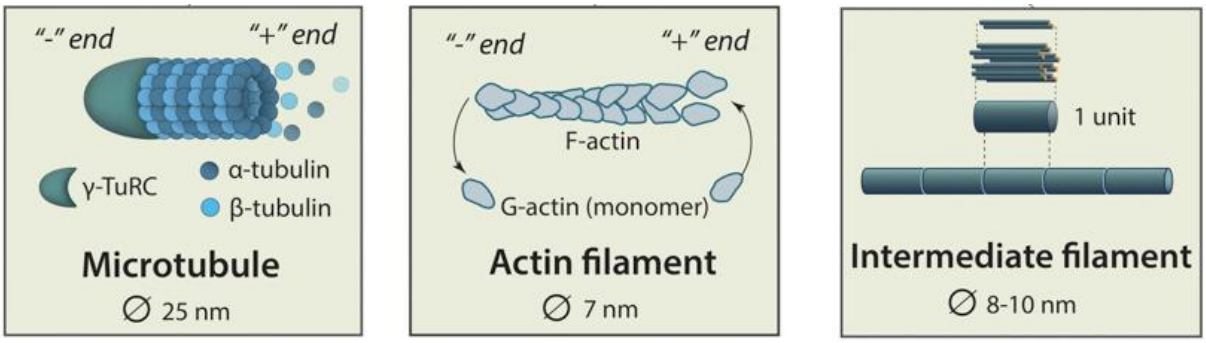

Figure 7. The three main components of the cytoskeleton. Microtubules are hollow tubes of ~25 nm diameter, formed of α- and β-tubulin dimers. On the minus end microtubules are nucleated by γ-tubulin and polymerizes towards the plasma membrane in the direction of the plus end. Microfilaments are thin ~7 nm, double-stranded filaments built of G-actin (monomer). The plus end grows by fast addition of G-actin. Intermediate filaments are rigid structures of cell-type specific components, they provide resistance to mechanic stress. (picture adapted from: MBINFO defining Mechanobiology, accessed 1 September 2019, (https://www.mechanobio.info/cytoskeleton-dynamics/what-is-the-cytoskeleton/).

1.4.1. Microtubules

Microtubules' subunits are formed of heterodimers of α-tubulin and β-tubulin. α/β-tubulin polymerize in the presence of GTP to form protofilaments, which when aligned in parallel (13 protofilaments) form hollow cylinders of about 25 nm in diameter (Alberts *et al.*, 2002).

Microtubules follow cycles of fast assembly and disassembly, a phenomenon called dynamic instability. GTP bound tubulin dimers are incorporated into the growing filament, where a stabilizing cap is formed. Below the cap, hydrolysis of GTP to GDP occurs at the β-tubulin subunit after incorporation into the plus-end of the growing microtubule. GTP hydrolysis causes a conformational change that generates tension within the filament. If the rate of GTP hydrolysis is faster than the incorporation of tubulin subunits, the tension causes fast depolymerization, an event known as "catastrophe". A catastrophic event is often followed by rescue, when polymerization is favored again (Jens Lüders, 2016). Another feature of microtubules is polarity, which is conferred by the orientation of the α/β-tubulin dimers. As they are assembled, α-tubulin is facing the bottom (minus end) and β-tubulin the top (plus end) of the filament. This polarity guides molecular motor proteins to move materials in a certain direction (Alberts *et al.*, 2002; Jens Lüders, 2016).

Nucleation of microtubules occurs from the minus end by γ-tubulin. γ-tubulin is anchored at the microtubule-organizing center (MTOC) called centrosome, which is often associated with the nuclear envelop. Therefore in interphase, the cells' microtubules normally expand from the MTOC towards the periphery of the cell (Alberts *et al.*, 2002; Schatten, 2015).

Microtubules can acquire specialized functions in different cell types. They can form cilia and flagella allowing movement of migrating cells along a surface. They can also create bundle tracks for the transport of vesicles along the axon of neurons. A particular specialized structure of microtubules is the mitotic spindle and mid-body that form during cell division and is essential for proliferation of all types of cells (Alberts *et al.*, 2002; Janke and Chloë Bulinski, 2011).

1.4.1.1. The mitotic spindle

The mitotic spindle mediates the segregation of chromosomes towards the two daughter cells. Tight control of the assembly and organization of the mitotic spindle is required for proper bipartition of the genetic material. Several pathways and mechanisms have been described to be involved in the reorganization of the microtubules during this process. One of the earliest and most important events is the maturation and duplication of the centrosome. Centrosome maturation promotes the recruitment and upregulation of nucleation factors, which form a major nucleation complex called the γ-tubulin ring complex (TUBGCP2) (Oakley, Paolillo and Zheng, 2015; Jan Lüders, 2016). Mainly three proteins are important in this pathway: NEDD1, RanGTP and Aurora kinase A (AURKA). NEDD1 targets TUBGCP2 to the centrosomes and promotes nucleation of microtubules. RanGTP, bound to the kinetochores at the center of the chromosomes, creates a gradient that induces the nucleation of microtubules. RanGTP also activates TPX2, which in turn binds and activates AURKA. Full activation of AURKA is achieved by 1) protection from the inhibitory activity of protein phosphatase 1 (PP1) and 2) a change in conformation that promotes the autophosphorylation at T288. Subsequently, AURKA triggers a phosphorylation cascade that promotes the stabilization of microtubules at the kinetochores and centrosomes.

1.4.2. The actin cytoskeleton

Microfilaments, or F-actin, are two-stranded helical structures of about 7 nm in diameter composed of globular (G)-actin that binds ATP. Similar to microtubules, which bind GTP, the ability to hydrolyze ATP confers microfilaments dynamic instability. F-actin is more dynamic that microtubules and single filaments can be nucleated and be quickly assembled practically at any point of the cells. A number of accessory proteins participates in anchorage, ramification, stabilization and disassembly of F-actin (Alberts et al. 2002). Nucleation promoting factors (NPFs), such as formins and the actin related protein complex 2/3 (ACTR2/3), integrate incoming signals and coordinate actin filament polymerization

1.4.2.1. Redox regulation of F-actin by MICALs

The most broadly studied mechanism of regulation of actin by redox modifications is the one mediated by the oxidation of actin methionines by MICALs. MICALs are a family of flavoprotein monooxygenases that bind FAD and use NADPH and O_2 to oxidize methionine 44 (M44) and M47 of actin. Oxidation at these methionines reduces the strength of the interaction between actin subunits, resulting in depolymerization of F-actin. The role of multiple members of the MICAL family has been evidenced in different cellular processes. MICAL1 accumulates at the mid-body and at the abscission site during cytokinesis. Depolymerization of F-actin at the last step of cytokinesis is indispensable for separation of the daughter cells (Frémont, Hammich, *et al.*, 2017). MICAL2, localized in the nucleus, promotes depolymerization and reduction of local levels of actin. Depletion of nuclear G-actin, enables SRF/MRTF-A complex formation and activation of gene transcription in response to serum withdrawal (Lundquist *et al.*, 2014). MICAL3 mediates the transport of Rab8A-possitive vesicles to the mid-body, although the mechanism seems to be independent on the redox-function (Frémont and Echard, 2018).

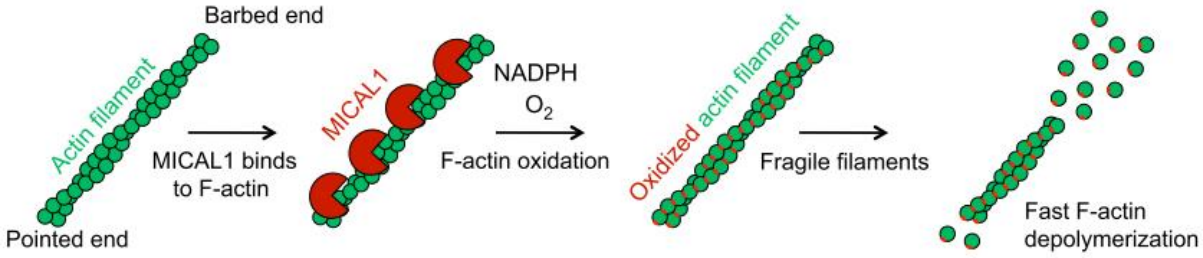

Figure 8. MICAL-mediated actin depolymerization (taken from Frémont, Romet-Lemonne, et al., 2017). MICAL1 is a monooxygenase that binds to actin filaments and uses NADPH and O2 to oxidize the methionines M44 and M47 of actin. Oxidation of these residues diminishes the binding affinity of actin monomers, resulting in turn in fast depolymerization of the microfilament.

1.4.3. Intermediate filaments

Intermediate filaments are ropelike fibers of about 10 nm in diameter. They are more stable than microtubules and microfilaments, and provide resistance to mechanical stress, especially to tensile forces, and assist in intercellular communications. Unlike the first two types, which

subunits can only be isoforms of α/βtubulin or actin, intermediate filaments come from different families and are expressed in a cell type specific manner. The three largest families of intermediate filaments are: keratins, found in epithelial cells, neurofilaments, which constitute the neuronal axons, and vimentins. Vimentins are expressed by mesenchymal cells and their derivates in cells of mesenchymal origin, for example, the glial fibrillaric acid found in glial cells, and desmins in muscle cells (Alberts *et al.*, 2002; Schatten, 2015). Another widely expressed family of intermediate filaments is the nuclear lamins. Lamins constitute the nuclear lamina, they assist in important nuclear functions, provide structural support to the nucleus and organization sites for interphase chromatin (Tsai *et al.*, 2006; Fletcher and Mullins, 2010). Phosphorylation of lamins by cyclin-dependent kinases (CDKs) induce the breakdown of the nuclear envelop at the start of mitosis (Tsai *et al.*, 2006).

1.5. Moonlighting proteins

The term “moonlighting proteins” was first presented in 1999 by Jeffery to describe proteins that have additional functions beyond the ones originally identified or predicted. This term excludes proteins from gene fusions, splice variants, or proteolytic fractions. Moonlighting proteins have been proposed to enable organisms to increase complexity in cellular function based on the available protein repertoire (Jeffery, 1999). Not surprisingly, many of the identified moonlighting proteins are evolutionarily conserved, including various cytosolic and mitochondrial metabolic enzymes (Boukouris, Zervopoulos and Michelakis, 2016), components of the cytoskeleton, receptors and transcription factors (Monaghan and Whitmarsh, 2015; Monaghan *et al.*, 2015; Jeffery, 2016; Qvit *et al.*, 2016). Proteins can acquire alternative functions through different subcellular localization, differential expression, oligomerization and/or complex formation, ligand or substrate concentration, changes in redox state of the cells or by acquisition of different posttranslational modifications (PTMs).

The best examples of moonlighting proteins come from glycolytic enzymes, which are often overexpressed in cancer and are increasingly being described to have additional functions in cancer. These enzymes do not restrict to their canonical localization and have been found to

translocate to other subcellular compartments where they perform completely unpredicted functions. Two of the most studied versatile enzymes are Pyruvate kinase (PKM2) and Glyceraldehyde-3-phosphate dehydrogenase (GAPDH), the functions of which drastically variate and have been found to act as trans-activators of transcription factors and chromatin modifiers to affect gene expression, regulators of apoptosis, cytoskeleton dynamics, membrane trafficking, autophagy, etc. (Min, Lee and Baek, 2016; Sirover, 2018; Amin, Yang and Li, 2019).

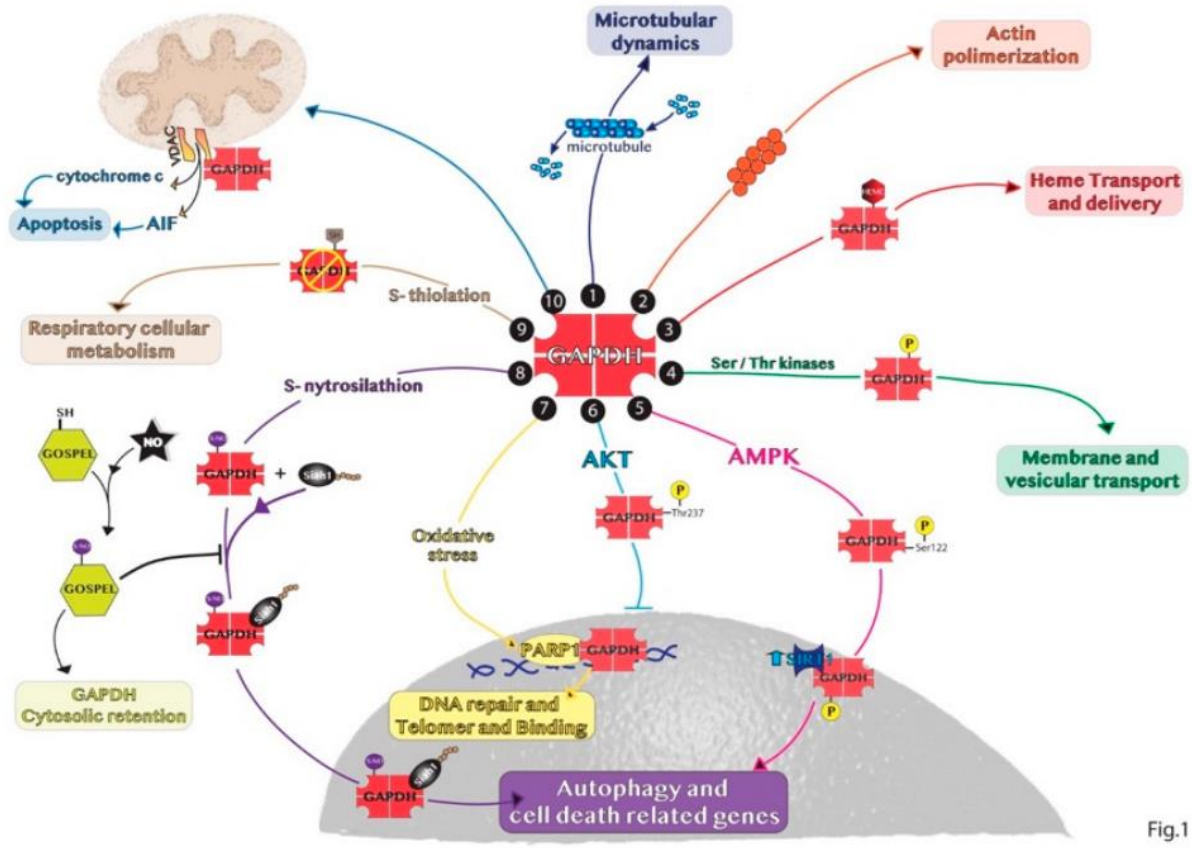

Figure 9. Pleiotropic functions of GAPDH. GAPDH is used to exemplify the variety of moonlighting functions that one protein can have. In different type of cells and under diverse stimuli, GADPH acquires PTMs or forms complexes with proteins that affect its subcellular localization and function (taken from Sirover, 2018).

2. Aims of the study

In prior work, our group has identified the metabolic enzyme BCAT1 as novel pro-tumorigenic factor in glioblastoma. More recently, we proposed that BCAT1 supports tumor growth by depleting intracellular α-KG levels and thus limiting the activity of α-KG-dependent enzymes, rather than by mediating BCAA anaplerosis, as originally hypothesized.

In my doctoral work presented here, I aimed to study the mode of action of BCAT1 in glioblastoma, using the α-KG-depletion model proposed by Raffel *et al.* in 2017 as a working hypothesis. However, initial experiments revealed evidence of a previously unappreciated non-canonical mechanism that is independent of BCAT1 catalytic activity. I therefore focused my work on elucidating this novel mode of action of BCAT1 and its impact on glioblastoma phenotype by:

1. determining the subcellular localization of BCAT1
2. identifying its interaction partners
3. characterizing the consequences of BCAT1 knockout on redox- and cytoskeleton-dependent cellular processes
4. analyzing the relevance of the catalytic transaminase function and the novel mode of action in glioblastoma cells

3. Results

3.1. Subcellular localization of BCAT1

To study the subcellular localization of BCAT1, immunofluorescence (IF) and confocal microscopy were performed in multiple glioblastoma cell lines. To address possible specificity effects of a single antibody, two different BCAT1 antibodies were used. One of them is a commercially available, monoclonal antibody produced in mouse (BD, Biosciences Eca39). The other a polyclonal antibody raised in rabbit that was developed by the group of Myra Conway, Bristol, U.K. To control for artifacts in immunostaining, an N-terminal green fluorescence protein (GFP) was fused to BCAT1 (GFP-BCAT1) and transfected into glioblastoma cells for visualization of BCAT1 in living cells.

3.1.1. BCAT1 localizes to the nucleus of glioblastoma cell lines

Immunostaining with the two antibodies showed comparable BCAT1 localization patterns in two glioblastoma cell lines. As expected, BCAT1 was homogeneously distributed in the cytoplasm of the cells. Additionally, a clear signal of BCAT1 could be observed in the nucleus (Figure 10A). This pattern was not restricted to cells in culture, since IF performed on slices of glioblastoma xenografts in mouse, also showed BCAT1 staining in the nucleus of the tumor cells (Figure 10B). As an antibody-independent validation strategy, GFP-BCAT1 was transiently transfected into three different cell lines: U251MG, U87MG and HEK293. Confocal microscopy performed on living and fixed cells, confirmed the presence of GFP-BCAT1 in the nucleus. Interestingly, the percentage of cells presenting localization of GFP-BCAT1 in the nucleus differed between cell lines. Whilst most of the U251MG cells showed GFP-BCAT1 expression in the nucleus (Figure 10C), only ~50 % of the U87MG exhibit nuclear GFP-BCAT1 (Figure 10D). In sharp contrast, the cell line HEK293 did not have any GFP-BCAT1 in the nucleus (Supplementary Figure. S1).

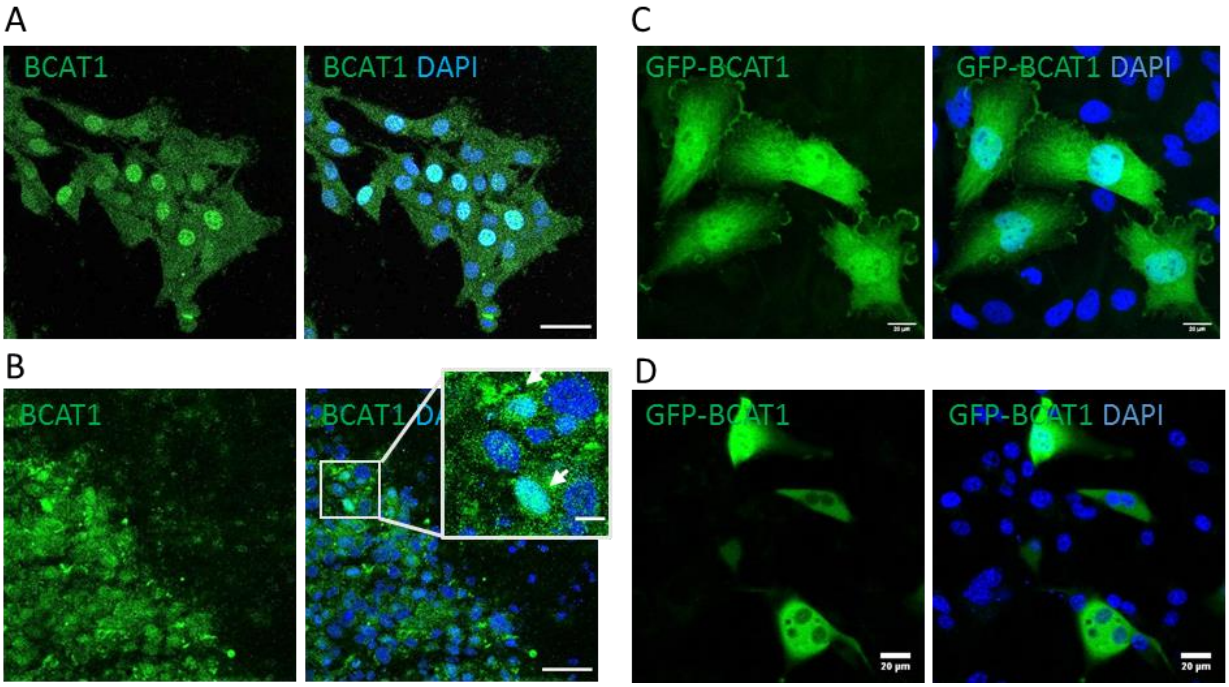

Figure 10. BCAT1 localizes to the nucleus of glioblastoma cells. (A) Immunofluorescence of BCAT1 in U87MG cells in culture. Scale bar: 30 µm (B) immunofluorescence of U87MG xenografts in mouse showing localization of BCAT1 in the nucleus of engrafted cells (inset, arrow). Scale bar: 50 µm, inset scale bar: 10 µm (C) Fluorescence imaging of GFP-BCAT1 in U251MG (D) Fluorescence imaging of GFP-BCAT1 in U87MG transfected. Scale bar: 20 µm.

3.2. Development of FRET sensors to study live-cell fluctuations of α-KG

In order to determine whether BCAT1 can regulate α-KG levels in the nucleus, it was necessary to measure concentrations of α-KG in this specific compartment. However, the current lack of extraction methods yielding sufficient amounts of clean nuclear extracts in a short time represents a serious limitation. In the available prolonged protocols for cell fractionation, unstable or very reactive metabolites might be lost. Furthermore, these methods are not suitable for monitoring temporal changes of α-KG in living cells or unperturbed tissues. We therefore opted to develop a biosensor based on Förster Resonance energy transfer (FRET) and used it as a tool to measure fluctuations of α-KG after manipulation of BCAT1 in living cells.

A first part of this project focused on engineering the FRET sensor and characterizing the dynamic range *in vitro*. The α-KG-sensor was engineered based on the signal transduction protein PII from *Synechococcus elongatus* PCC 7942 *(S. elongatus)*. Two fluorescent proteins, mVenus and mCerulean, acting as FRET acceptor and donor, respectively, were linked to the α-KG-binding domain of the PII protein. Upon α-KG binding, the PII protein suffers a conformational change, such that the distance between the two fluorescent proteins increases. Upon excitation with an UV laser, the transfer of energy from mCerulean to mVenus decreases relative to the unbound protein. Therefore, the FRET ratio, measured as the ratio of the signal emitted by the acceptor divided by the signal emitted by the donor, decreases as the concentrations of α-KG increase (Lüddecke, Francois et al., 2017).

A modified version of the α-KG sensor was generated by introducing a R9P mutation in the PII protein (TC3-R9P). This change shifted the detection range to 10 µM - 10 mM α-KG, suitable to detect physiologically relevant fluctuations of α-KG in mammalian cells. The TC3-R9P sensor showed to be functional to monitor intracellular fluctuations of α-KG. Dose-dependent changes of the FRET ratios were observed upon addition of precursors of α-KG such as the dimethyl-α-KG (dm-α-KG), a cell permeable derivative of α-KG that is demethylated to α-KG by cytosolic demethylases, and citrate, which is processed by the IDH enzymes (Figure 11).

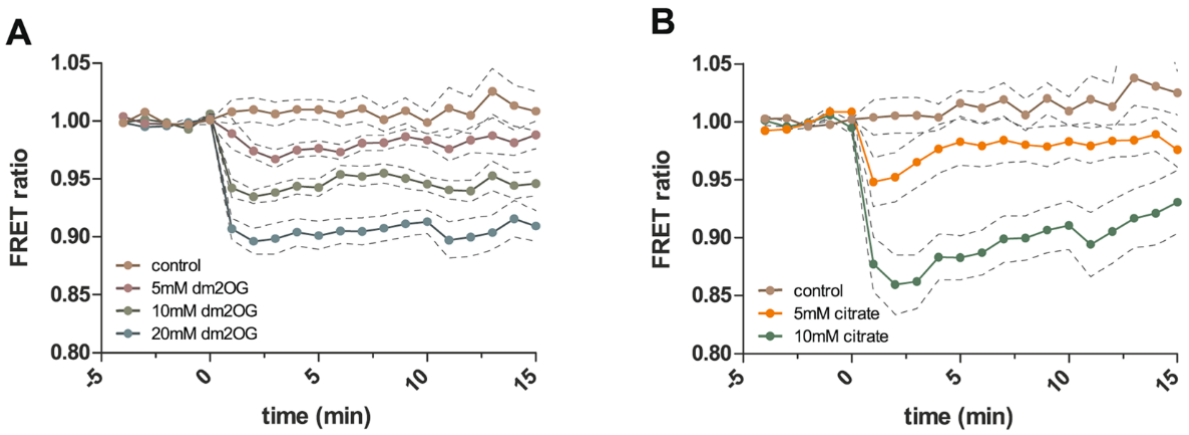

Figure 11. Effects of dimethyl-α-KG (dm-α-KG) and citrate on FRET signal emitted by the α-KG-sensor in U87MG cells. Taken from (Lüddecke, Francois et al., 2017). U87MG transfected with TC3-R9P were seeded in chambered coverslips (µ-slides) for life-cell imaging. 48hr after transfection, cells were imaged for 5 min (baseline), then treated with dm-α-KG (A) or citrate (B) and imaging was resumed. At each timepoint, FRET ratio of 3-6 cells per field was measured and normalized to the baseline FRET ratio. During each experiment, 3 fields per condition were imaged (in total ~20-50 cells per experiment were quantified). Graphs shows the average of 3 independent experiments. Gray dotted lines = S.E.M.

Having shown that our FRET-based sensor can be used to monitor metabolism of α-KG in living cells, we evaluated whether it could detect changes in α-KG levels after manipulation of BCAT1 activity. We made use of a small molecule inhibitor that targets the catalytic activity of BCAT1 (BAY1900489). This compound was previously shown to have an IC50 of 10-20 µM in cell-based assays (Martje Tönjes, personal communication). Using the α-KG-sensor, we could show that treatment of U87MG cells with 30 mM of BAY1900489 leads to a rapid increase in intracellular α-KG levels, as evidenced by a decrease in FRET ratio of ~10 %. This suggests that BCAT1's transaminase activity is rapidly inhibited by 30 µM of the drug. Lower concentrations did not appear to significantly affect BCAT1 activity, at least not within the detection limits of the sensor (Figure 12A).

We further validated the functionality of our α-KG-FRET sensors by manipulating BCAT1 expression. U87MG cells expressing the α-KG sensor were evaluated before and after BCAT1 knockdown. A decrease in FRET ratio, corresponding to increased α-KG concentrations, was

observed 24 h after induction of BCAT1 knockdown, suggesting that already at this time-point, reduction of BCAT1 levels have effect on total intracellular α-KG levels (Figure 12B). These results are consistent with our previous observations (Raffel *et al.*, 2017).

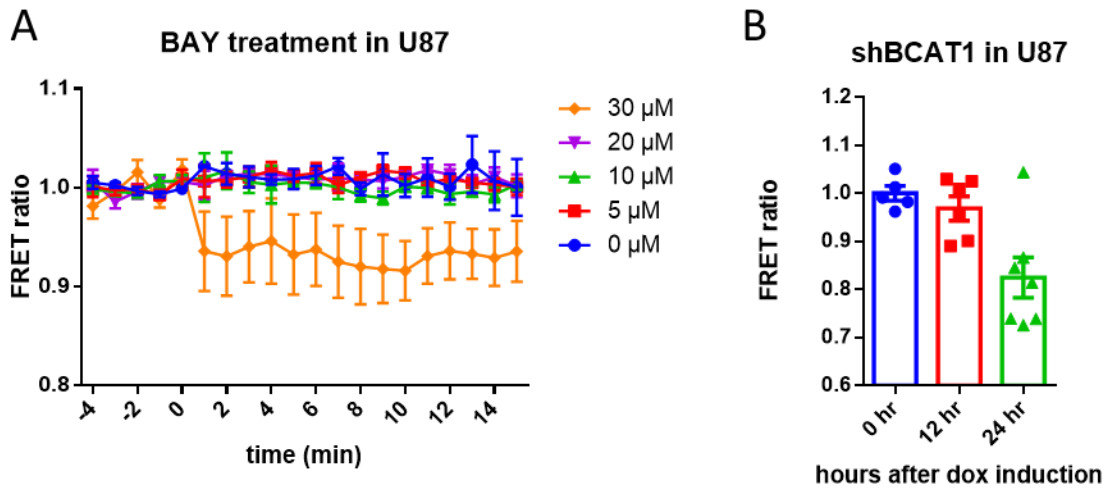

Figure 12. Changes in α-KG levels monitored in living cells using FRET sensor after manipulation of BCAT1 activity and expression. A) U87MG transfected with TC3-R9P were seeded in µ-slides. Cells were imaged for 5 min (baseline), then treated with 0-30 µM of BAY1900489 and imaging was resumed. At each timepoint, FRET ratio of 3-6 cells per field was measured and normalized to the baseline FRET ratio. During each experiment, 3 fields per condition were imaged (in total ~20-50 cells per experiment were quantified). Graphs show the average of 3 independent experiments. B) BCAT1 shRNA knockdown was induced by addition of doxycycline (dox, 1:20 000) and imaged after 12 and 24 h of dox treatment. At each timepoint, FRET ratio of 10-20 cells was measured and normalized to the baseline FRET ratio. Error bars = S.E.M.

3.2.1. Targeting α-KG FRET sensors to the nucleus

Targeting of the α-KG-FRET sensor to the nucleus was accomplished by adding three SV40 nuclear localization sequences (NLS) $(PKKKRK)_3$ at the C-terminal end of the TC3-R9P construct (TC3-R9P-NLS). Microscopic evaluation showed that the sensor was efficiently targeted to the nucleus of cells transfected with the TC3-R9P-NLS (Figure 13). To test the sensor, U87MG cells

expressing TC3-R9P-NLS were treated with different concentrations of dm-α-KG. However, under the conditions assayed, the FRET ratio emitted by the nuclear sensor remained unchanged. This could mean that either nuclear α-KG levels were not affected by the conditions we tested, or that the concentrations of α-KG in the nuclear compartment are beyond the detection range of our α-KG-FRET sensor.

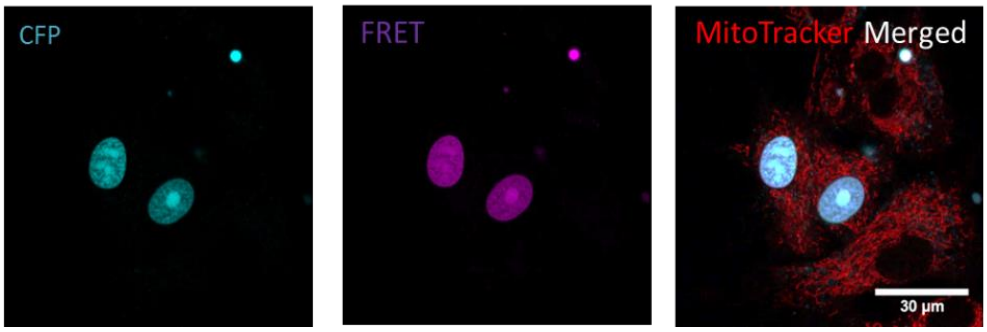

Figure 13. The α-KG FRET sensor targeted to the nucleus of GB cell lines. U87MG cells were transfected with the TC3-R9P-NLS and imaged 48 h after transfection. Mitochondria were counterstained using MitotrackerRed to deliniate the cells.

3.3. Identifying nuclear BCAT1 binding partners by IP-MS

To determine whether BCAT1 associates with α-KG-dependent enzymes in the nucleus, we performed immunoprecipitation (IP) followed by mass-spectrometry (MS) analysis (IP-MS). To this end, lysates from nuclear and cytoplasmic fractions from U251MG cells were subjected to IP with a BCAT1 specific antibody (kindly provided by Myra Conway, Bristol) or the appropriate IgG control. Immunoprecipitated complexes from the nuclear and cytoplasmic fractions were sent for MS analysis to the Krijgsveld group at the DKFZ where the samples were processed and analyzed by Dr. Gianluca Sigismondo.

IP-MS resulted in a large list of binding candidates. 151 proteins were found in the cytoplasmic fraction and 252 proteins in the nuclear compartment. Ingenuity pathway analysis (IPA) detected enrichment of proteins associated with canonical cellular processes and pathways (Figure 14). IPA grouped most of the proteins (229 out of 251) to be associated to cancer, indicating that BCAT1 directly participates in oncogenic processes. The analysis also revealed a significant enrichment of binding candidates that are involved in cytoskeleton-associated functions and signaling pathways, such as cell cycle, cellular assembly and organization, and clathrin-mediated endocytosis signaling (Figure 14). The complete lists of associated proteins can be found in the supplementary section (Tables S1, S2 and S3). Selected examples of identified proteins from these three categories are listed below in Table 1. These include well-known regulators of mitosis, the actin and tubulin cytoskeletons, and vesicle-mediated signaling pathways such as EGFR signaling (Sigismund *et al.*, 2008; Tomas, Futter and Eden, 2014).

To our surprise, none of the binding candidates were known α-KG-dependent proteins, as we expected to find based on my working hypothesis that BCAT1 might regulate chromatin structure and gene expression by controlling local α-KG concentrations. Instead, most of the potential BCAT1-binding partners identified through IP-MS analysis were proteins involved in cytoskeleton-related processes. This unexpected finding suggested that BCAT1, in addition to its classic catalytic activity as a transaminase, might have additional, “moonlighting” functions, as have been described for other metabolic enzymes (Luo *et al.*, 2011; Yang *et al.*, 2011; Yang,

Xia, Hawke, Li, Liang, Xing, Aldape, Hunter, Alfred Yung, *et al.*, 2012; Min, Lee and Baek, 2016; Zhang *et al.*, 2017).

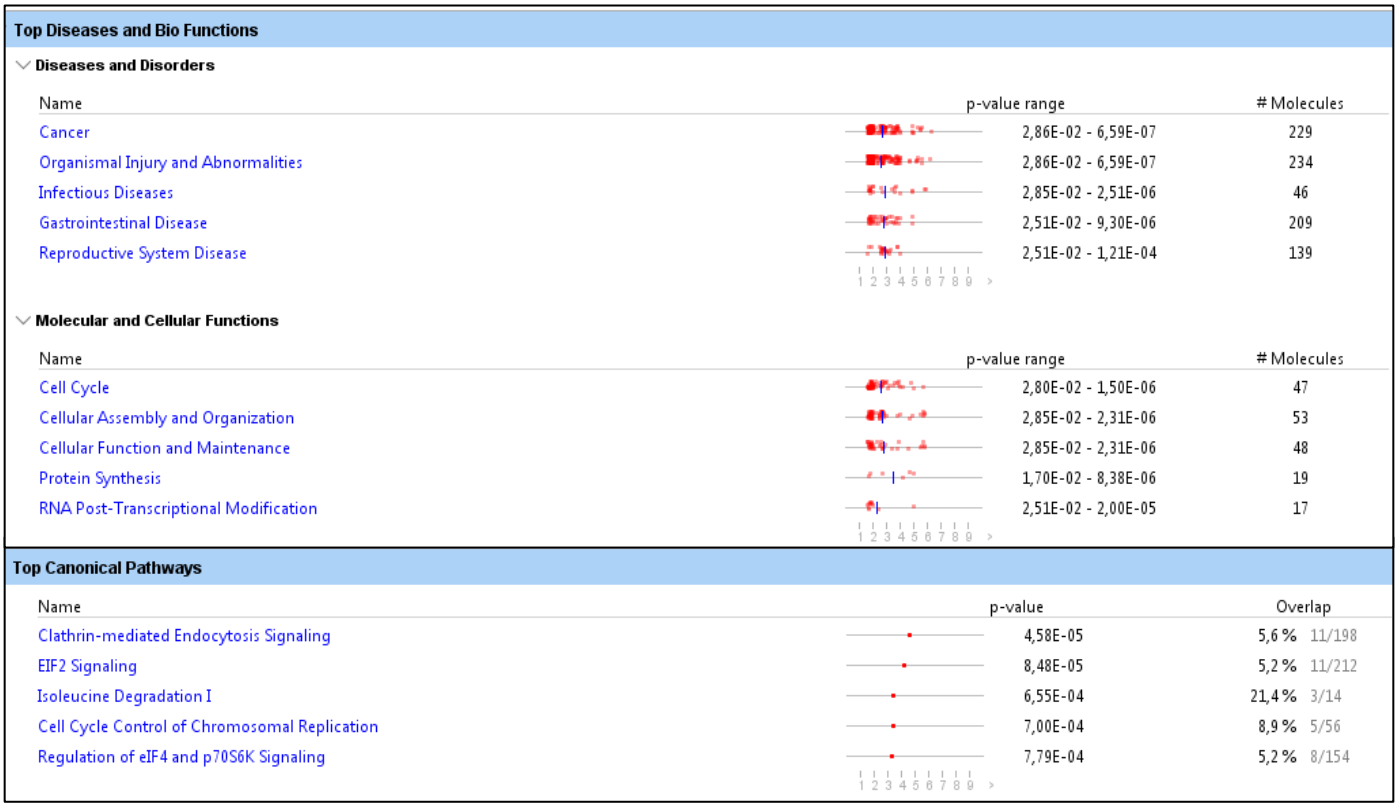

Figure 14. Top diseases, bio-functions and canonical pathways of BCAT1 binding partners. The 251 binding candidates obtained by IP-MS of the nuclear fraction of U251MG cells was analyzed with the Ingenuity Pathway Analysis (IPA) software.

Table 1. Examples of proteins belonging to each of the groups that showed significant enrichement by IPA analysis.

Cell cycle	Cellular assembly and organization	Clathrin mediated Endocytosis signaling
AURKA	ACTR3	AP2M1
CDK1	KIF18B	CDC42
CDC20	MAP2	CLTB
EWSR1	MICAL2	MYO1E
NUSAP1	TUBA1A	PIK3C2A

3.4. Validation of IP-MS binding candidates

3.4.1. BCAT1 co-localizes with AURKA during mitosis and cytokinesis

AURKA has essential roles during cell division, it mediates centrosome maturation and assists the formation of a bipolar spindle (Vader and Lens, 2008). AURKA is often amplified in tumors, including glioblastoma, and is associated with sustained growth, migration and resistance to therapy (Mannino *et al.*, 2014; Willems *et al.*, 2017, 2019). To investigate the possible interaction between BCAT1 and AURKA, co-immunofluorescence (Co-IF) and confocal microscopy was performed. Co-localization analysis showed that BCAT1 and AURKA co-localized at the mitotic spindle (Figure 15). BCAT1 and AURKA were observed at the same sites as soon as the centrosomes formed in prophase and remained at the mitotic spindle during metaphase. At anaphase, BCAT1 was additionally localized at the cleavage furrow, followed by its appearance at the mid-body and contractile ring by the end of cytokinesis (Figure 16). All these structures are rich in cytoskeletal proteins, and their assembly is essential for successful cell division. The presence of BCAT1 at these mitotic structures was not restricted to glioblastoma cell lines. Similar localization patterns were observed in immortalized normal human astrocytes, and in U2OS, an osteosarcoma cell line (Figure 17).

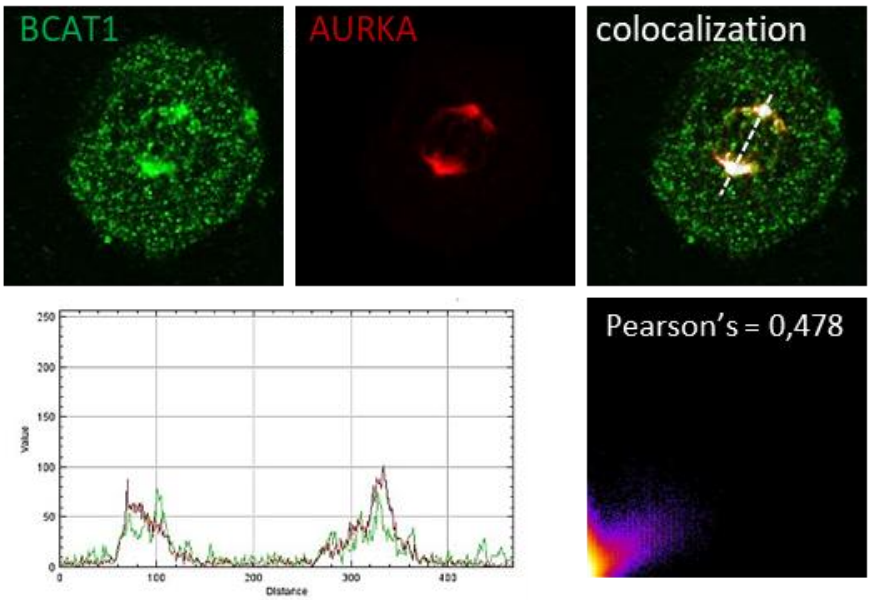

Figure 15. BCAT1 colocalizes with AURKA. Co-staining of AURKA and BCAT1 showing colocalization at the mitotic spindle. Colocalization analysis, intensity histogram and Pearson's correlation score was calculated with Fiji (Image J).

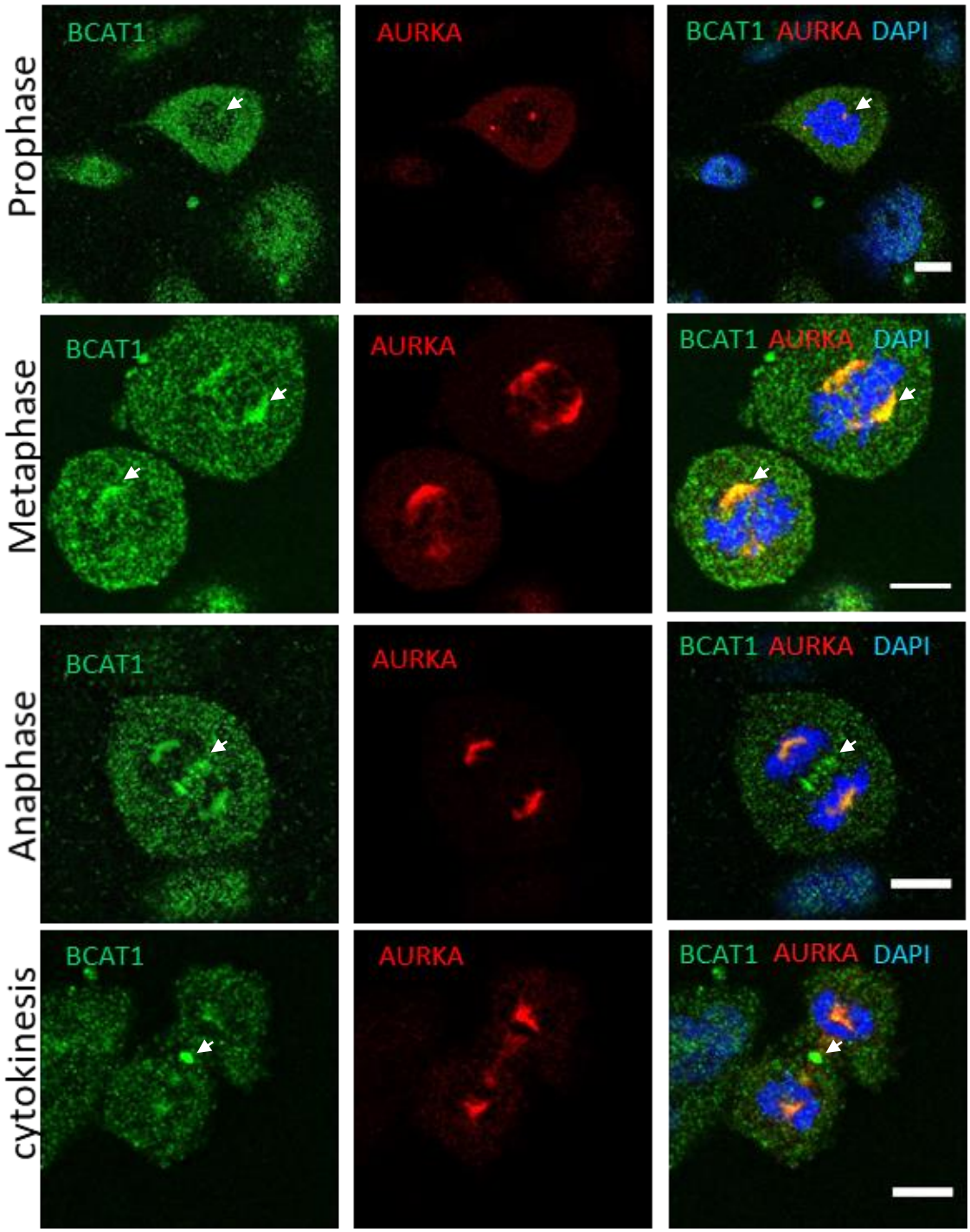

Figure 16. Co-Immunofluorescence of BCAT1 and AURKA in mitotic cells. BCAT1 appears at the centrosomes in prophase, at the mitotic spindle during metaphase and at the cleavage furrow and midbody during anaphase and cytokinesis, respectively. White arrows show the localization of BCAT1 each mentioned structure. Scale bar = 5 µm

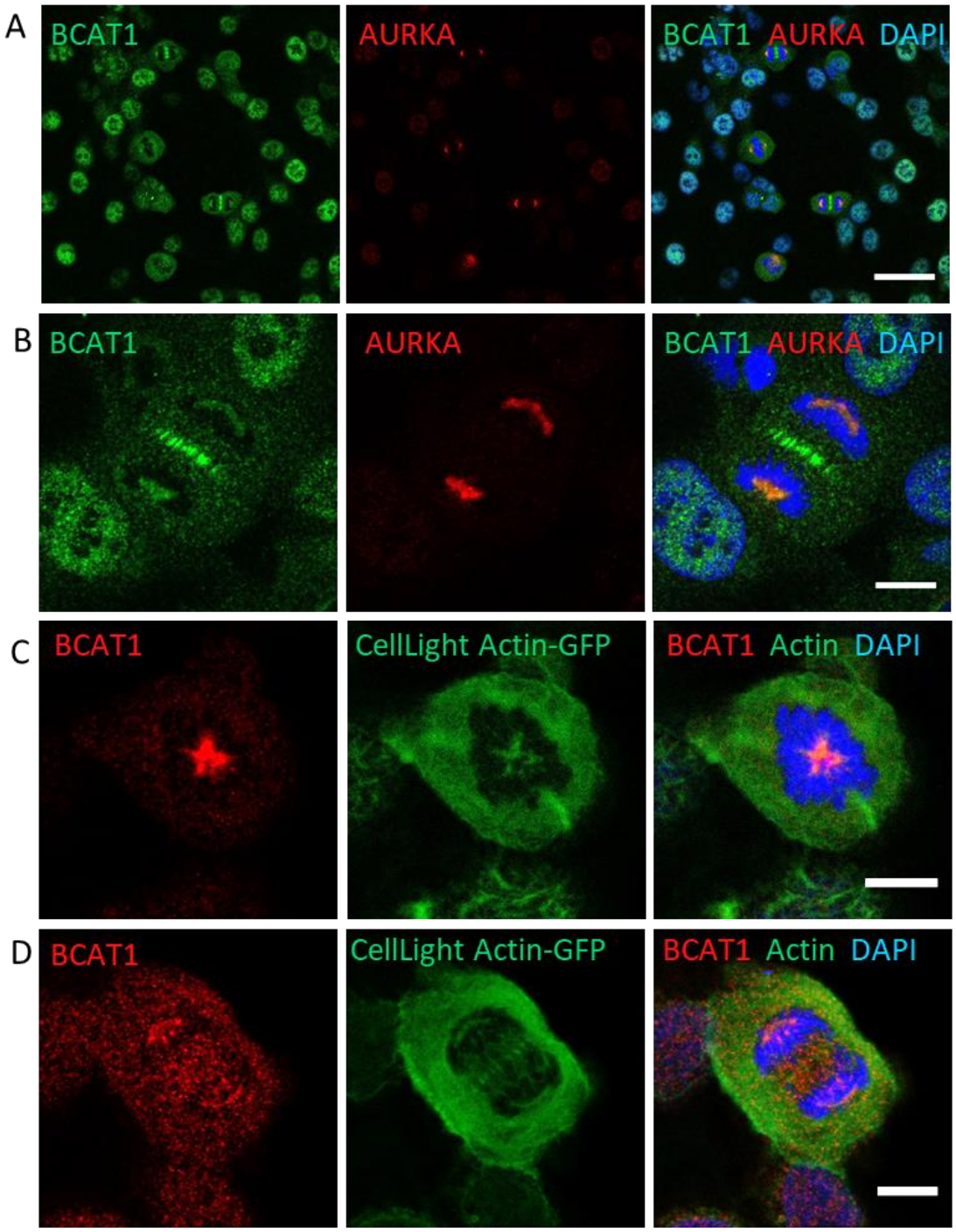

Figure 17. Localization of BCAT1 during mitosis of additional cell lines. A) and B) Normal human astrocytes A) showing a strong signal of BCAT1 in the nucleus of cells in interphase and some mitotic cells B) mitotic cells with localization of BCAT1 at the cleavage furrow. C) and D) U2OS osteosarcoma cell line expressing CellLight® Actin-GFP. BCAT1 in green: immunostaining with a mouse monoclonal antibody (BD-biosciences) and anti-mouse A488. BCAT1 in red: immunostaining with a rabbit polyclonal antibody and anti-rabbit A564. Scale bars in A= 30 µm, in B, C and D = 5 µm.

3.4.2. BCAT1 interacts with the cytoskeleton

Another group of proteins significantly enriched in IP-MS was associated with cytoskeleton assembly and organization (Table 1, Supplementary table S2). Proteins from this group were found in both nuclear and cytoplasmic fractions. This group included the main components of the cytoskeleton: actin (ACTA1), tubulin (TUBA1A, TUBGCP2) and vimentin (VIM). Additionally, cytoskeletal accessory proteins such as the actin related protein 3 (ACTR3), and microtubule associated proteins (MAP1S and MAP2) were also found. These data, together with the clear localization of BCAT1 at the mitotic spindle and contractile ring, strongly suggest that BCAT1 interacts with the cytoskeleton. It is possible that the BCAT1 and cytoskeleton interactions are not restricted to mitosis but might also take place during other processes.

3.4.3. BCAT1 is present at cell protrusions and co-localizes with cytoskeletal components

Confocal microscopy showed that BCAT1 is widely distributed in the cell. To investigate whether BCAT1 co-localizes with the cytoskeleton other than the spindle apparatus, GFP-BCAT1 expressing cells were stained with a cell-permeable probe specific for microtubules (SiR-tubulin) and analyzed them by time-lapse imaging. GFP-BCAT1 was not only localizing with the microtubules, but also formed part of cell protrusions, where microtubules were not present (Figure 18A, arrows). GFP is a large protein that could affect localization and interactions of BCAT1. To avoid possible artifacts caused by the GFP-tag, we created an HA-tagged BCAT1 (HA-BCAT1). By indirect IF using antibodies against the HA-tag and α-tubulin, we could confirm the localization of BCAT1 in tubulin-rich and tubulin depleted areas at the edges of cell protrusions (Figure 18 B, inset). Counterstaining of HA-BCAT1 expressing cells for F-actin with fluorescently labeled phalloidin revealed that BCAT1 was co-localizing with F-actin bundles near the cell membranes of these protrusions (Figure 18 C, arrows).

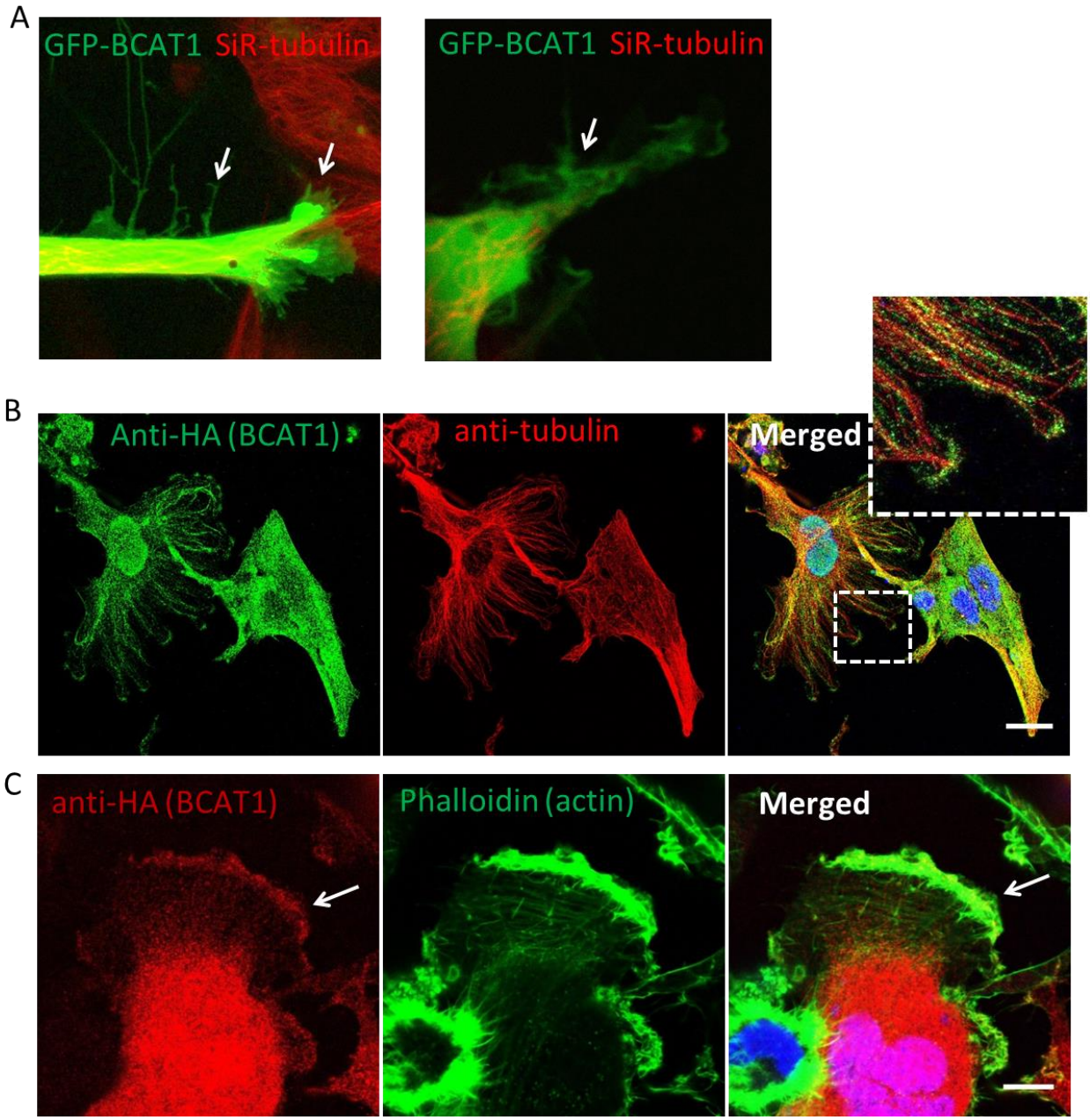

Figure 18. BCAT1 localizes at cytoskeleton structures. A) Live-cell imaging of U87MG cells transfected with GFP-BCAT1 and counterstained with SiR—tubulin to visualize microtubules, showing GFP-BCAT1 forming part of extensions of the cell membrane. B) U251MG cells expressing HA-BCAT1 were immuno-stained for HA-tag and tubulin. Insets showing HA-BCAT1 staining at the tips of cells protrusions. Scale bar= 20 µm C) U251MG cells expressing HA-BCAT1 were immuno-stained against HA-tag and counterstained with phalloidin-A488 to visualize F-actin. HA-BCAT1 localizes at F-actin bundles. Scale bar =10 µm.

3.5. BCAT1 knockout affects proliferation and cytoskeleton related processes

We then questioned whether the association of BCAT1 with cytoskeleton component has a functional role in cancer-relevant phenotypes. To address this, we created BCAT1 knockout (BCAT1-KO) cells and evaluated cytoskeleton-dependent processes. Complete knockout of BCAT1 was achieved using CRISPR/cas9 technology on three different glioblastoma cell lines: U251MG, U87MG and LN229. Of the clones evaluated, CRISPR/cas9 resulted in complete depletion of BCAT1 proteins levels and resulted in a 40-50 % decrease in proliferation compared to control cells using a non-target gRNA (cNT). The proliferation phenotype of CRISPR-mediated BCAT1-KO was comparable to what was previously achieved using shRNA-mediated knockdown (Tönjes *et al.*, 2013; Raffel *et al.*, 2017). Flow cytometric analysis using propidium iodide (PI) and EdU incorporation (Click-iT®) showed that BCAT1-KO induces a G2/M arrest. The percentage of cells in G2/M phase in BCAT1-KO compared to cNT cells increased by 2.1 fold in U251 cells and by 3.4 fold in LN229 cells (Figure 19B).

3.5.1. BCAT1-KO affects cell morphology

BCAT1-KO severely affected the morphology of the cells. U251 BCAT1-KO cells appeared thin and developed long projections (Figure 20A). The mean cell area of U251 BCAT1-KO cells was ~30 % smaller than U251cNT when analyzed by microscopy (Figure 20B).

Quantifications by flow cytometry (Figure 20D) showed that the cell size, measured by the mean intensity of the forward scatter channel (FSC), was about ~20 % lower in BCAT1 depleted cells compared to the cNT cells (Figure 20C). Additionally, the side scatter channel (SSC), which is an indication of the internal complexity of the cell, gave a mean intensity 50 % lower in U251 BCAT1-KO than U251cNT cells. In LN229 cells, BCAT1-KO led to a 15 % and 32 % decrease in the FSC and SSC signal, respectively, compared to the LN229cNT cells (Figure 20C).

3.5.2. BCAT1-KO affects migration of glioblastoma cells

To assess the role of BCAT1 in migration, another cytoskeleton dependent process, transwell migration assays were used. The migration capacity was evaluated in two different cell lines, U251MG (Figure 21 top) and U87MG (Figure 21 bottom). BCAT1-KO impaired the ability of glioblastoma cell lines to migrate towards 10% FCS or 50 ng/ml of epidermal growth factor (EGF).

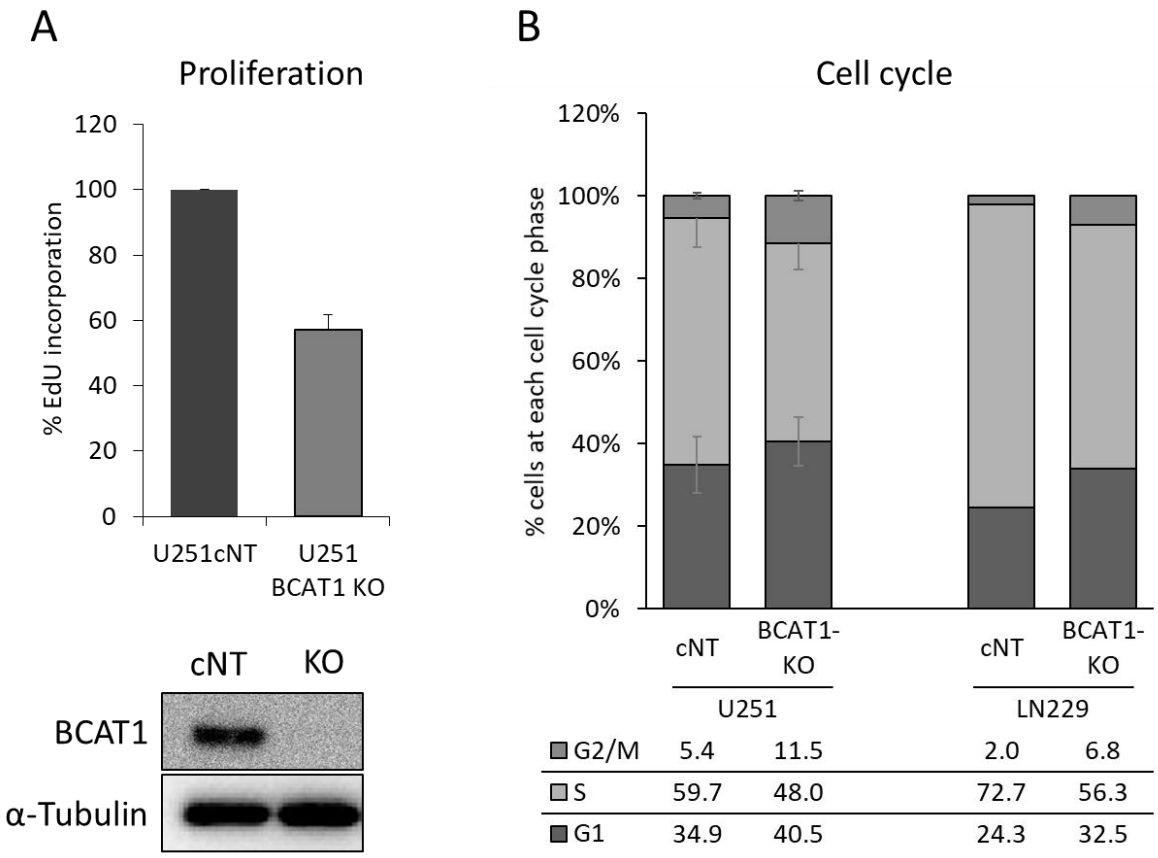

Figure 19. CRISPR/Cas9 mediated BCAT1-KO decreases proliferation and induces G2/M arrest of glioblastoma cell lines. A) Complete depletion of BCAT1 causes impaired proliferation of glioblastoma cells by ~ 50-60%. B) Cell cycle analysis of glioblastoma cell lines showing a larger percentage of cells in G2/M phase was higher in BCAT1-KO cells compared to cNT cells. The bars represent the mean of 6 independent experiments for the U251 cells and 2 experiments for LN229 (error bars = s.e.m.). The table shows the percentage of cells at each cell cycle phase.

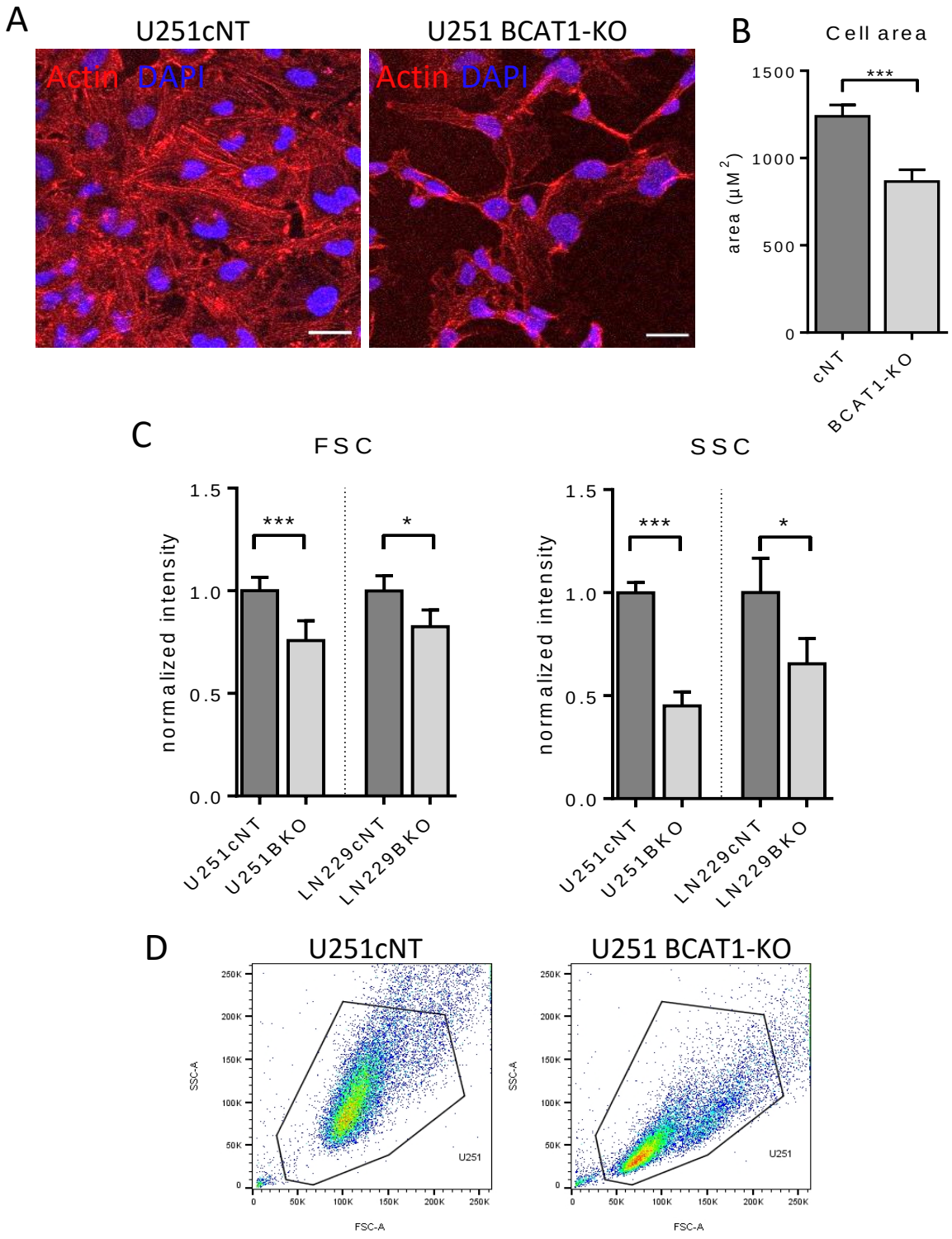

*Figure 20. Effects of BCAT1-KO (BKO) on cell morphology. A) U251 cells counterstained with Acti-stain-A647 (Cytoskeleton, Inc) B) cell area obtained from fluorescence images using Fiji (ImageJ). 5 fields with at least 50 cells were quantified C) Flow cytometry analysis of FSC and SSC of U251 and LN229. D) Dot plot (SSC vs FSC) showing the changes in the cell population caused by depletion of BCAT1. At least 3 independent experiments were performed. Mean + s.e.m. *p<0.05 ***p<0.001, ****p<0.0001 (two-tailed Student's t test)*

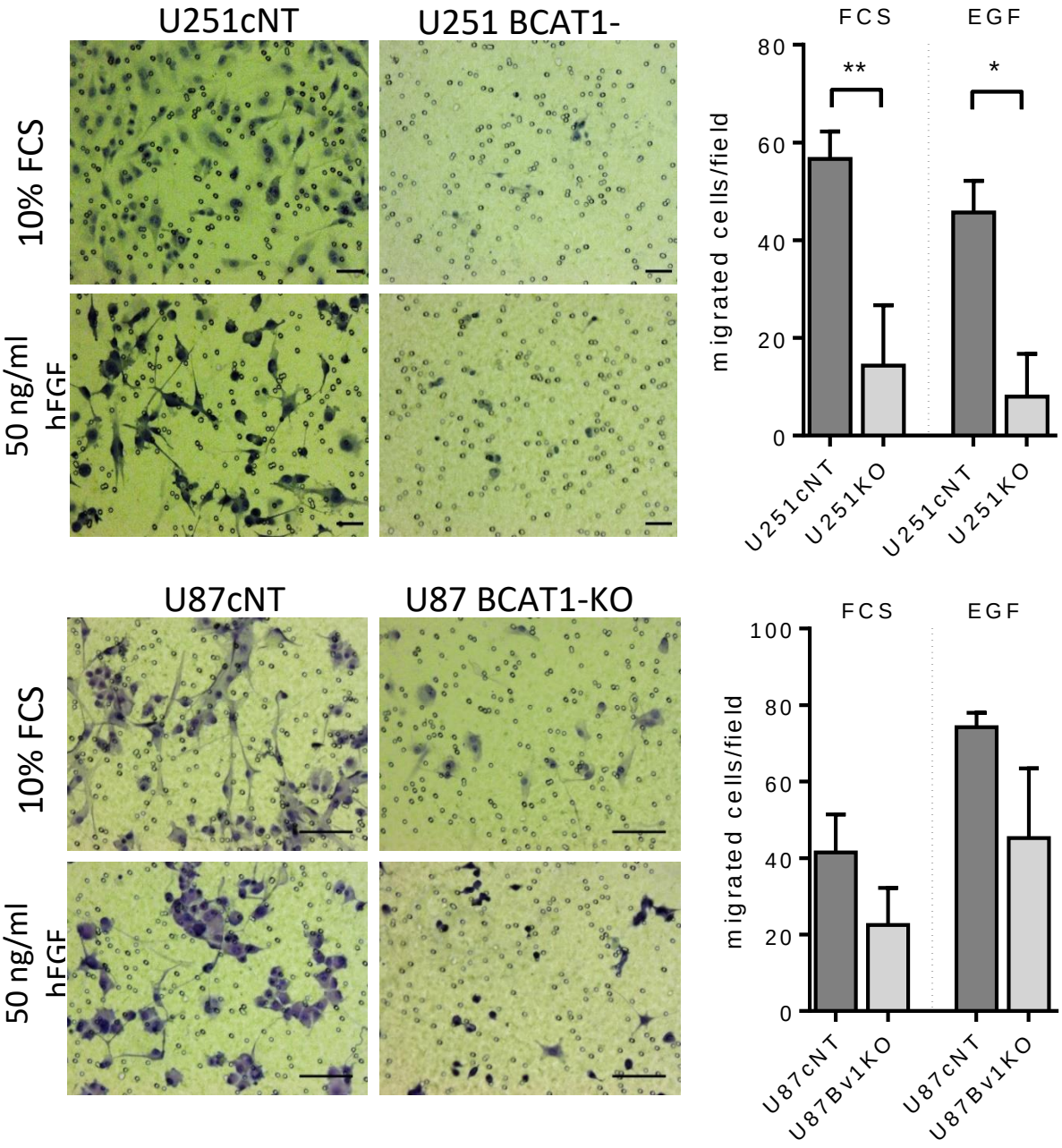

*Figure 21. BCAT1-KO impairs migration in glioblastoma cell lines assessed by transwell migration assay. 1x10^4 serum starved cells were placed into each insert and allowed to migrate for 24 h towards medium containing 10 % FCS or 50 ng/ml of EGF. Migrated cells were fixed and stained with hematoxylin. 4-5 fields per condition were imaged and migrated cells were counted. For U251MG cells, 3 independent experiments were performed (mean + s.e.m.) *p<0.05, **p<0.01 (two-tailed Student's t test). One experiment was performed with U87MG cells.*

3.5.3. BCAT1 affects endocytic trafficking of EGFR

Another important group of proteins found by IP-MS was associated with endocytosis and vesicle trafficking. Endocytosis mediates the translocation of membrane bound proteins from the outer cell membrane to other subcellular compartments. This process is coordinated by the cytoskeleton. F-actin is required for the invagination of cargo vesicles at the cell membrane, which are then transported along the microtubules to other sites inside the cell (Anitei and Hoflack, 2012). Endocytosis is important for regulating the activity of cytokine receptors, such as the epidermal growth factor receptor (EGFR). Internalized EGFR in endosomes can have different fates: 1) Activated EGFR can be released from its ligand and be recycled back to the membrane, ready to be reactivated by other extracellular ligands; 2) ligand-bound receptor in the membrane of endosomes can be mobilized to certain areas to activate diverse downstream effectors; 3) EGFR can be delivered to lysosomes for degradation. This last, terminates the signal and reduces the number of receptors presented at the cell membrane. EGFR signaling promotes proliferation and migration and is dysregulated in tumors including glioblastoma (Tomas, Futter and Eden, 2014). Among other mechanisms, aberrant endocytosis contributes to sustained activation of EGFR in cancer (Huang, Xu and White, 2009; Pike *et al.*, 2018).

To investigate whether BCAT1 plays a role on EGFR internalization, U251 BCAT1-KO and U251cNT were treated with EGF and fixed after 5, 15 and 30 minutes. Fixed cells were stained for EGFR and F-actin. U251cNT cells, formed EGF-induced actin bundles within the first 15 minutes. After 30 minutes of EGF stimulation, the distribution of EGFR changed from a homogenous distribution at the cell membrane to a perinuclear localization (Figure 22, left panel). The formation of actin bundles and the obvious change in EGFR localization suggest that endocytosis of EGFR is efficient in BCAT1 expressing cells. However, this was not observed in BCAT1-KO cells. U251 BCAT1-KO cells failed to induce cytoskeletal rearrangements at the cells' cortex and F-actin could be observed as stiff stress fibers along the cell. In line with inefficient F-actin dynamics, the localization of EGFR was not affected by EGF treatment (Figure 22, right panel).

Endocytosis is a dynamic process; therefore, examination of fixed samples by IF might cause loss of short time events. To learn more about the dynamics of EGFR internalization, live cell imaging using a GFP-labeled EGFR (EGFR-GFP) was performed. EGFR-GFP was transfected in U87cNT or in U87 BCAT1-KO and imaged before and during treatment with 100 ng/ml of hEGF. Time-lapse imaging revealed differences in initial distribution and dynamics of EGFR-GFP in response to its ligand EGF. Under basal conditions, EGFR-GFP was concentrated at the cell periphery of U87cNT, while in U87 BCAT1-KO, it was homogenously distributed in the cytoplasm (Figure 23. upper panel). Within 5 minutes of starting EGF treatment, U87cNT formed vesicles of about 5-15 µM in diameter that persisted in the cytoplasm for 10 to 20 minutes. U87 BCAT1-KO showed a delayed response and formed mostly small vesicle of < 5 µM in diameter. Only few larger vesicles were formed after 30 minutes, but different than in U87cNT cells, these remained in the cell periphery for a short time and seemed to disappear after few minutes. The most common type of vesicles observed in U87cNT cells appeared to be devoid of internal EGFR-GFP staining, but displayed strong staining at the periphery (Figure 23 lower left panel). On the contrary, the vesicles in U87 BCAT1-KO cells were observed as dense vesicles with EGFR-GFP (Figure 23 lower right panel).

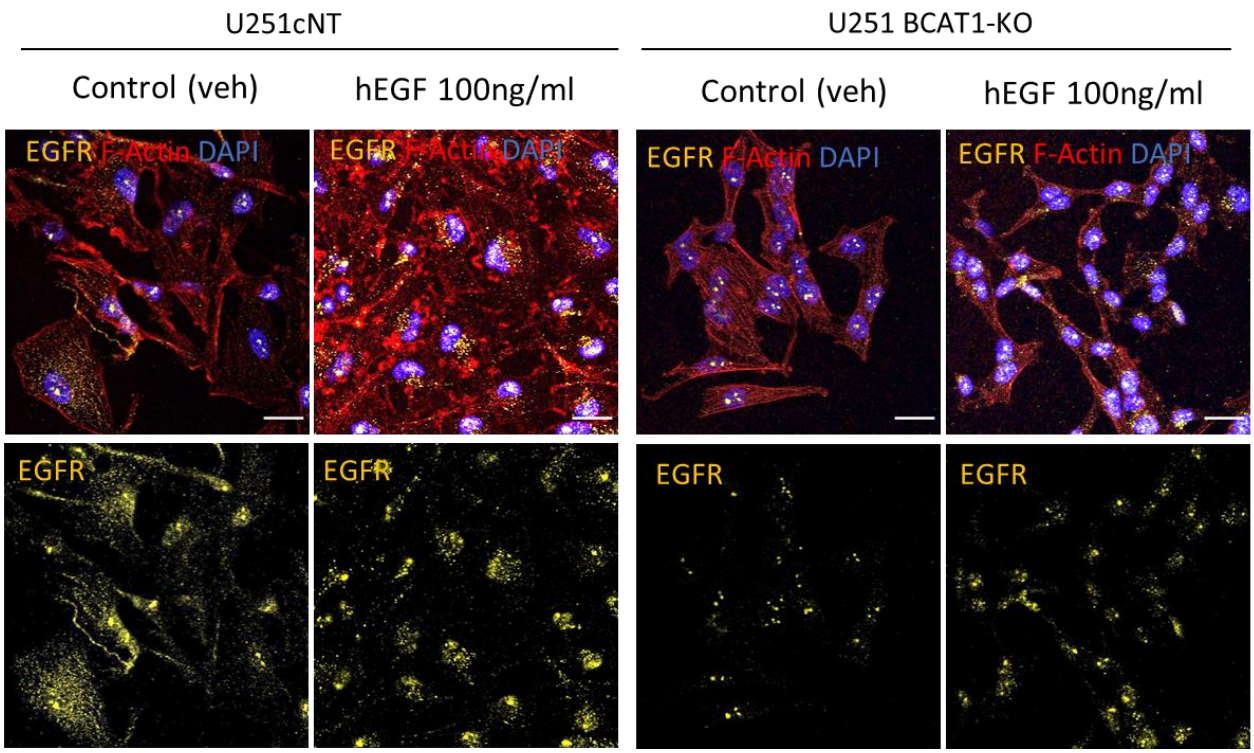

Figure 22. Immunofluorescence of U251cNT and U251 BCAT1-KO treated with 100 ng/ml of EGF for 30 min. Cells were seeded in 12 chambered coverglass, allowed to attach and starved overnight. Cells were treated with media without (Veh) or supplemented with hEGF (100 ng/ml) for 30 minutes. Cells were immunostained for EGFR (sc-003) and counterstained with Acti-stain (phalloidin-A647) and DAPI for visualization of F-actin and nuclei, respectively. Samples were imaged using a laser scanning confocal microscope Leica SP8. The pictures shown here are representative of 3 independent experiments, per experiment at least 4 fields per condition were imaged.

Figure 23 (next page). Imaging of EGFR-GFP endocytosis by time-lapse imaging (snapshots). U87cNT and U87 BCAT1-KO transiently expressing EGFR-GFP were seeded in 8-chambered coverglass and starved for 4 hr. The localization of EGFR-GFP was imaged before and after treating with 100 ng/ml of hEGF. Cells were imaged for 90 min after the addition of hEGF. Top: localization of EGFR-GFP before treatment with hEGF. Bottom: EGFR-GFP internalization after 25 min of stimulation with hEGF. Insets: zoom to show different EGFR-EGF vesicle formed in the two cell lines. Histograms shows the signal density of the horizontal line drawn over the vesicle. The pictures shown here are representative of 2 independent experiments, where at least 3 fields of view per condition were imaged. As a negative control, a GFP-only protein was expressed. No GFP-vesicles were observed upon treatment with hEGF. Scale bars= 30 µm (top), 20 µm (middle) and 5 µm (insets)

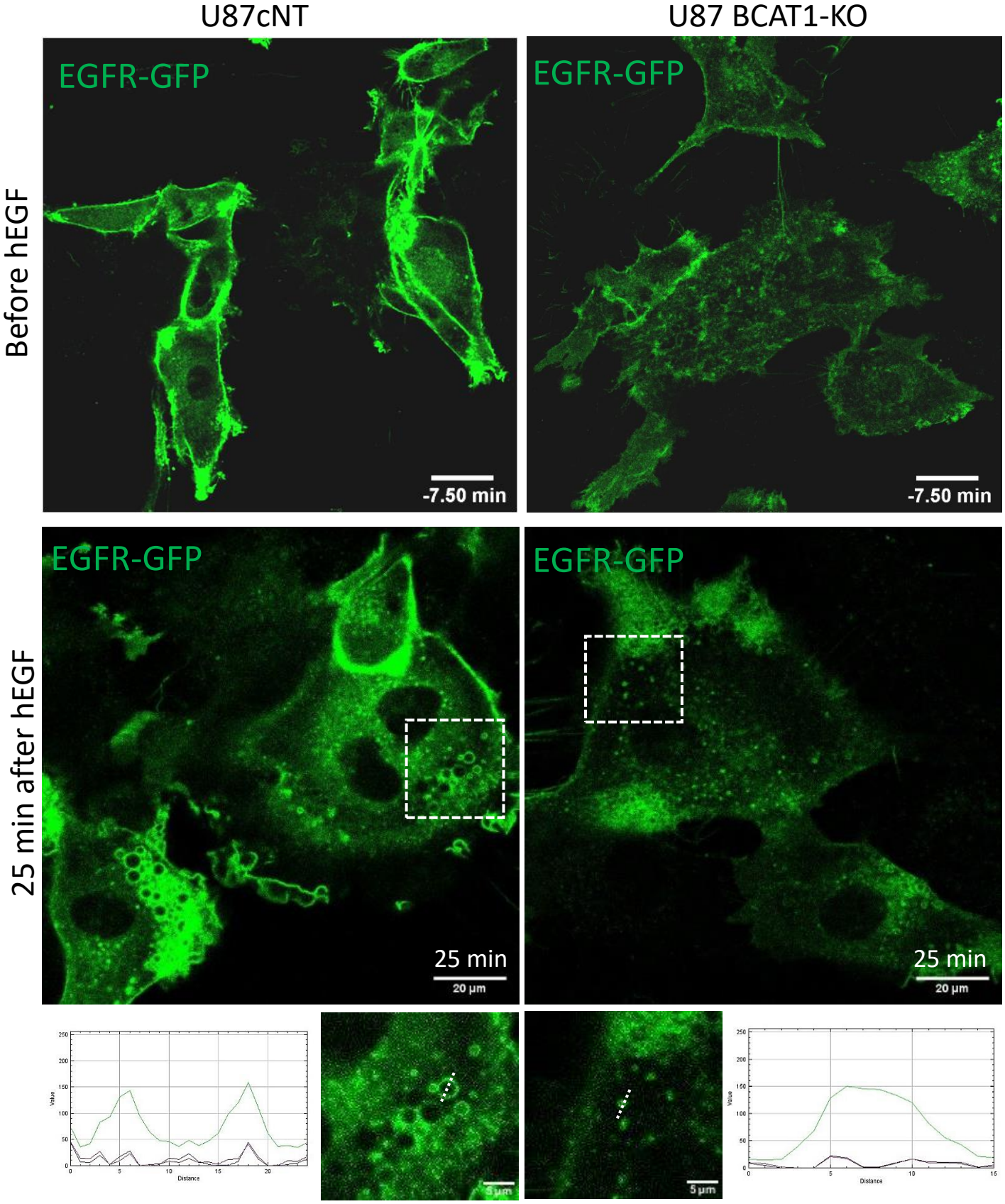
U87cNT
U87 BCAT1-KO
Before hEGF
25 min after hEGF
EGFR-GFP
EGFR-GFP
-7.50 min
-7.50 min
EGFR-GFP
EGFR-GFP
25 min
20 µm
25 min
20 µm
Value
Distance
5 µm
5 µm
Value
Distance

3.6. The non-canonical role of BCAT1 in glioblastoma

Thus far, research aiming to understand the role of BCAT1 in tumorigenesis focused exclusively on the metabolic function of BCAT1. Raffel et al., (2017) proposed that decreased α-KG levels, caused by high expression of BCAT1, affects the activity of α-KG and Fe (II) dependent enzymes. However, IP-MS data in the present study failed to identify BCAT1 binding partners that depend on α-KG. Furthermore, the cytoskeleton-dependent phenotypes observed after BCAT1-KO (see section 3.5) cannot be explained by changes in α-KG levels. We reasoned then that BCAT1 might contribute to tumorigenesis due to non-canonical functions.

Besides the transamination activity, another feature of BCAT1 is a CXXC motif near the active site (Figure 3 and section 1.1.2.). It has been suggested that these two thiols not only affect the transaminase activity of BCAT1 but can also mediate interactions with other redox-sensitive proteins (Conway *et al.*, 2008). More recently, affinity column pull-down assays were used to show that BCAT1 interacts in a redox-dependent manner with a number of cytoskeletal and cell cycle proteins (Hindy and Conway, 2019). Taken together, studies published by others and our own data (IP-MS and phenotypic), support the hypothesis that BCAT1 interacts with cytoskeleton and cell cycle proteins and might affect their function through redox regulation.

We thus aimed to determine whether the metabolic or redox activities of BCAT1 have functional relevance in redox associated phenotypes. To asses this, BCAT1 mutants were constructed and ectopically overexpressed in U251 BCAT1-KO cells. A metabolically dead mutant was created by mutating the lysine at position 222, the binding site of the Vitamin B_6 co-factor, to alanine ($BCAT1^{K222A}$)(Kingsbury, Sen and Cardenas, 2015). A redox-insensitive mutant was created by mutating the cysteines C335 and C338, which form the CXXC motif, to serines ($BCAT1^{SXXS}$). All BCAT1 variants were C-terminal FLAG-tagged and inserted into the pLVX-hygro vector for lentiviral transduction. Cyan fluorescent protein (CFP) instead of BCAT1 constructs were used as control.

3.6.1. BCAT1 has redox balancing functions

CXXC-motifs are conserved amongst oxidoreductases such as TRXs and GLRX. As their name implies, their function is to reduce oxidized proteins. Their activity helps to maintain the intracellular environment in a reduced state, necessary for cellular function (Groitl and Jakob, 2014).

To determine whether BCAT1 assist in balancing of ROS, we measured the response of U251cNT and U251 BCAT1-KO cells to exogenous H_2O_2. Intracellular levels of ROS were quantified with the fluorescent dye2',7'–dichlorofluorescin diacetate (DCFDA) which emits fluorescence upon oxidation. Under normal conditions, without H_2O_2 challenge, intracellular ROS increased steadily over the 25 minutes test period, with the rate of ROS production being lower in BCAT1-KO than in control cells (Figure 24A, Supplementary Figure S3). This difference in steady states probably is due to presumably lower mitochondrial ROS production in the slower proliferating U251 BCAT1-KO cells. The opposite trend was observed when cells were challenged by exogenous addition of H_2O_2. In U251 BCAT1-KO treated vs. untreated cells, DCFDA oxidation increased by ~ 8-fold with 100 µM H_2O_2 (Figure 24B) and ~ 10-fold with 500 µM H_2O_2 treatments (Figure 24C). In response to the same treatments, control U251cNT cells, displayed increases of only 4 to 5 fold, respectively (Figure 24B and C, blue line), indicating that control cells have a higher capacity for ROS buffering than BCAT1-KO cells.

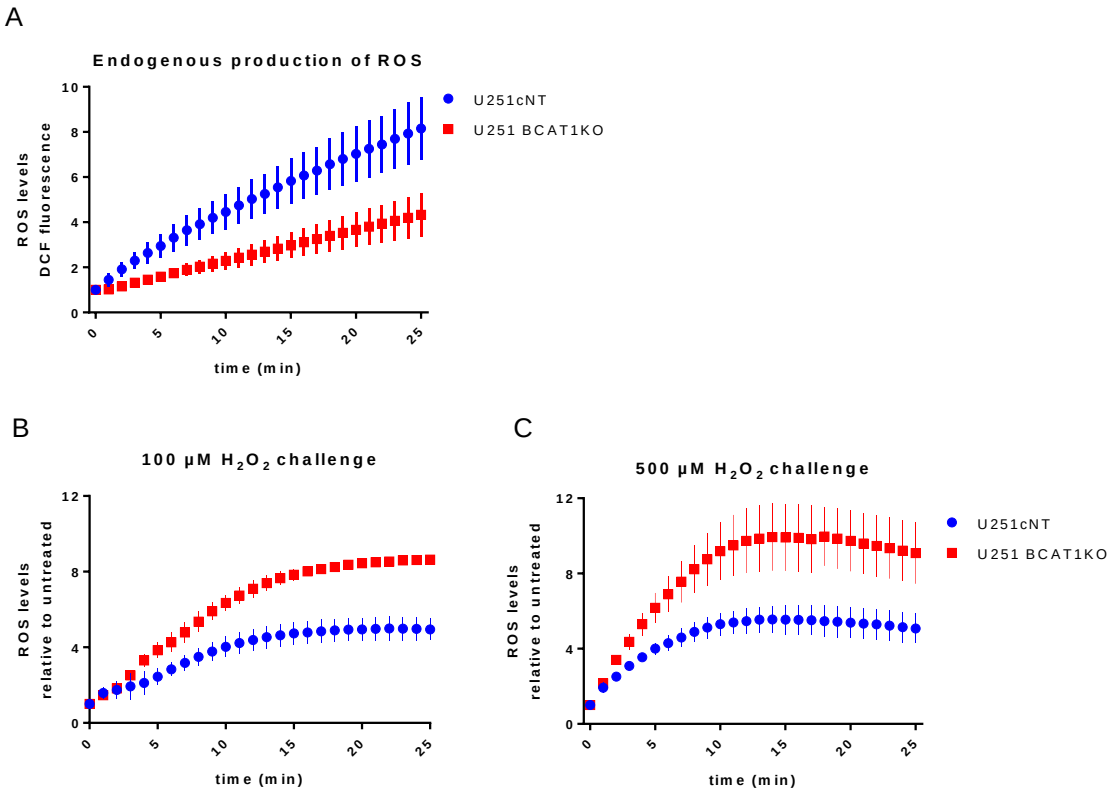

Figure 24. Intracellular ROS production in U251cNT and U251 BCAT1-KO cells. Oxidation of DCFDA was monitored before and after addition of H_2O_2 for a period of 25 minutes. After blank subtraction, change in ROS was calculated by dividing the emitted fluorescence at the time measured by the initial fluorescence (T0). A) endogenous ROS production. B) ROS production in response to H_2O_2 500 µM. Fluorescence intensity emitted by treated cells was normalized to the fluorescence of untreated cells. Data of 3 independent experiments (mean + s.e.m)

We next examined whether ROS buffering capacity was dependent on the CXXC motif. Towards this end, cells expressing the different BCAT1 mutants were challenged with H_2O_2 and intracellular ROS levels measured over a 30-minute period. Overexpression of $BCAT^{WT}$ and $BCAT1^{K222A}$ resulted in a partial rescue of ROS buffering capacities after H_2O_2 challenge. In contrast, H_2O_2 treatment of U251 BCAT1-KO cells expressing $BCAT1^{SXXS}$ resulted in the same high ROS levels as treatment of the BCAT1 depleted cells (Figure 25). These results show that the CXXC-motif of BCAT1 helps maintaining a balanced redox-state.

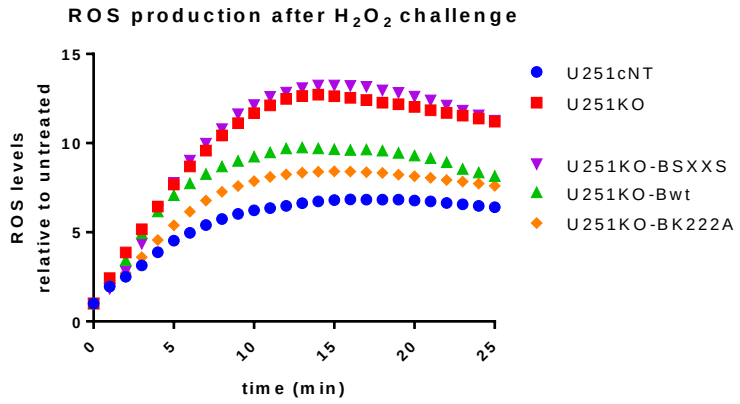

Figure 25. Intracellular ROS production of U251cNT and U251 BCAT1-KO rescued cells after treatment with 500 µM H_2O_2. Oxidation of DCFDA was monitored before and after addition of H_2O_2 for a period of 25 minutes. After blank subtraction, change in ROS was calculated by dividing the emitted fluorescence at the time measured by the initial fluorescence (T0). Fluorescence intensity emitted by treated cells was normalized to the fluorescence of untreated cells.

3.6.2. BCAT1-KO reduces sensitivity of EGFR to activation by H_2O_2

Consistent elevated ROS in cancer contributes to activation of signaling pathways that control proliferation, survival, migration, glucose metabolism and others (Liou and Storz, 2010). Carroll and co-workers, showed that EGFR contains a H_2O_2-sensitive C797 in the vicinity to the active-site (Thu Truong *et al.*, 2016). Upon EGF binding, EGFR dimerizes and activates nearby NOX, resulting in the production of intracellular H_2O_2. This local increase in H_2O_2, induces the oxidation of EGFR at C797 which results in a conformation change that brings the autophosphorylation sites (Y1068 and Y1086) of EGFR in close proximity. Autophosphorylation at these residues leads to full activation of EGFR and initiation of signaling cascades (Lladó *et al.*, 2008; Pike *et al.*, 2018).

To determine whether BCAT1 affects redox-induced EGFR signaling, U251cNT and U251 BCAT1-KO cells were treated for 5 minutes with H_2O_2 in the presence or absence of 4 ng/ml EGF. BCAT1 expressing cells, but not BCAT1-KO cells, showed a significant activation of pY1068 EGFR in response to 500 µM of H_2O_2 alone (Figure 26). In fact, H_2O_2 alone causes only a small increase in pY1068 EGFR levels in U251 BCAT1-KO. However, the addition of EGF was able to activate EGFR, suggesting that the receptor is still active and responsive to its ligand. We then determined whether pY1068 EGFR induced by H_2O_2 was able to activate downstream signaling

pathways. Since the EGFR-pathway kinases AKT and ERK can be activated by H_2O_2 independently of EGFR, we instead analyzed phosphorylation of PLC-γ, which is stimulated by ROS induced EGFR signaling (Bae *et al.*, 1997). Addition of 500 µM of H_2O_2, regardless of the presence or absence of EGF, induced a strong activation of PLC-γ (pY783) in U251cNT. Contrastingly, U251BCAT1-KO did not exhibit any pY783 PLC-γ under the tested conditions.

Similar responses to H_2O_2 were observed in the LN229 glioblastoma cell line. LN229cNT and BCAT1-KO were treated for 5 minutes with increasing concentrations of H_2O_2 (0-500 µM) in the absence of EGF. In line with the observed phenotype in U251, BCAT1 depleted LN229 cells exhibited reduced pY1068 EGFR activation in response to H_2O_2 (Figure 27).

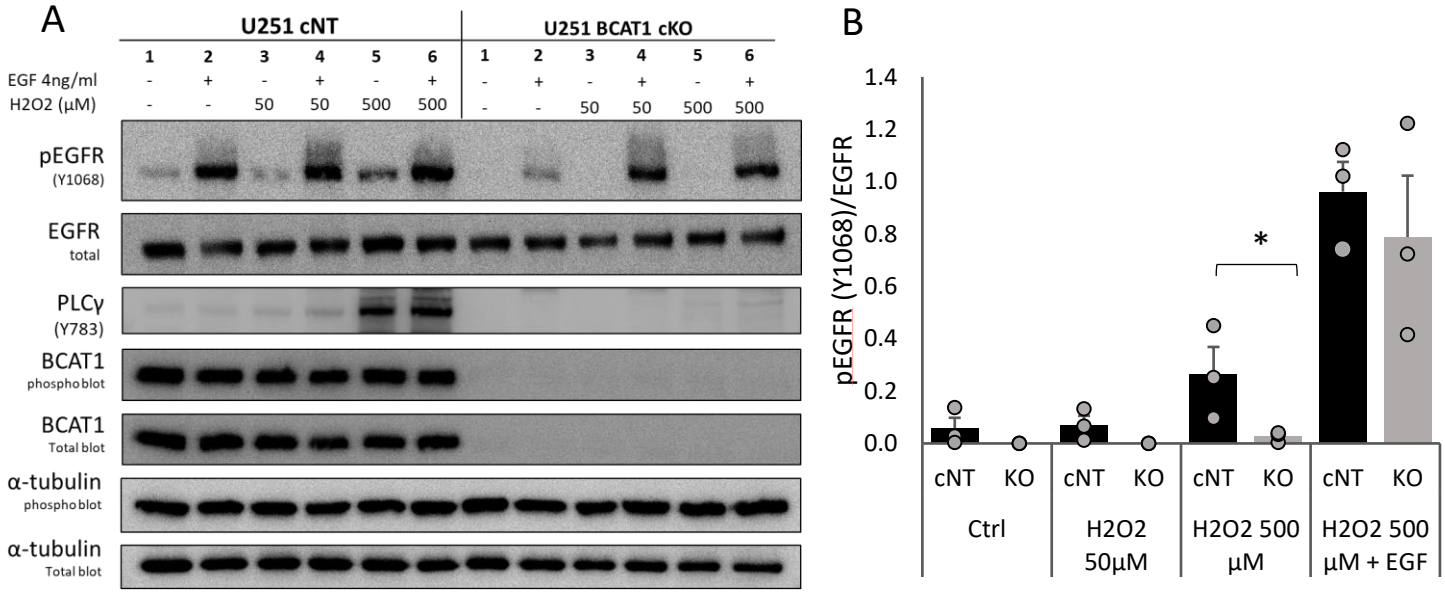

*Figure 26. Effects of BCAT1-KO on EGFR signaling induced by H_2O_2 in U251MG. Cells were starved for 16 h prior treatments with H_2O_2 (50 µM or 500 µM) in the presence or absence of EGF (4ng/ml). After 5 minutes, cells were washed once with ice cold PBS and lysed on ice. All solutions contained protease and phosphatase inhibitors. A) Western blot representative of 3 independent experiments. A) expression of pEGFR Y1068 relative to the total levels of EGFR (each first normalized to tubulin) mean of the densitometric quantification of 3 independent experiments. Error bars = s.e.m. * p<0.05 student's t-test.*

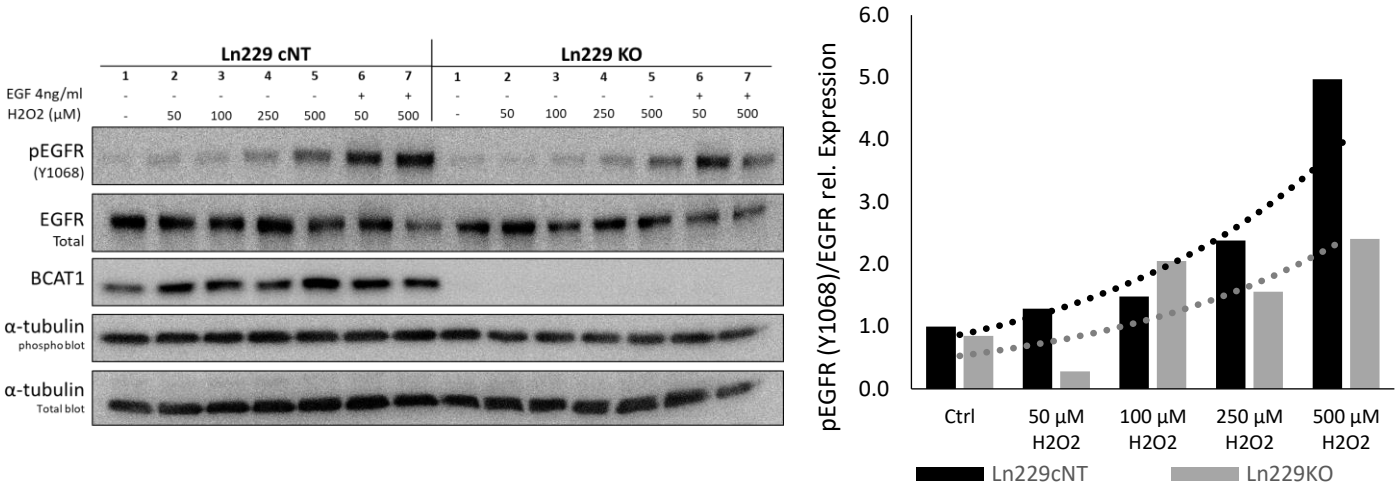

Figure 27. Effects of BCAT1-KO on EGFR signaling induced by H_2O_2 in LN229MG. Cells were starved for 16 h prior treatments with H_2O_2 in the presence or absence of EGF (4 ng/ml). After 5 minutes, cells were washed once with ice cold PBS and lysed on ice. All solutions contained protease and phosphatase inhibitors. Western blot and densitometric quantification of the expression of pEGFR Y1068 relative to the total levels of EGFR (each first normalized to tubulin). One experiment performed.

3.6.3. BCAT1 affects F-actin depolymerization

Actin dynamics are influenced via oxidation by H_2O_2 or through the activity of MICALs (DalleDonne, Milzani and Colombo, 1995; Hung, Pak and Terman, 2011). We therefore investigated whether BCAT1 could affect F-actin dynamics in a similar way. Towards this end, HA-tagged BCAT1 was overexpressed in 293FT cells and purified using α-HA-magnetic beads. Thereafter, purified HA-BCAT1 was used in an in vitro biochemical co-sedimentation assay with F-actin to confirm their interaction. This method uses high centrifugation speeds to separate non polymerized, monomeric actin (G-actin) from F-actin. Thus, G-actin is found in the supernatant and F-actin in the pellet. If a test protein interacts with F-actin, it precipitates together and occur in the pelleted fraction. Purified HA-BCAT1 was incubated with F-actin and subjected to centrifugation at high speed for one hour. A fraction of BCAT1 precipitated with F-actin, indicating that BCAT1 can bind to F-actin (Figure 28 A).

A variation of this method can be used to detect whether the test protein can affect F-actin bundling. This variation is based on the ability of F-actin to form bundles that precipitate at lower centrifugation speed (14 000 rpm). Under these conditions, BCAT1 affected F-actin bundling activity, as can be seen by a decreased in precipitated F-actin and an increased G-actin. This suggest that BCAT1 interferes with filament assembly or promotes F-actin disassembly (Figure 28B).

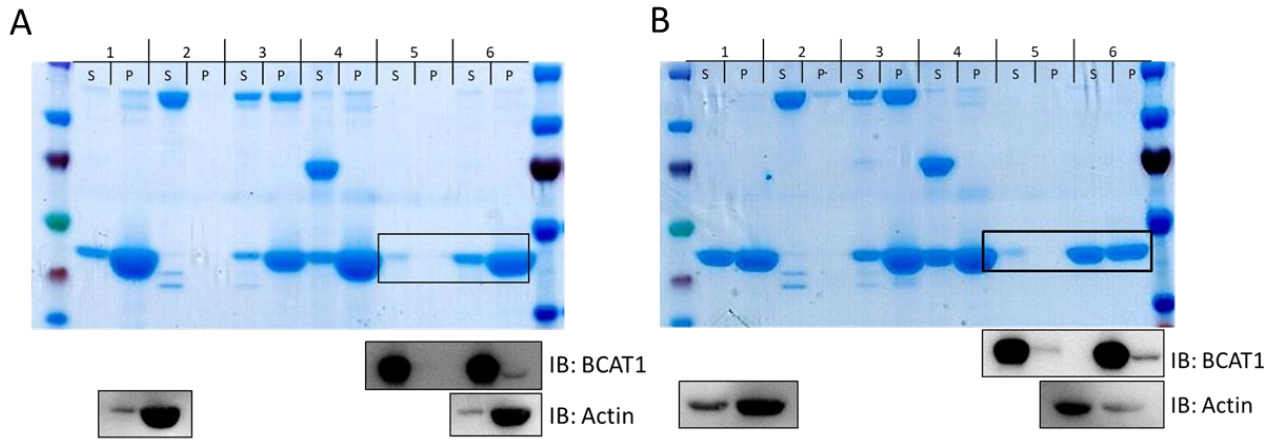

Figure 28. BCAT1 co-sediments with F-actin in an in vitro biochemical assay (cytoskeleton, Inc.) (A) „method 1". Purified HA-BCAT1 co-sediments with F-actin. (B) „method 3". Purified HA-BCAT1 affects bundling activity of F-actin. Lanes: 1) F-actin control (only), 2) α-actinin control (only), 3) α-actinin + F-actin „positive control", 4) BSA + F-actin „negative control" 5) HA-BCAT1 only, 6) HA-BCAT1 + F-actin. S= supernatant fraction, P= pellet fraction.

3.6.3.1. Effects of BCAT1 on actin dynamics is dependent on the CXXC-motif

In another attempt to understand how BCAT1 affects F-actin dynamics, a fluorometric assay, using pyrene-labeled actin (Pyr-actin) was performed. Pyr-actin is covalently linked at C347 to a pyrene group, which fluorescence is enhanced by its polymerization into filaments. The emitted florescence can be then measured with a plate reader and allow one to study the dynamics of actin assembly or disassembly under different experimental conditions. A first test determined that HA-BCAT1 had minimal effects on actin polymerization and had a stronger impact on F-actin depolymerization (supplementary Figure S3).

To determine whether the CXXC-motif of BCAT1 was playing a role on the dynamics of F-actin, polymerized Pyr-actin was incubated with HA-BCAT1^{WT}, HA-BCAT1^{SXXS} or HA-BCAT1^{K222A}. The ability of the mutants to induce F-actin depolymerization, was compared to the F-actin in the presence of 20 mM of H_2O_2, which oxidizes actin cysteines and induces F-actin depolymerization (DalleDonne, Milzani and Colombo, 1995). This showed that HA-BCAT1^{WT} induced depolymerization by a factor of 1.3. The catalytic mutant HA-BCAT1^{K222A} was found to have an intermediate effect (1.15-fold) on actin polymerization, while the redox mutant HA-BCAT1^{SXXS} did not cause any additional effect compared to F-actin treated with the solvent PBS only (Figure 29).

Altogether, these *in vitro* assays suggest that HA-BCAT1 interacts with F-actin and influences its dynamics. These results show that HA-BCAT1 induces depolymerization of F-actin, possibly by affecting its redox state, as suggested by the failure to induce depolymerization when the redox-center in mutated (HA-BCAT1^{SXXS}).

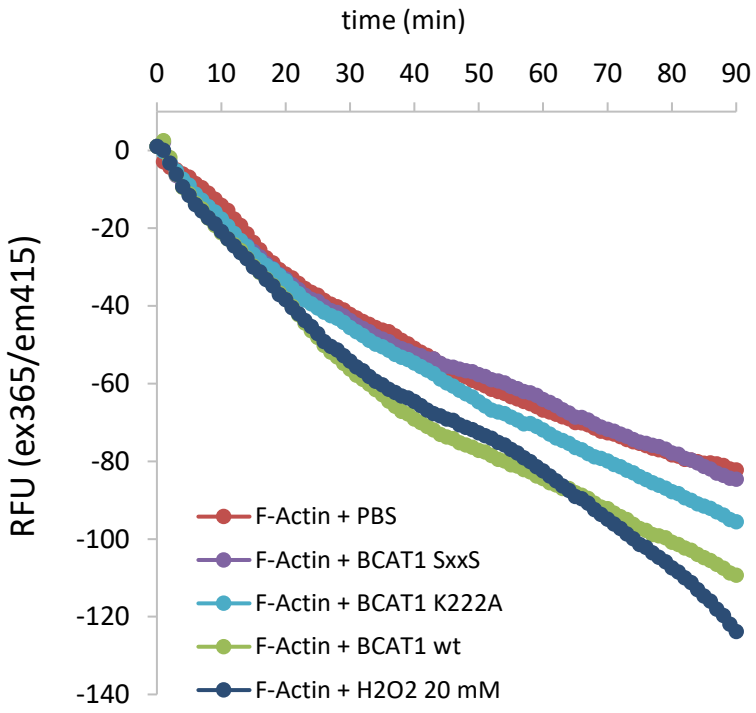

Figure 29. Effects of BCAT1 mutants on pyrene-labeled F-Actin depolymerization. 1.2 µM F-actin was allowed to depolymerize in the presence of 500 nM of HA-BCAT1 mutants, 20 mM of H_2O_2 or vehicle (PBS). Change in fluorescence at ex 365nm/em415-445nm was measured in a plate reader every 60 sec.

3.6.4. ROS induce the formation of BCAT1 high molecular weight aggregates.

Oxidation of redox-regulated proteins by ROS frequently induces the formation of disulfide bonds that affect the activity or function of proteins. Disulfide bonds can form between thiols of the same protein (intramolecular) or between thiols of two proteins (intermolecular).

In-vitro studies using recombinant BCAT1 purified from *E.coli* have shown that BCAT1 treated with H_2O_2 forms dimers that could be observed a slow-migrating band in non-reducing SDS-PAGE (Conway *et al.*, 2008). Whether BCAT1 can also form disulfide bonds in its native, cellular environment is not clear. Therefore, I treated U251 cells with increasing concentrations of H_2O_2 (0-500 µM) for 10 to 300 seconds and analyzed total cell protein by non-reducing SDS-PAGE. Treatment with 50 or 100 µM of H_2O_2 for only 2 minutes induced the formation of high molecular weight (HMW) bands > 100 KDa under non-reducing conditions (Figure 30A). To determine, whether the formation of HMW BCAT1 bands was mediated by the thiols forming the CXXC-motif or by C242, another solvent accessible cysteine (Conway *et al.*, 2008), LN229 BCAT1-KO cells overexpressing $BCAT^{WT}$ or single cysteine mutants (C242S, C335S, C338) as well as the SXXS mutant were treated with H_2O_2. Analysis by non-reducing SDS-PAGE showed that all mutants formed HMW in response to H_2O_2 (Figure 30B blot on the left). Addition of the reducing agent dithiothreitol (DTT) to the sample reverted this effect, indicating that these HMW species are thiol-disulfide bonded (Figure 30B blot on the right). These data suggest that intermolecular disulfide bond formation of BCAT1 does not require the tested cysteines or involves multiple cysteines that can substitute for one another. For solving the mechanism of BCAT1 intermolecular disulfide bonding, future extensive mutagenesis studies will be required.

From these experiments, we can conclude that BCAT1, like other redox-regulated proteins, can form intermolecular thiol-disulfide bonds, as evidenced by the appearance of HMW bands in non-reducing gels. Whether these are BCAT1 dimers or mixed-disulfide interactions with other proteins, remains to be determined.

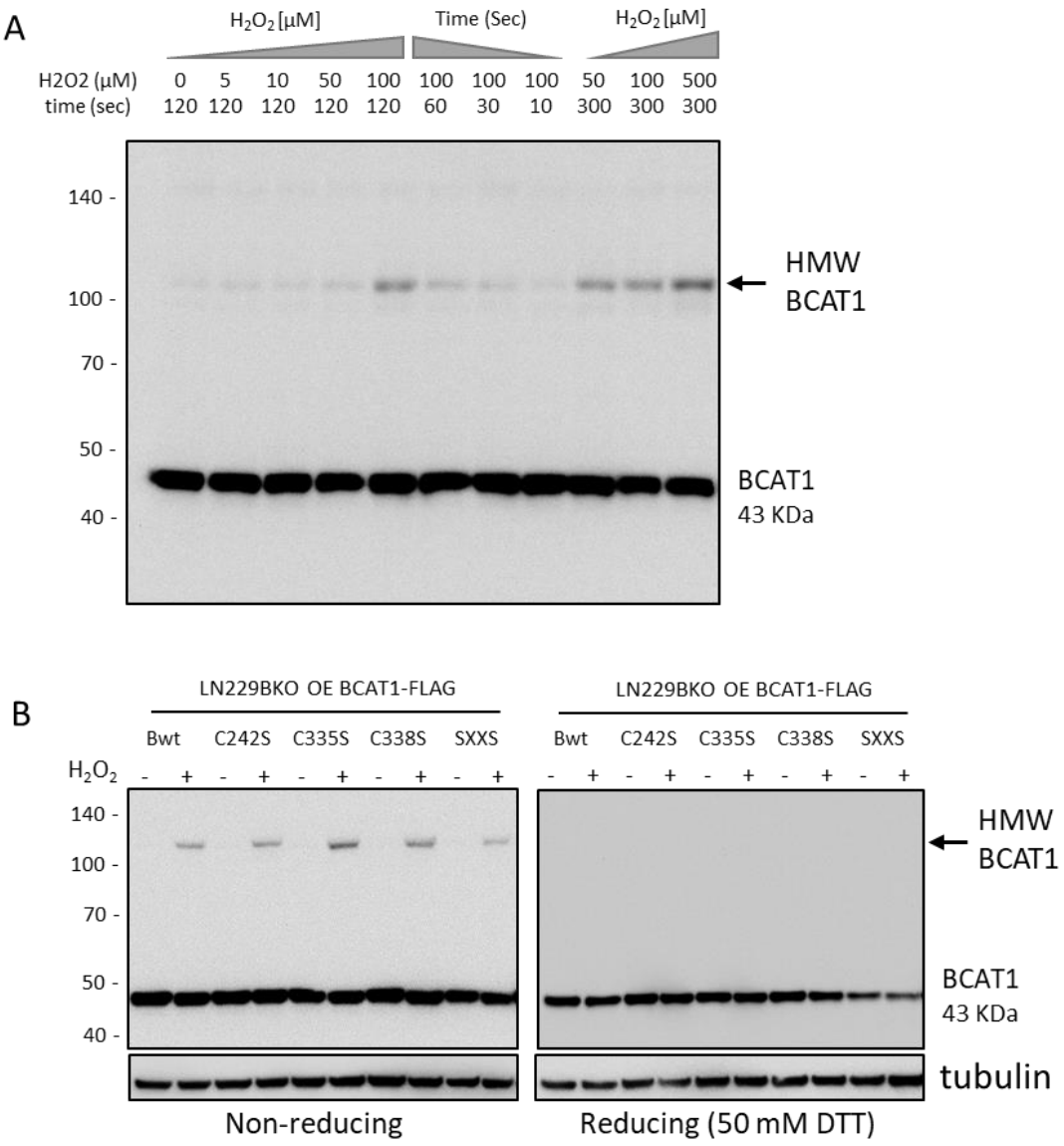

Figure 30. H_2O_2 induces the formation of BCAT1 high molecular weight species. A) U251MG cells were treated with H_2O_2 for the indicated concentrations and times. B) LN229 BCAT1-KO cells overexpressing (EO) BCAT1 mutants, treated with 100 µM of H_2O_2 for 3 minutes. In all experiments, free thiols were blocked with NEM (100 mM in PBS) for 5 minutes on ice, followed by lysis (1% tritonX100, 10mM NEM). Cleared lysates were run on 4-12% SDS-PAGE gels under non-reducing or reducing (50 mM DTT) conditions.

3.6.5. BCAT1 is oxidized and forms mixed-disulfide intermediates in mitosis

The cellular redox environment varies throughout the cell cycle (Figure 31A). Cells go from a reduced state in G1, towards a high oxidative state during mitosis. After cell division, the reducing environment is restored in the daughter cells and the redox-cycle restarts (Sarsour *et al.*, 2009). Having shown that exogenous H_2O_2 can induce BCAT1 oligomerization in glioblastoma cells (section 3.6.4), we questioned whether endogenous increases of ROS could also cause this. Knowing that ROS levels are high in mitotic cells, we investigated whether BCAT1 becomes oxidized during mitosis. To test this, U251 cells were synchronized using double thymidine block or nocodazole and harvested at different cell cycle phases. Analysis by non-reducing SDS-PAGE and immunoblot against BCAT1 showed the appearance of HMW bands as the cells progressed throughout the cell cycle and were more abundant in mitotic cells (Figure 31B). This suggests that endogenous ROS produced during mitosis induces BCAT1 oxidation and formation of mixed-disulfide intermediates.

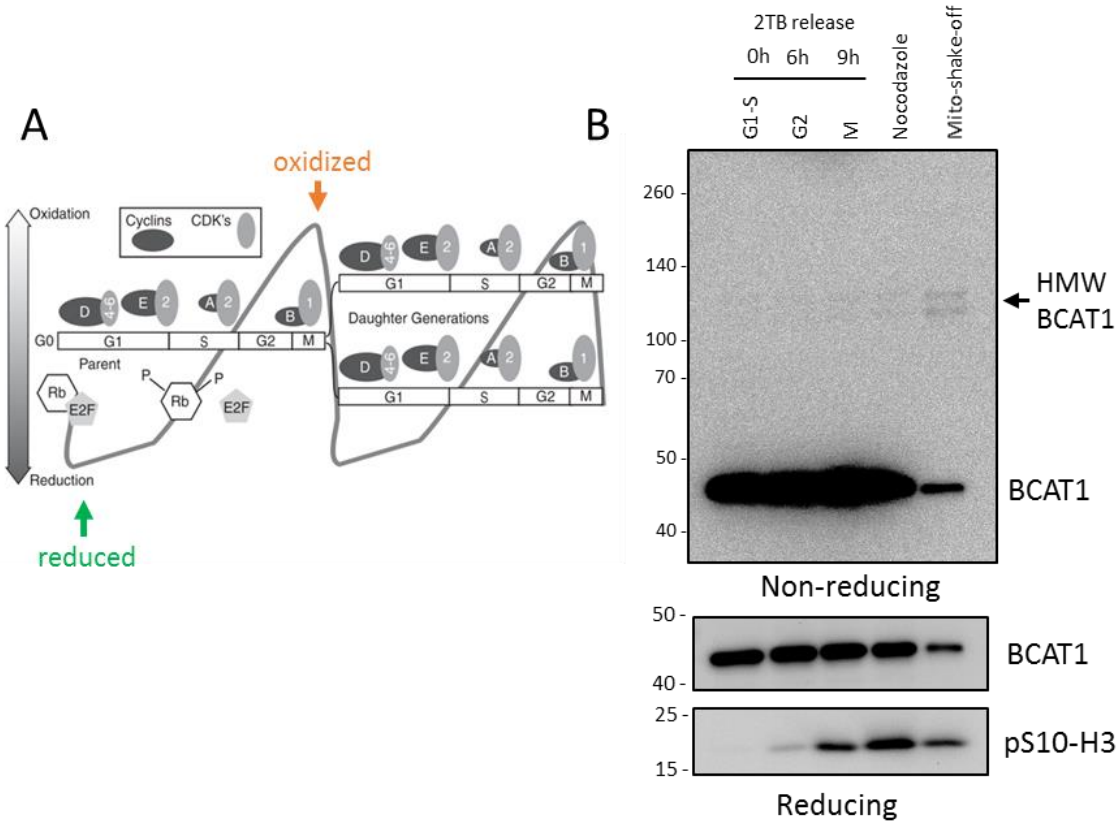

Figure 31. (previous page) Oxidative environment during mitosis promotes the formation of BCAT1 mixed-disulfides. A) variations in the redox environment during the cell cycle. Adapted from Sarsour et al, 2009. B) Oxidation of BCAT1 in the cell cycle. U251MG were synchronized using double thymidine block (2TB) to enrich for G1/S cells or G2 and Mitosis (M) after releasing for 6 and 9 h, respectively. Alternatively, cells were synchronized at mitosis using nocodazole and shacked-off to enrich for mitotic cells (mito-shake-off). Prior to harvesting and lysis, free thiols were blocked using 10 mM NEM in PBS for 5 min on ice to prevent loss of mixed-disulfide bonds.

3.7. BCAT1 depletion causes cytokinesis failures

Normal cytoskeleton function is required for mitosis progression and cytokinesis (Woolner *et al.*, 2008; De Wever *et al.*, 2014; Frémont, Hammich, *et al.*, 2017; Gerien and Wu, 2018). Distribution of the chromosomes into the two daughter cells relies on the coordinated function of microtubules and accessory proteins that form the mitotic spindle (Jens Lüders, 2016). Once the sister chromatids have been efficiently separated to the opposite poles of the dividing cells, the cleavage furrow starts to form, initiating the separation of the plasma membrane into two (Pollard and O'Shaughnessy, 2019).

Having shown that BCAT1 localizes at cytoskeleton structures during cell division (see section 3.4), interacts and affects the F-actin dynamics (section 0), and BCAT1KO cause a G2/M arrest (Figure 19), we questioned whether BCAT1 affects mitosis and/or cytokinesis. To assess this, we performed live-cell imaging on U251cNT and U251 BCAT1-KO cells undergoing cell division. Time-lapse imaging revealed that about 50 % of BCAT1-KO cells had mitotic failures. On the other hand, more than 80% of the BCAT1 expressing cells divided properly. A live-cell dye specific for F-actin (SiR-actin) and tubulin (SiR-tubulin) revealed that BCAT1-KO cells were incapable to form a functional mitotic spindle (Figure 32, top panels), and could not accomplish adequate separation of the sister chromatids (Figure 33, lower panels). The cleavage furrow was therefore unable to form, which ultimately lead to incomplete abscission in ~ 50 % of BCAT1-KO cells. In line with abnormal cytokinesis of BCAT1-KO cells, we observed a higher percentage of cells presenting aneuploidies in BCAT1-KO than in control cells (Figure 33). Live-cell imaging and analysis was performed by Dr. Matthias Plessner of the group of Prof. Dr. Robert Grosse (University of Freiburg) on a collaborative basis.

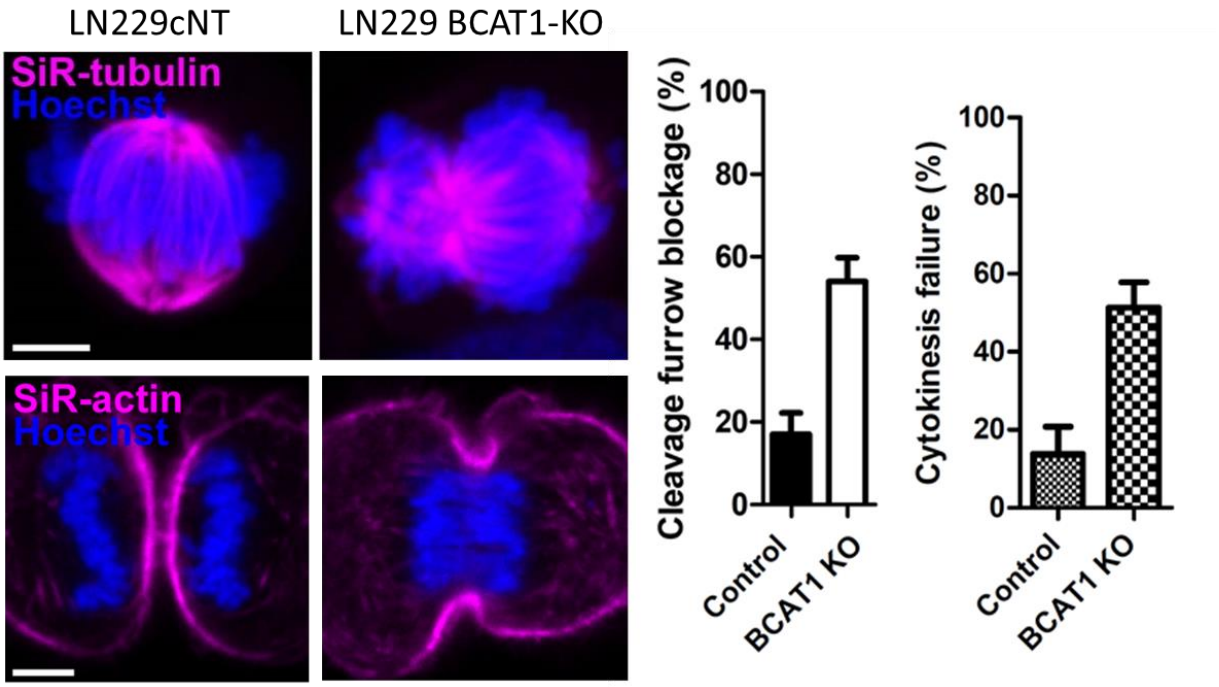

Figure 32. BCAT1-KO glioblastoma cells exhibit mitotic failure. Glioblastoma cells (U251 or Ln229) were synchronized in mitosis using nocodazole. After release from nocodazole, cells stained with the live-cell dyes SiR-actin or SiR-tubulin were imaged. The percentage of cells exhibiting cleavage furrow blockage and cytokinesis failure was quantified. Data generated by Dr. Matthias Plessner, Robert Grosse's group (University of Freiburg).

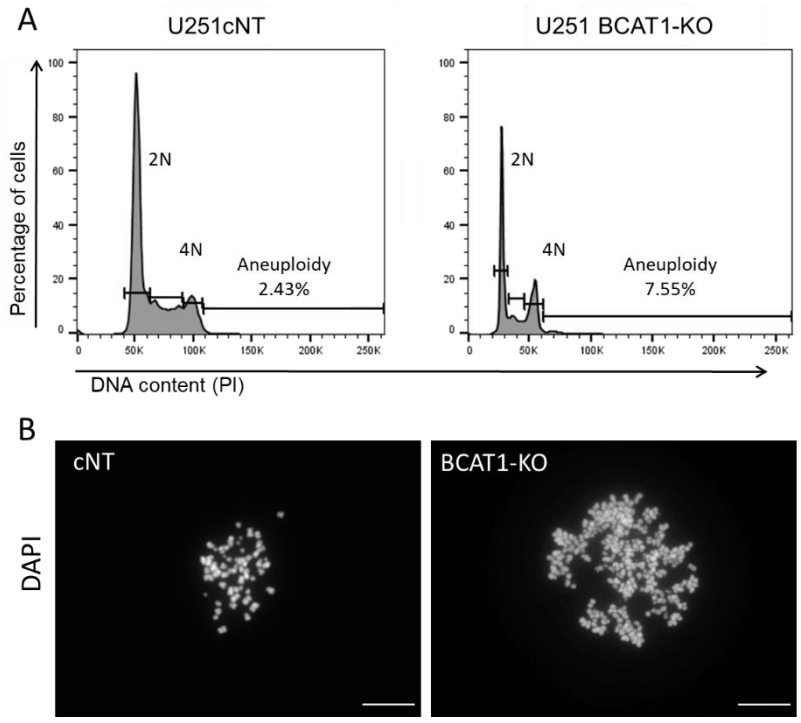

Figure 33. BCAT1 depletion causes aneuploidy of glioblastoma cells. A) cell cycle analysis of unsynchronized cells using propidium iodide (PI) showing the percentage of cells at each cell cycle phase and presenting aneuploidy B) Metaphase spreads of LN229 cells arrested at metaphase using 50 ng/ml of nocodazole for 24 h (performed with the help of Dr. Manasi Ratnaparkhe).

3.7.1. BCAT1 interacts with tubulin in mitotic cells

The mitotic spindle, constituted of microtubules, is essential for the separation of the chromosomes during cell division. Prolonged and/or failed mitosis is frequently related to abnormal mitotic spindle function (Gadde and Heald, 2004).

In our IP-MS analysis (section 3.3), we identified tubulins (TUBA1A and TUBGCP2) and microtubule binding proteins, as well as a great number of cell cycle regulators including AURKA, CDK1 and CDC20, key players of the spindle assembly and check point control (see section 3.3, Table 1, Supplementary tables S1, S2). We also showed that BCAT1 co-localizes with AURKA at the mitotic spindle and is present at other cytoskeletal-rich structures during mitosis (see section 3.4.1, Figure 15, Figure 16). Furthermore, we have observed that BCAT1-KO cause severe impairments of the mitotic spindle function and cause mitotic failures. All together, these results suggest a close association of BCAT1 with the mitotic machinery. Aiming to understand more about the mechanism by which BCAT1 induces mitotic failure in glioblastoma cells, we investigated the direct association of BCAT1 and tubulin in cells undergoing mitosis. To approach this, cells were arrested in mitosis and subjected to co-immunoprecipitation (co-IP) using anti-FLAG beads or an antibody against α-tubulin (supplementary Figure S4). Co-IP confirmed the direct interaction of BCAT1 and tubulin in mitotic cells (Figure 34). We also attempted to determine if the CXXC-motif of BCAT1 directly participates in thiol-disulfide interactions with tubulin. If this was the case, mutation of the CXXC-motif (SXXS) would decrease or impair the interaction between BCAT1 and tubulin. As can be observed in Figure 34, the mutant $BCAT1^{SXXS}$ also co-immunoprecipitated with tubulin, suggesting that these cysteines are not the main residues participating in the interaction between BCAT1 and tubulin.

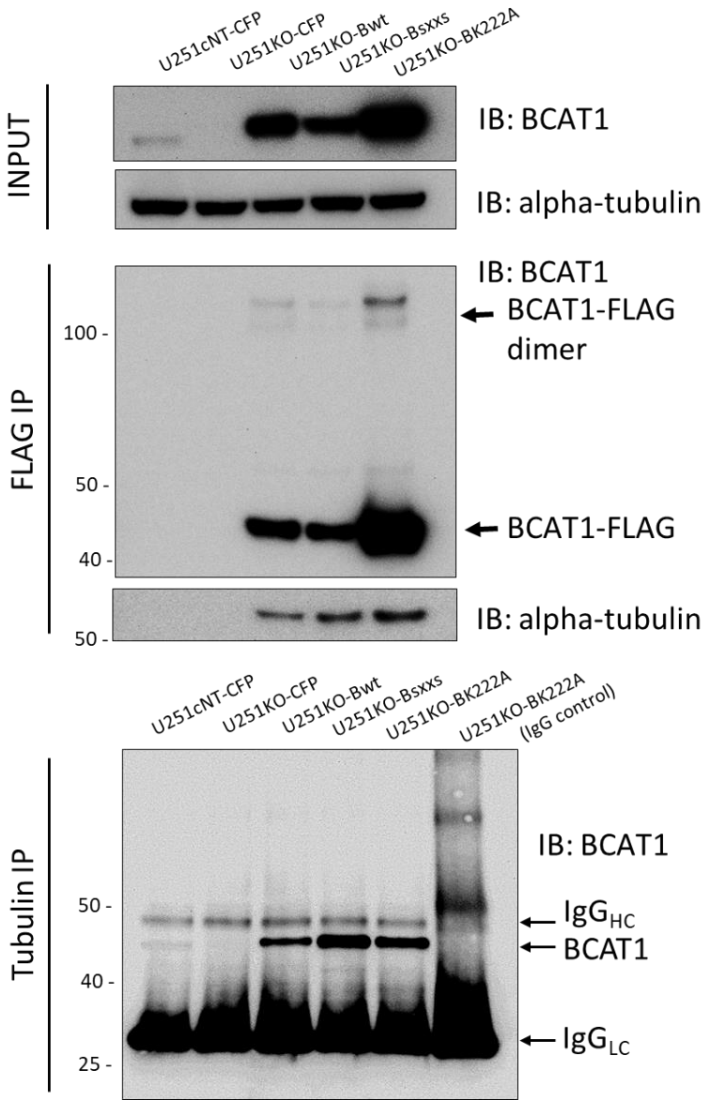

Figure 34. BCAT1 and tubulin Co-IP in LN229 cells arrested in mitosis. LN229 overexpressing CFP-FLAG or BCAT1-FLAG mutants were harvested by mitotic shake-off, followed by blockage of free thiols using 100 mM of NEM in PBS for 5 min on ice. After lysis and clearing, 300 µg of protein was used to pulldown using anti-FLAG magnetic beads or anti-tubulin antibody (TUBA4A). Eluted complexes were subjected to non-reducing SDS-PAGE and immunoblotting. The blots showed here are representative of 3 independent experiments performed in LN229 and U251 cell lines with comparable results.

3.8. Redox-dead BCAT1 mutant fails to rescue proliferation of glioblastoma cells

So far, I provided evidence that BCAT1 affects cytoskeleton dynamics and has an essential role during cytokinesis. However, whether this is dependent on its catalytic or redox function is still unclear.

The contribution of the redox and metabolic activity to cell proliferation was determined with the Click-iT® EdU cell proliferation assay. U251 BCAT1-KO cells were rescued by overexpression (OE) of either $BCAT1^{WT}$ or the metabolic mutant $BCAT1^{K222A}$, which showed ~ 18 % higher proliferation rates than U251 BCAT1-KO control cells (Figure 35). On the other hand, overexpression of the redox mutant $BCAT1^{SXXS}$ did not increase cell proliferation. These results show that overexpression of $BCAT1^{WT}$ and $BCAT1^{K222A}$, but not $BCAT1^{SXXS}$, can partially rescue the proliferation of BCAT1 deficient cells when compared to U251cNT cells. These results also suggest that the CXXC-motif, the center of the redox activity of BCAT1, plays a more important role in proliferation than the metabolic activity of the enzyme.

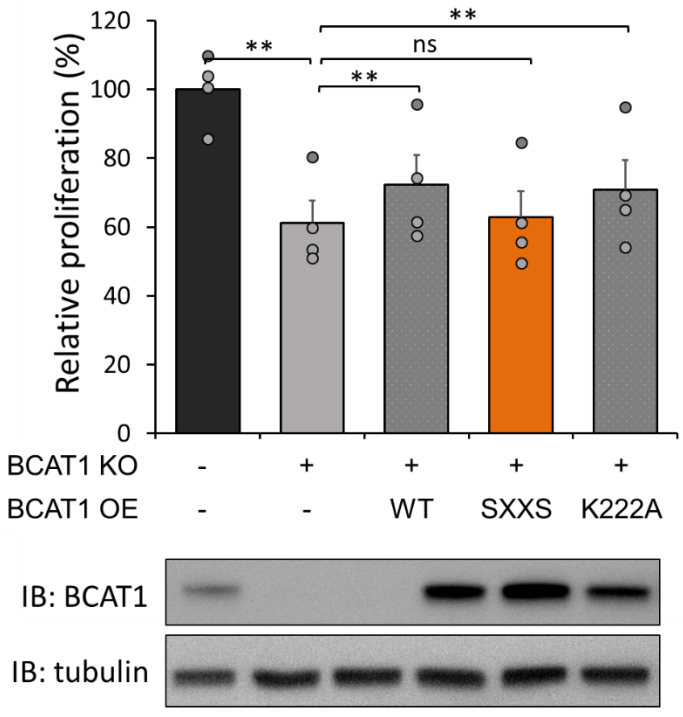

*Figure 35. Click-iT EdU incorporation proliferation assay in U251cNT and BCAT1-KO after depletion of BCAT1 and rescue with BCAT1 mutants. U251cNT and U251 BCAT1-KO overexpressing (OE) control plasmid (-) or BCAT1 mutants (WT, SXXS, K222A) were incubated with 10 nM EdU for 6-8 hr. EdU incorporation was determined using the Click-iT assay. Four independent experiments were performed. **p<0.01 paired Student's t test. Bars = Mean ± S.E.M.*

4. Discussion

Since its first identification as a potential oncogenic driver in glioblastoma (Tönjes *et al.*, 2013) and nasopharyngeal carcinoma (Zhou *et al.*, 2013), BCAT1 has been shown to be essential for cell proliferation in several more cancer entities (Tönjes *et al.*, 2013; Wang *et al.*, 2015a; Mayers *et al.*, 2016; Zheng *et al.*, 2016; Raffel *et al.*, 2017; Thewes *et al.*, 2017). Different hypotheses for the tumor-promoting BCAT1 mode of action have been proposed, implicating BCAT1 transaminase function and either increased BCAA or reduced α-KG levels as the key events.

With this thesis, I aimed to contribute to the understanding of the mode of action of BCAT1 in glioblastoma. The results that I obtained suggest that BCAT1, in addition to its canonical metabolic function, has a non-metabolic mode of action in glioblastoma. In this context, I uncovered novel information regarding the subcellular localization of BCAT1 and potential interaction partners. Furthermore, I showed functional evidence supporting a novel redox function of BCAT1 that appears to play a role in cell signaling and cell division events. Such alternative functions of a protein that often depend on different interaction partners, subcellular localizations, and post-translational modifications are also referred to as "moonlighting" functions (Jeffery, 1999).

4.1. FRET sensors to study live-cell fluctuations of α-KG

At the time this project started, FRET-based sensors for other metabolites such as lactate, pyruvate and glucose were increasingly being developed and employed by many groups, revolutionizing the way of studying metabolism. Compared to biochemical methods, genetically encoded FRET sensors provide spatial and temporal resolution to study metabolites in living systems (Fehr *et al.*, 2003; Hou *et al.*, 2011; San Martín *et al.*, 2013). Accordingly, this technology was utilized to generate an α-KG specific FRET sensor that enabled measurements of live-time fluctuations of cytoplasmic α-KG in a variety of cells (Lüddecke and Francois, *Sci Rep*, 2017). However, when using our FRET sensor to study α-KG levels in the nucleus, several

limitations of this technology became apparent. The sensor we developed was unable to detect small localized fluctuations of α-KG in the nucleus. The reasons for this remain unclear, however, technical limitations of FRET sensor technology could play a role. These include (1) the frequently small dynamic range, (2) a low signal-to-noise ratio due to autofluorescence, photobleaching and background noise, and (3) phototoxicity of the light source due to the high laser power necessary for excitation of fluorescent proteins.

To overcome these inherent problems of FRET-based sensors, metabolite sensors have been developed that use a single modified fluorescent protein (e.g. circular permutated) or bioluminescent proteins (Zhao *et al.*, 2015; Goyet *et al.*, 2016). The latter offer the advantage that no excitation laser is needed. However, bioluminescent reactions are typically slower than fluorescence reactions, thus limiting the detection of short fluctuations of the metabolite.

To further improve our α-KG sensor, I created a bioluminescence resonance energy transfer (BRET) sensor by combining the PII α-KG-binding protein with a NanoLuc® luciferase (Promega) donor and an acceptor fluorescent protein. Similar BRET sensors have been developed by others and used *in vitro* and *in vivo* (Bakayan *et al.*, 2011; DE *et al.*, 2013; Yang *et al.*, 2016; Arts, Aper and Merkx, 2017). My own construct generated a 10-times improved dynamic range compared to our original FRET sensor (Supplementary Figure S5). Using signal peptides for compartment targeting and different combinations of fluorescent proteins, these constructs could be used for multicolor imaging, enabling simultaneous measurements in different cellular compartments (Suzuki *et al.*, 2016). These improved sensors could be used in future studies to better understand the role of α-KG in different cellular compartments.

4.2. BCAT1 localization, interaction partners, and redox mechanism

It is widely accepted that a certain protein is not necessarily restricted to one cellular compartment (Jeffery, 1999, 2016; Min, Lee and Baek, 2016). Particularly in cancer, metabolic enzymes are often found taking part in nuclear functions affecting proliferation, apoptosis, migration, angiogenesis, and metabolism, which often vary between different types of tumors

(Luo *et al.*, 2011; Yang *et al.*, 2011; Yang, Xia, Hawke, Li, Liang, Xing, Aldape, Hunter, Alfred Yung, *et al.*, 2012; Yang, Zheng, *et al.*, 2012; Butera *et al.*, 2019). Glycolytic enzymes that localize to the nucleus have been found to perform functions that are not related to their canonical metabolic function. For example, under hypoxic conditions pyruvate kinase M1/2 (PKM) is hydroxylated at P403/408 by Egl-9 family hypoxia inducible factor 1 (EGLN1) and directly binds to activate transcriptional activity of HIF1A (Luo *et al.*, 2011). Others have shown that EGFR-induced PKM binds to β-catenin and is translocated as a complex to the nucleus. Nuclear PKM is required for the dissociation of histone deacetylase 3 from the promotors of cyclin D1 (*CCND1*) and the *MYC* proto-oncogene, and for the phosphorylation of T11 of histone H3, which results in the activation of *CCND1* and *MYC* transcription (Yang, Xia, Hawke, Li, Liang, Xing, Aldape, Hunter, Alfred Yung, *et al.*, 2012).

In this thesis, I show that BCAT1 is distributed in the cytoplasm and also localizes to the nucleus of glioblastoma cells. This finding, although unexpected, seemed consistent with the concept of BCAT1 limiting α-KG concentrations and thus the activities of α-KG dependent chromatin modifier enzymes such as the TET DNA demethylases and lysine demethylases (KDMs). Our group recently provided evidence in support of this hypothesis by showing that α-KG depletion, due to BCAT1 overexpression, can result in DNA-hypermethylation in AML cells (Raffel *et al.*, 2017). However, the immunoprecipitation (IP) and mass spectroscopy (MS) experiments of glioblastoma cell nuclear fractions reported here did not identify any proteins with α-KG-related functions as potential BCAT1 binding partners. These data suggest that BCAT1 has additional, non-metabolic functions in the nucleus of glioblastoma cells.

Ingenuity Pathway Analysis (IPA) of the IP/MS data showed an enrichment of proteins in the categories of cell cycle control, cellular assembly and organization, and clathrin-mediated endocytosis signaling. The experimental approach I employed depended on antibody-based IP of native BCAT1 protein from cell lysates (rather than overexpressed or tagged). This method permitted the detection of endogenous BCAT1-complexes and naturally occurring protein interactions in the cells. Of note, interactions with some of the proteins I identified were also described in recent work of Myra Conway focusing on the role of BCAT1 in Alzheimer's disease (Conway *et al.*, 2008; Hindy and Conway, 2019). In these studies, BCAT1 interaction partners

were identified by using trapping approaches consisting of affinity columns loaded with immobilized recombinant human BCAT1 generated in *E. Coli*. The overlapping findings of these independent studies provide strong support for the association of BCAT1 with elements of the cytoskeleton and the cell cycle. Furthermore, this suggests possible common mechanisms by which BCAT1 contributes to the development of glioblastoma and Alzheimer's disease. In both pathologies, dysregulation of BCAA metabolism and oxidative stress plays an important role in the disease development and progression (Galeffi and Turner, 2012; El Hindy *et al.*, 2014; Hull and Patel, 2015; Salazar-Ramiro *et al.*, 2016).

When the crystal structures of BCAT1 and BCAT2 were resolved, it was shown that both enzymes are susceptible to oxidation by air and by oxidants in solution (Yennawar *et al.*, 2001; Goto *et al.*, 2005). A conserved redox-sensitive CXXC-motif near the active-site cavity was initially shown to act as a redox-switch that regulates the catalytic activities of the enzyme (Conway *et al.*, 2002). It was later shown that CXXC-motif was implicated in the interaction of BCAT2 and the E1 decarboxylase subunit of the branched-chain α-keto acid dehydrogenase enzyme, which interaction was shown to be dependent on the redox status of the CXXC-motif (Islam *et al.*, 2010). So far, the redox-related functions of BCAT1 have been studied using purified proteins, and to a limited extent, in the context of neurodegenerative diseases. Despite these limitations, these biochemical studies have contributed to our understanding of how BCAT1 responds to different oxidants, and have drawn our attention to the similarities of BCAT1 and other CXXC possessing oxidoreductases, i.e. thioredoxins (TRX) and glutaredoxins (GLRX) (Conway *et al.*, 2008; Coles, Hancock and Conway, 2012; El Hindy *et al.*, 2014). Therefore, in my doctoral work, I aimed to extend the study of BCAT1 redox-functions of BCAT1 in cancer using mostly cell-based assays.

ROS are naturally produced as a byproduct of metabolism and regulate multiple signaling pathways by reversible modification of key cysteines of target proteins. Cancer cells exhibit high ROS production, which contributes to activation of signaling pathways that promote proliferation, migration and survival (Liou and Storz, 2010). Here, I showed that under normal conditions glioblastoma cells generates high amounts of ROS, presumably since their metabolism is altered to promote fast proliferation. Consequently, ROS production was

reduced in BCAT1-KO cells which have a lower proliferative rate. Moreover, I showed that BCAT1 helped maintaining redox homeostasis after a H_2O_2 challenge and that this function was dependent on its CXXC-motif. This suggests that BCAT1, might have antioxidant functions similar to TRX and GLRX, which catalyze the reduction of proteins via formation of thiol disulfide exchange reactions through their CXXC-motif (Coles, Hancock and Conway, 2012; El Hindy *et al.*, 2014). Upregulation of these antioxidant systems and of peroxiredoxins (PRDX) is a strategy of cancer cells to prevent damage of biomolecules caused by sustained oxidative stress (DeNicola *et al.*, 2011).

ROS and oxidative stress can also impact chromatin state and gene expression in multiple ways. Many chromatin remodeling proteins and transcription factors are regulated by oxidation at sensitive cysteines affecting their translocation to the nucleus or binding affinity to the DNA (Kreuz and Fischle, 2016). Histones and DNA themselves are subjected to modification by oxidants, which directly impact chromatin structure and genomic stability. The most common lesion associated with DNA damage is 8-oxoguanine, which preferentially occurs at guanines and is repaired by base excision repair (Kreuz and Fischle, 2016). In a recent study, overexpression of BCAT1 in lung cancer cells was shown to prevent DNA damage and confer resistance to EGFR tyrosine kinase inhibitors (TKI). It was proposed that the glutamate produced by metabolic activity of BCAT1, is converted by glutamate-cysteine ligase to glutathione (GSH). Thus, BCAT1-derived GSH would protect against ROS-induced DNA damage and prevent apoptosis of lung cancer cells treated with EGFR TKI (Wang *et al.*, 2019). The data presented in this thesis suggests that BCAT1-dependent maintenance of cellular redox homeostasis could also depend on the redox-active CXXC-motif of BCAT1 rather than on its catalytic transaminase function. This alternative explanation of the correlation of BCAT1 expression and TKI resistance should be further evaluated.

4.3. BCAT1 affects cytoskeleton-related processes in glioblastoma cells

The cytoskeleton is an elaborate network of filaments that plays a crucial role in most cellular processes. Cancer cells implement ways to enhance cytoskeleton remodeling to promote changes in cell growth, cell polarity, movement and invasiveness, among other. This perspective is supported by the large number of cytoskeleton-accessory proteins that are implicated in cancer (Brodsky *et al.*, 2015; Yang and Lin, 2018). For example, overexpression of ARP2/3 is associated with increased tumor growth, invasion and metastasis in colorectal gastric and hepatocellular carcinomas (Zheng *et al.*, no date; Iwaya *et al.*, 2007; Yang *et al.*, 2013). Additionally, proteins not described before as cytoskeleton-associated, have been discovered do so in cancer. For example, the glycolytic enzyme phosphoglycerate mutase 1 (PGAM1) has been shown to interact with actin (ACTA2) and ACRP2/3 to promote cell migration and metastatic potential of breast cancer cells *in vitro* and *in vivo* (Zhang *et al.*, 2017).

Clinical data analyses have shown an association of high BCAT1 expression and metastasis in patients of hepatocellular carcinoma, ovarian and colorectal cancer (Yoshikawa *et al.*, 2006; Wang *et al.*, 2015b; Xu *et al.*, 2016). Furthermore, BCAT1 knockdown impairs migration and invasion of different types of cancer cells including glioblastoma and breast carcinoma (Tönjes *et al.*, 2013; Thewes *et al.*, 2017). Despite the increasing evidence of BCAT1 conferring motility to cancer cells, not much is known about the underlying mechanism. In the present study, I found that BCAT1 localizes at cytoskeleton structures and binds to multiple accessory components, which suggests that BCAT1 directly interacts and affects the dynamic properties of the cytoskeleton. Functionally, I not only showed that BCAT1 is required for migration of glioblastoma cells but might also play a role during other active processes such as endocytosis and cell division.

Clathrin-mediated endocytosis is the preferred route for inactivation and degradation of EGFR and other receptor tyrosine kinases (RTKs). The process of endocytosis is tightly linked to the cytoskeleton and is regulated by a variety of elements that mediate the recognition of the cargo and formation of coated vesicles (Kaksonen, Toret and Drubin, 2006; Bezanilla *et al.*, 2015). Dysregulation of these regulatory elements in cancer contributes to sustained RTK signaling and

tumorigenesis (Mosesson, Mills and Yarden, 2008). For example, the huntingtin interacting protein 1 (HIP1), which is involved in connecting clathrin coats to actin filaments, is often dysregulated in cancer affecting EGFR endocytosis and degradation. HIP1 overexpression is correlated with high EGFR expression and poor prognosis in several cancer entities, including breast cancer and glioblastoma (S. V Bradley *et al.*, 2007; S. V. Bradley *et al.*, 2007; Li *et al.*, 2017).

The results presented here, showed that BCAT1 depletion causes abnormalities in phenotypes associated to endocytosis of EGFR. On the first place, BCAT1-KO cells did not show the characteristic remodeling of actin bundles at the cell membrane when stimulated with the EGFR ligand EGF. Actin nucleation at sites of endocytosis invaginations is mainly coordinated by the activities of myosin (MYO1E) and the ACRP2/3 complex that recognize and bind clathrin-coated pits (Kaksonen, Toret and Drubin, 2006; Cheng, Grassart and Drubin, 2012). This is preceded by the assembly of the clathrin coats at the cell membrane, which is assisted by the adaptor protein (AP2) (Kelly *et al.*, 2014). Secondly, BCAT1-KO cells failed to induce re-localization of EGFR from the periphery to the perinuclear compartment. Active movement of trafficking vesicles along microtubules is enabled by kinesins (Sorkin and von Zastrow, 2009; Anitei and Hoflack, 2012). Many of these mentioned accessory proteins were found as candidate binding partners of BCAT1 (Supplementary table S3), suggesting that BCAT1 participates in protein complexes that coordinate the organization of the cytoskeleton during endocytosis. Additionally, I found that the morphology of the endocytic vesicles largely differed between control cells and BCAT1 depleted cells. Interestingly, in control cells, EGFR appeared to be distributed at the surface of the endocytic vesicles. This could indicate that the active receptor could still be exposed to the cytoplasm and thus be able to continuously transmit its signal to downstream effectors. Whether EGFR was active in these large vesicles was not determined in the present study, but could be investigated by immunofluorescence against the active phospho-EGFR and quantification of vesicles exhibiting phospho-EGFR in BCAT1-KO and to control cells (Campion *et al.*, 2018). Altogether, these results suggest that BCAT1 plays a role in clathrin-mediated endocytosis of EGFR. However, whether this mechanism contributes to sustained EGFR signaling in glioblastoma requires further investigations.

EGFR signaling is also affected by oxidation at a conserved cysteine (C797) near the ATP binding site of the catalytic domain of EGFR. H_2O_2-induced sulfenylation at C797 increases the kinase activity of EGFR, a mechanism that frequently contributes to the sustained activation of signaling pathways under conditions of prolonged oxidative stress (Truong and Carroll, 2013; Thu Truong *et al.*, 2016). Here I showed that BCAT1 can influence H_2O_2-dependent EGFR signaling. Control glioblastoma cells showed steady state active phosphorylated EGFR (pY1068-EGFR), even in the absence of its ligand, which could be expected considering the elevated levels of ROS that BCAT1 expressing cells exhibit. Interestingly, the presence of BCAT1 seemed necessary to enhance activation of pY1068-EGFR by exogenous H_2O_2. BCAT1 depletion, did not affect the responsiveness of EGFR to its ligand EGF, demonstrating that BCAT1 only affects the sensitivity of EGFR to H_2O_2. This last observation suggests that BCAT1 participates in redox signaling events.

Overall, I showed that BCAT1 plays a role in two important regulatory mechanisms of EGFR, endocytosis and redox signaling. This is of particular importance in glioblastoma since ~43 % of patients present *EGFR* gene amplification and many have *EGFR-VIII* mutations that lack the ligand binding domain and have constitutively active downstream signaling (Sturm, Bender, D. T. W. Jones, *et al.*, 2014). Most glioblastoma are resistant or respond poorly to available targeted therapies using small molecule kinase inhibitors (e.g. Gefitinib, Afatinib) or antibodies (e.g. Cetuximab) that block EGFR signaling (An *et al.*, 2018; Saleem *et al.*, 2019). Whether BCAT1 is associated to EGFR-therapy resistance in glioblastoma has not been studied. Thus, the data presented here should encourage us to address this important question.

4.4. BCAT1 plays an essential role in cell division of glioblastoma cells

One of the most interesting findings of the present thesis is that depletion of BCAT1 in glioblastoma cells causes mitotic failures. Mitosis is one of the most critical processes of living cells, in which a great number of proteins orchestrate the equal separation of genetic material into the daughter cells. The central structure mediating the separation of chromatids is the

mitotic spindle, which is mainly formed of microtubules. Here, I showed that BCAT1 localizes to the mitotic spindle along with AURKA, which have a key role in centrosome maturation and formation of a bipolar mitotic spindle (Willems *et al.*, 2018). I also showed by co-IP that BCAT1 and tubulin directly interact in mitotic cells. Furthermore, when BCAT1 was depleted, half of the cells failed to form a functional spindle. Thus, BCAT1-KO cells were unable to achieve separation of the sister chromatids, which physically blocked the contractile ring and eventually lead mitotic failure. Altogether, these data suggest that BCAT1 directly participates in the assembly of the mitotic spindle and thus is essential for proliferation of glioblastoma cells.

Fast dividing cells inherently rely on the function of the cytoskeleton to form the mitotic spindle and contractile ring. Many successful anticancer drugs currently used in the clinics act by disrupting microtubule dynamics or AURKA activity. They are referred to as anti-mitotics since they prevent the cells from accomplishing mitosis and thus stop tumor growth. Despite their broad usage, these drugs exhibit high toxicity to the surrounding tissue and the response to therapy is highly variable from patient to patient (Wilson, Panda and Jordan, 1999; Katayama and Sen, 2010; Dominguez-Brauer *et al.*, 2015; Henriques *et al.*, 2019). To minimize toxicity and potentiate the effectiveness of such drugs, combination therapies can be devised to simultaneously attack multiple key players of the tumor pathomechanism. I have shown that BCAT1-KO causes severe defects of the mitotic spindle and induces mitotic arrest in glioblastoma cells, indicating that BCAT1 could be a potential therapeutic target. If BCAT1 influences the spindle function by direct interaction with tubulin and AURKA, an approach could consist on designing a compound that target the binding site and disrupts their interaction. This would prevent side effects of the drug on other cellular processes and would only target dividing cells with high BCAT1 expressing (tumor cells). To design such compound, however, more information about the precise amino acid residues involved in these interactions will be necessary.

Although the CXXC-motif did not appear to be exclusively necessary for the interaction between BCAT1 and tubulin, this redox center of BCAT1 was found to be essential for promoting proliferation of glioblastoma cells. This was done by showing that the proliferation phenotype of BCAT1 depleted cells could be partially rescued by overexpression of wild-type ($BCAT1^{WT}$)

and catalytically dead (BCAT1^{K222A}) enzymes, but not by the redox dead (BCAT1^{SXXS}) enzyme. The fact that complete rescues could not be achieved might be explained by irreversible damage that the BCAT1-KO cells might have suffered due to spindle dysfunction during the lengthy generation of CRISPR/cas9 BCAT1-KO clones. To overcome this limitation, the use of an inducible knockdown system could be a better approach.

Despite the limitations of these experiments, the fact that BCAT1^{SXXS} failed to improve the proliferation of BCAT1-KO cells, while BCAT1^{WT} and BCAT1^{K222A} did improve proliferation, supports the hypothesis that BCAT1 regulates redox-dependent pathways of cell division. As discussed above, ROS constitute an important signal to promote cell cycle progression and play essential roles throughout cell division. Firstly, elevation of ROS promotes initiation of mitosis by oxidation of conserved cysteines affecting the catalytic loop of phosphatases and kinases regulating mitosis (Rudolph, 2005; Lim *et al.*, 2015; Byrne *et al.*, 2019; Patterson, Joughin, Prota, *et al.*, 2019). Since BCAT1 was found to interact with a number of these redox-sensitive mitotic proteins (AURKA, CDK1, PP1, CDC20) we are currently investigating whether BCAT1 forms mixed disulfide bonds to transmit redox modifications to key mitotic regulators. Secondly, if ROS levels are not well balanced, overoxidation of cysteines could induce mitotic arrest and eventually lead to DNA damage and induction of apoptosis (D'Angiolella, Santarpia and Grieco, 2007; Patterson, Joughin, van de Kooij, *et al.*, 2019). In this context, BCAT1 might act to maintain redox homeostasis during mitosis and thus prevent overoxidation of cysteines and mitotic arrest. Lastly, redox reactions have also been implicated in cytoskeleton remodeling by direct oxidation of its components during mitosis and cytokinesis. A very well studied example is the oxidation of M44 and M47 on F-actin by the monooxygenase activity of MICAL1 at the final step of cytokinesis, allowing cleavage and complete separation of the daughter cells (Frémont, Hammich, *et al.*, 2017). Since I have provided evidence that BCAT1 affects cytoskeleton functions and I showed ROS-mediated dimerization of BCAT1 in mitosis, it is possible that BCAT1 influence the assembly of the mitotic spindle and contractile ring via a redox-dependent mechanism.

4.5. BCAT1 modes of action in cancer

Previous to the work presented here, several hypotheses for the BCAT1 mode of action in tumor cells have been proposed by us and others. At the time of the discovery of BCAT1 as an oncogene in glioblastoma we had hypothesized that the BCKAs that are produced by the BCAT1 reaction would be further catabolized in the mitochondria and that BCAA carbon would replenish the TCA cycle to fuel anaplerosis (Tönjes *et al.*, 2013). This hypothesis was later falsified by us by showing that BCAA carbon does not enter the TCA but is excreted by the tumor cells in the form of BCKAs that possibly contribute to immune-suppression (Silva *et al.*, 2017). Most recently, we showed that BCAT1 stabilizes HIF1A by suppressing the activity of EGLN1 which targets HIF1A for proteosomal degradation. Similarly, α-KG depletion also might suppress the activity of other α-KG and Fe (II)-dependent dioxygenases including DNA and histone demethylases (Raffel *et al.*, 2017). Other authors have suggested that high BCAT1 expression leads to the accumulation of BCAAs in chronic myeloid leukemia (CML) and breast cancer (Hattori *et al.*, 2017; Zhang and Han, 2017; Gu *et al.*, 2019). BCAAs, and particularly leucine, are important activators of the mammalian target of rapamycin (MTOR), a master regulator of growth, proliferation and metabolic pathways (Guertin and Sabatini, 2007). In this context, the reverse reaction of BCAT1 would generate BCAA rather than consuming them. It remains unclear, however, how the required BCKA substrate would be supplied, since BCKAs cannot be synthesized by human cells. Together, these studies suggest that the BCAT1 mode of action in cancer could vary dependent on the tumor type and maybe even on the conditions in the tumor microenvironment. Nevertheless, the modes of action that were proposed so far all are based on the classic catalytic activity of BCAT1 as a BCAA transaminase.

In the thesis presented here, I provide evidence for a novel mode of action of BCAT1 that is dependent on the redox-activity of its CXXC-motif. In the case of glioblastoma, this redox-dependent mechanism appeared to be more important for tumor proliferation than the catalytic mechanism. Therefore, it is important to evaluate the previously reported BCAT1 modes of action in the light of these new findings.

EGLN family of proteins, for example, has been shown to be inhibited by oxidative stress in different ways. On the one hand, ROS act as chelators of the cofactor Fe(II) by oxidizing it to Fe(III), thus limiting the catalytic activity of EGLNs (Pan *et al.*, 2007). Furthermore, high ROS can also lead to inactivation of EGLN1 by homo-dimerization through disulfide bond formation between C326 of each molecule. This mechanism has been proposed for increased HIF1A activity in osteosarcoma and lung cancer cell lines (Lee *et al.*, 2016). Therefore, redox-dependent regulatory mechanisms could provide an alternative explanation to the previously reported low activity of EGLN1 in high BCAT1 expressing cancer cells (Raffel *et al.*, 2017). As I showed here, BCAT1 expressing cells exhibited high ROS production, which could then cause oxidative-mediated inactivation of EGLN1. Thus, upon BCAT1 depletion and consequent reduction of ROS levels, the activity of EGLN1 could be restored leading to degradation of HIF1A. In summary, the BCAT1-dependent stabilization of HIF1A that has been observed in AML, glioblastoma and breast cancer cells could be also explained by its redox-related function.

Raffel et al., also proposed that BCAT1 controls epigenetic modification via the modulation of α-KG and Fe (II)-dependent TET DNA demethylases and the histone lysine demethylases (KDMs) of the JmJC family. Analysis of molecular and clinical data from AML patients showed an association between high BCAT1, DNA hypermethylation and adverse prognosis. The causal link between BCAT1 expression and DNA hypermethylation was studied *in vitro* by showing that overexpression of BCAT1 in AML cell lines resulted in DNA hypermethylation. However, these results need to be interpreted with caution. Firstly, the AML cell lines that already express high BCAT1 have low α-KG levels. Thus, according to the α-KG depletion hypothesis, the activity of TET enzymes in these cells should already be limited by low α-KG availability. Therefore, the physiological relevance of increasing BCAT1 levels to further impact α-KG levels and TET enzyme activity should be carefully considered.

Regulation of TETs and KDMs could also occur through redox-mediated mechanisms (Pastor, Aravind and Rao, 2013; Kreuz and Fischle, 2016; Lamadema, Burr and Brewer, 2019). Oxidative stress induced by treatment with H_2O_2 or other pro-oxidant compounds, have been shown to inhibit TET1 and TET2 *in vitro* and *in vivo*. Since the activity of TETs could be restored by ascorbate (vitamin C), which specifically reduces Fe(III) to Fe(II), ROS-mediated oxidation of

Fe(II) is thought to be one of the mechanisms regulating TET demethylase activity (Blaschke *et al.*, 2013; Delatte *et al.*, 2015; Niu *et al.*, 2015). In addition, these particular chromatin modifier enzymes contain a cysteine-rich zinc finger (ZF-CxxC) domain, characterized by 8 conserved cysteines arranged in two clusters and coordinated by two Zn^{2+} ions. This ZF-CxxC domain is essential for recognition and interaction with DNA at non-methylated CpGs (Long, Blackledge and Klose, 2013). Therefore, due to the high content in cysteines, TET and KDMs are also sensitive to oxidative stress, and inactivation by oxidation-induced homodimer formation has also been proposed (Ma *et al.*, 2016). Considering these aspects, it is important to examine more carefully whether BCAT1 affects the activity of these and other chromatin modifier enzymes in a redox-dependent or in an α-KG-dependent manner.

Regarding BCAT1-dependent MTOR activation, Zhang et al. showed that BCAT1 overexpression in breast cancer cell lines was associated with mitochondria biogenesis, shown by mtDNA content and RNA expression of mitochondrial genes (e.i. PGC1A, NRF-1 and TFAM). BCAT1 knockdown was shown to downregulate markers of mitochondrial function and antioxidant genes, including the superoxide dismutases SOD1 and SOD2, catalase and the glutathione peroxidase 1. Additionally, BCAT1 knockdown caused increased levels of mitochondrial superoxide (Zhang and Han, 2017). This effect could be explained by the observed downregulation of SOD1 and SOD2, key enzymes that convert superoxide to H_2O_2 in the cytoplasm and mitochondrial matrix. Thus, it is likely that levels of H_2O_2 were reduced upon BCAT1 knockdown, which would be consistent with my data showing lower ROS production in BCAT1-KO cells compared to control cells. Furthermore, downregulation of important H_2O_2 scavengers, such as catalase and GPX1, would render BCAT1-depleted cells more sensitive to oxidative stress. Zhang and Han attempted to show that these effects were dependent on MTOR activation by BCAA produced by BCAT1. However, the metabolic function of BCAT1 seemed only partially responsible for MTOR activation and proliferation of breast cancer cells *in vitro*.

MTOR is directly and indirectly regulated by oxidation and the effects are dependent on the level and duration of the oxidation (Heberle *et al.*, 2015). Inhibition by oxidation of upstream regulators such as tuberous sclerosis complex (TSC1/2) and PTEN and activation of downstream

effectors like p70 ribosomal S6 kinase 1 (S6K1) contributes importantly to MTOR-dependent pathomechanism in cancer (Bae *et al.*, 1999; Yoshida *et al.*, 2011; Heberle *et al.*, 2015; Oka *et al.*, 2017). Thus, the possible missing link between BCAT1 and MTOR activity in cancer could be related to the BCAT1 redox-function instead of, or in addition to its catalytic activity.

An important function of MTOR is initiation of protein translation, which is promoted by phosphorylation of S6K1 or the eukaryotic translation initiation factor 4E (eIF4E)-binding protein 1 (4EBP1). Phosphorylation of 4EBP1 results in loss of interaction with eIF4E, which in turn associates into a complex to initiate cap-dependent translation (Laplante and Sabatini, 2009). eIF4E has been shown to play a role in oncogenic transformation by selectively promote the translation of genes involved in detoxification and control of ROS levels. Modulation of eIF4E levels, thus affects endogenous ROS production and sensitivity to exogenous ROS treatment (Truitt *et al.*, 2015). Interestingly, our list of candidates BCAT1 binding partners revealed a significant enrichment of proteins associated with EIF2A signaling (see section 3.3, Figure 14). These included eIF4A and eIF2A other important translation factors that integrate signals from MTOR and more stress sensors (Pavitt, 2018). Investigating the mechanistic link between BCAT1, EIF2 signaling and MTOR, was beyond the scope of this thesis, but is an important aspect to investigate.

In summary, I have provided evidence in support of a novel, redox-mediated mode of action of BCAT1 in glioblastoma that is independent of its catalytic function. I described here a close interaction of BCAT1 with the cytoskeleton, which seems to be important in multiple cellular processes. I showed that BCAT1 interacts with proteins involved in EGFR signaling and modulates H_2O_2-mediated activation of EGFR. Furthermore, I found that BCAT1 interacts with the mitotic machinery, which is essential for mitosis progression. My data indicate that the BCAT1 redox mechanism might be the primary determinant of BCAT1-dependent proliferation in glioblastoma cells. Additional work will be needed to elucidate the details of the catalytic and redox mechanisms and their possible interdependence in glioblastoma, additional cancer entities, as well as other diseases.

5. Materials

5.1. Cell culture material

material name	distributor
µ-slide 8 well	ibidi GmbH
µ-Slide 8 Well (collagen IV)	ibidi GmbH
12 Well Chamber, removable	ibidi GmbH
96 well plate Black	Greiner Bio-One GmbH
96 well plate white	Greiner Bio-One GmbH
CD 293 Medium (1X)-1,000 mL	Life Technologies
Cell culture flasks and multi-well plates	Tritech Research, Los Angeles, USA
Costar Polycarbotate Membrane Transwell inserts (8 µm pores)	Corning
Dimethyl sulphoxide (DMSO)	Sigma-Aldrich, Munich, Germany
Dulbecco's Modified Eagle's Medium - high glucose	Sigma-Aldrich, Munich, Germany
Dulbecco's Modified Eagle's Medium - low glucose	Sigma-Aldrich, Munich, Germany
Einweg-Zählkammer C-Chip	Biochrom, Berlin, Germany
Fetal Calf serum (FCS)	Merck Millipore, Darmstadt, Germany
hEGF	Life Technologies
L-Glutamine	Thermo Fischer Scientific, Langenselbold, Germany
OptiMEM	Thermo Fischer Scientific, Langenselbold, Germany
Penicillin/Streptomycin (10000 U/ml, 100 µg/ml)	Thermo Fischer Scientific, Langenselbold, Germany
Polyethylenimine	Polysciences Europe GmbH
Spinner flask	Weaton DWK LifeSciences
Tet System Approved FBS	Takara Bio Clontech
TRANSIT®-LT1 TRANSFECTION REAGENZ	mirus-VWR
Trypsin EDTA solution (0.5 %)	Sigma-Aldrich, Munich, Germany

5.2. Buffers and solutions

solution	Composition
1x Transfer buffer	25 mM Tris, 200 mM glycine, 20 % methanol, pH 8.8
1x TRIS buffered saline (TBS)	150 mM NaCl, 10 mM Tris, pH 7.5
TBS-T	TBS 1X, 1:1000 (v/v) Tween 20
Blocking buffer (WB)	5% milk or BSA in TBS-0.1% Tween20
Blocking buffer (IF)	3% BSA PBS 0.1% triton-X100

Cell cycle staining solution (PI staining)	0.1 % Triton X-100/PBS, 200 µg/ml DNAse-free RNAse, 250 µg/ml propidium iodide
FACS buffer	1 % BSA in DPBS
LB (Luria Bertani) medium	0.5 % (w/v) NaCl, 1 % (w/v) Tryptone, 0.5 % (w/v) Yeast extract
LB Agar	0.5 % (w/v) NaCl, 1 % (w/v) Tryptone, 0.5 % (w/v) Yeast extract, 1.6% (w/v) Agarose

5.3. Reagents

5.3.1. Antibiotics and inhibitors

Selection antibiotics and inhibitors	**Distributor**
Ampicillin	Roche diagnostics, Mannheim, Germany
Geneticin Selective Antibiotic (G418 Sulfate)	Thermo Fischer Scientific, Langenselbold, Germany
Hygromycin B 100mg	MP Biomedicals
Kanamycin Solution	Sigma-Aldrich, Munich Germany
Nocodazole	Sigma-Aldrich, Munich Germany-Aldrich
Puromycin	Merck Millipore, Darmstadt, Germany
Thymidine	Biolmol GmbH, Hamburg, Germany

5.3.2. Immunoprecipitation material

Immunoprecipitation	**Distributor**
Pierce concentrator, PES, 10K MWCO	Thermo Fischer Scientific, Langenselbold, Germany
Pierce™ Anti-HA Magnetic Beads	Thermo Fischer Scientific, Langenselbold, Germany
Pierce™ Anti-DYKDDDDK Magnetic Agarose	Thermo Fischer Scientific, Langenselbold, Germany
Pierce 3x DYKDDDDK Peptide-5 mg	Life Technologies
HA Peptide	Hölzel Diagnostika -
Dynabeads protein G	Invitrogen

5.3.3. Cytoskeleton related products

Cytoskeleton related products	**Company**
Actin Binding Protein Biochem Kit	Cytoskeleton, Inc
Actin Polymerization Biochem Kit	Cytoskeleton, Inc
acti-stain 670(phalloidin)	Cytoskeleton, Inc
Alexa Fluor ™ 488 Phalloidin	Invitrogen

microtubule Binding protein Spin-down assay kit	Cytoskeleton, Inc
Muscle actin	Cytoskeleton, Inc
SiR-actin	Cytoskeleton, Inc
SiR-tubulin	Cytoskeleton, Inc

5.3.4. Fluorescent tools

Fluorescent dyes/kits	**Distributor**
Click-iT 647 (alexa fluor 647 picolyl azide)	Invitrogen
Click-iT™ EdU Alexa Fluor™ 488 Flow Cytometry Assay Kit	Invitrogen
propidium iodide	Sigma-Aldrich, Munich Germany
DCFDA/H2DCFDA - Cellular Reactive Oxygen Species Detection Assay Kit	Abcam

5.3.5. Protein preparation material

Material	**Distributor**
NuPAGE 4-12% bis-Tris 1,5mmx15well	Life Technologies GmbH
20xMOPS buffer	Life Technologies GmbH
NuPAGE 4xLDS sample buffer	Life Technologies GmbH
Pierce ECL Western Blotting Substrate	Thermo Fischer Scientific, Langenselbold, Germany
PVDF transfer membrane 0.45 µM	Merck Millipore, Darmstadt, Germany
GelCode Blue Safe Protein Stain-1 L	Thermo Fischer Scientific, Langenselbold, Germany
Pierce BCA Protein Assay	Thermo Fischer Scientific, Langenselbold, Germany
NuPAGE Sample Reducing Agent (10X)-10 mL	Life Technologies GmbH
PIERCE® IP LYSIS BUFFER, 100 ML	Thermo Fischer Scientific, Langenselbold, Germany
RIPA Buffer	Sigma-Aldrich, Munich Germany
cOmplete Mini, Edta free	Sigma-Aldrich, Munich Germany
GelCode Blue Stain Reagent	Thermo Fischer Scientific, Langenselbold, Germany

5.4. Cloning material

Material	**Distributor**
Precisor High-Fidelity DNA Polymerase	BioCat GmbH, Heidelberg, Germany
QIAGEN Plasmid Maxi Kit	Qiagen, Hilden, Germany
QIAGEN Plasmid mini Kit	Qiagen, Hilden, Germany
QIAquick Gel Extractions Kit	Qiagen, Hilden, Germany
Quick Ligation Kit	New England Biolabs, Massachusetts, United States
PCR nucleotide mix	Roche Diagnostics, Mannheim, Germany

QuickChange II XL site-directed mutagenesis kit	Agilent, California, United States
QuikChange Lightning Site-directed mutagenesis Kit	Agilent, California, United States
T4 DNA Ligase	New England Biolabs, Massachusetts, United States
BamHI	Thermo Fischer Scientific, Langenselbold, Germany
NdeI	Thermo Fischer Scientific, Langenselbold, Germany
XbaI	Thermo Fischer Scientific, Langenselbold, Germany
NotI	Thermo Fischer Scientific, Langenselbold, Germany
XhoI	Thermo Fischer Scientific, Langenselbold, Germany

5.5. Plasmids

5.6. Commertial plasmids

Plasmid	**company**
lentiCRISPRv2_52961	Addgene, Cambridge, USA
pLVX-Puro	Addgene, Cambridge, USA
pLVX-hygro	Addgene, Cambridge, USA
mCeruleanC1	Addgene, Cambridge, USA
mVenusC1	Addgene, Cambridge, USA
EGFR-GFP	Addgene, Cambridge, USA
psPAX.2 (#12260)	Addgene, Cambridge, USA
pMD2.G (#12259)	Addgene, Cambridge, USA

5.6.1. Generated plasmids

Generated plasmids
pLVX-puro_HA-BCAT1wt
pLVX-puro_HA-BCAT1-SXXS
pLVX-puro_HA-BCAT1-K222A
pLVX-hygro_BCAT1wt-FLAG
pLVX-hygro_BCAT1-SXXS-FLAG
pLVX-hygro_BCAT1-K222A-FLAG
pLVX-puro-HA-CFP
pLVX-hygro_CFP-FLAG
pLentiCRISPRv2_NT sgRNA

pLentiCRISPRv2_BCAT1 E3g1-sgRNA	
pcDNA3.1_TC3-R9P (FRET sensor)	
pcDNA3.1_TC3-R9L (FRET sensor)	

5.7. Biological material

cells	Distributor
293FT	provided by Rainer Will (Vectors Core facility, DKFZ)
DH5α Competent Cells	Life Technologies GmbH
LN-229	ATCC
Normal human Astrocytes (NHA)	provided by Thorsten Kolb (B060, DKFZ)
One Shot TOP10 Chemically Competent E.coli	Life Technologies GmbH
One Shot ™ Stbl3 ™ Chemically Competent E. coli	Life Technologies GmbH
U251-MG	ATCC
U2OS (live-Act transduced)	provided by Kendra Maaß (B060, DKFZ)
U87-MG	ATCC

5.7.1. Cell lines generated by stable lentiviral transduction

name of the cell line	plasmid transduced
U251cNT	lentiCRISPRv2 NT-sgRNA
U251cNT-CFP-FLAG	lentiCRISPRv2 NT-sgRNA + pLVX-hygro-CFP-FLAG
U251BKO	lentiCRISPRv2 BCAT1 E3g1-sgRNA (clone 4)
U251BKO-CFP-FLAG	lentiCRISPRv2 BCAT1 E3g1-sgRNA + pLVX-hygro-CFP-FLAG
U251BKO-BCAT1wt	lentiCRISPRv2 BCAT1 E3g1-sgRNA + pLVX-hygro_BCAT1-wt-FLAG
U251BKO-BCAT1-SXXS	lentiCRISPRv2 BCAT1 E3g1-sgRNA + pLVX-hygro_BCAT1-SXXS-FLAG
U251BKO-BCAT1-K222A	lentiCRISPRv2 BCAT1 E3g1-sgRNA + pLVX-hygro_BCAT1-K222A-FLAG
LN229cNT	lentiCRISPRv2 NT-gsRNA
LN229cNT-CFP-FLAG	lentiCRISPRv2 NT-gsRNA + pLVX-hygro-CFP-FLAG
LN229BKO	lentiCRISPRv2 BCAT1 E3g1-sgRNA
LN229BKO-CFP-FLAG	lentiCRISPRv2 BCAT1 E3g1-sgRNA + pLVX-hygro-CFP-FLAG
LN229BKO-BCAT1wt	lentiCRISPRv2 BCAT1 E3g1-sgRNA + pLVX-hygro_BCAT1-wt-FLAG
LN229BKO-BCAT1-SXXS	lentiCRISPRv2 BCAT1 E3g1-sgRNA + pLVX-hygro_BCAT1-SXXS-FLAG
LN229BKO-BCAT1-K222A	lentiCRISPRv2 BCAT1 E3g1-sgRNA + pLVX-hygro_BCAT1-K222A-FLAG
U87cNT	lentiCRISPRv2 NT-gsRNA
U87cNT-CFP-FLAG	lentiCRISPRv2 NT-gsRNA + pLVX-hygro-CFP-FLAG
U87BKO	lentiCRISPRv2 BCAT1 E3g1-sgRNA
U87BKO-CFP-FLAG	lentiCRISPRv2 BCAT1 E3g1-sgRNA + pLVX-hygro-CFP-FLAG
293FT-HA-BCAT1wt	pLVX-puro_HA-BCAT1-wt

293FT-HA-BCAT1-SXXS	pLVX-puro_HA-BCAT1-SXXS
293FT-HA-BCAT1-K222A	pLVX-puro_HA-BCAT1-K222A

5.8. Antibodies

5.8.1. Primary antibodies

target	number	company
Actin(I-19)	sc-1616-R	santa-cruz
Alexa Fluor(R) 488 anti-HA.11 Epitope Tag	BLD-901509	Biolegend
alpha-Tubulin	T9026	Sigma-Aldrich, Munich, Germany
Aurora A (D3E4Q)	14475	Cell Signaling Technology, Denver, USA Technology
Aurora Kinase A antibody - A594 conjugated	sc-373856 AF594	santa-cruz
BCAT1 (BCATc)		Myra cOnway (Bristol University)
BCAT1 (Eca39)	611271	BD-biosciences
CDK1 (A17.1.1)	MA5-11472	Thermo fisher
EGFR	E30	Dako
EGFR (1005)	sc-03 R	santa-cruz
EGFR-phospho (Tyr1068) (D7A5)	3777	Cell Signaling Technology, Denver, USA
EGFR-phospho (Tyr1068) Antibody #2234	2234	Cell Signaling Technology, Denver, USA Technology
HA tag antibody - ChIP Grade	(ab9110)	Abcam, Cambridge, UK
Phospho-Aurora A (Thr288) (C39D8)	#3079	Cell Signaling Technology, Denver, USA Technology
Phospho-Histone H3 (Ser10) (D2C8) XP® Rabbit mAb	#3377	Cell Signaling Technology, Denver, USA Technology
Phospho-p44/42 MAPK (Thr202/Tyr204)	9101S	Cell Signaling Technology, Denver, USA
Phospho-PLC gamma1 (Tyr783)	E-AB-20971.20	Biomol (Elabsciences)
PLCγ (D9H10) XP	590	Cell Signaling Technology, Denver, USA
Protein phosphatase 1 (PP1) E-9	sc-7482	Santa Cruz Biotechnology, Dallas, TX, USA

5.8.2. Secondary antibodies

target	number	company
anti-mouse alexa 488	A-11001	Invitrogen, California, USA
anti-Rabbit IgG Alexa Fluor 647	A-21245	Invitrogen, California, USA
anti-Rabbit IgG Alexa Fluor 488	A-11034	Invitrogen, California, USA
Alexa 594 anti Mouse	A-21203	Invitrogen, California, USA
HRP-anti-mouse	Sc-2004	Santa Cruz Biotechnology, Dallas, TX, USA

HRP-anti-Rabbit	Sc-2005	Santa Cruz Biotechnology, Dallas, TX, USA

5.9. Equipment

Equipment	company
Agarose gel electrophoresis	Biozym, Hamburg, Germany
Airfuge ultracentrifuge	Beckman Coulter GmbH, Krefeld, Germany
CO_2 incubator ThermoForma	Thermo Fischer Scientific, Langenselbold, Germany
Cytospin3-centrifuge	Thermo Fischer Scientific, Langenselbold, Germany
DynamagTM magnet	Thermo Fischer Scientific, Langenselbold, Germany
FACS Canto II™	BD biosciences, Heidelberg, Germany
FACS canto ™ II	BD biosciences, Heidelberg, Germany
Zeiss Axio Vert.A1	Carl Zeiss, Germany
GloMax® Discover	Promega, Madison, Wisconsin, USA
Heraeus Biofuge fresco	Thermo Fischer Scientific, Langenselbold, Germany
Leica TCS SP5 confocal microscope	Leica Mycrosystems, Wetzlar, Germany
Leica TCS SP8 confocal microscope	Leica Mycrosystems, Wetzlar, Germany
Mastercycler epgradient S	Eppendorf, Hamburg, Germany
Mithras LB 940 plate reader	Berthold Technologies, Bad Wilbad, Germany
NanoDrop® ND-2000C spectrometer	NanoDrop, Wilmington, USA
Shaker DRS-12	neoLab Migge GmbH
Sterile bench HERA safe	Thermo Scientific, Langenselbold, Germany
Thermal cycler PTC-200	MJ resear, BioRad, Hercules, USA
Vi-CELL XR 2.03	Beckman Coulter GmbH, Krefeld, Germany

5.1. Software

software	company
Leica LAS-X Life Science	Leica Mycrosystems, Wetzlar, Germany
Flowjo V10	Flowjo, LLC, USA
Microsoft office 365	Microsoft Corporation
Ingenuity Pathway Analysis (IPA)	QIAGEN bioinformatics
design of CRISPR guides	https://zlab.bio/guide-design-resources
Fiji	ImageJ, NIH, USA
Basic Local Alignment Search Tool (BLAST)	https://blast.ncbi.nlm.nih.gov/
Mendeley version 1.19.4	Mendeley Ltd.
GraphPath Prism version 6.01	https://www.graphpad.com/scientific-software/prism/

5.2. Primers

5.2.1. PCR amplification

BCAT1-BamHI frw	gcataGGATCCATGAAGGATTGCAGTAACGGATGCTCC
BCAT1-NotI-rev	agcatGCGGCCGCTCAGGATAGCACAATTGTCCAGTCGCTCTC
BCAT1-EcoRI-rev	agcatGAATTCTCAGGATAGCACAATTGTCCAGTCGCTCTC
HindIII_BCAT1_frw	tgGatcAAGCTTTGAAGGATTGCAGTAACGGATGCTCCG
BamHI_BCAT1_rev	gatcacGGATCCTCAGGATAGCACAATTGTCCAGTCGCTCTC
BCAT1-EcoRI-rev	agcatGAATTCTCAGGATAGCACAATTGTCCAGTCGCTCTC
BshTI-HA-BCAT1_frw	CGCCCACCGGTATGTATCCCTATGACGTGCCCGATTATGCCAAGGATTGCAGTAACGGATGCTCCGC AGAGTG
BCAT1_XbaI_rev	GcataTCTAGATCAGGATAGCACAATTGTCCAGTCGC
BCAT1_XhoI_frw	GcataCTCGAGATGTATCCCTATGACGTGCCCGATTATGCCAAGGATTGCAGTAACGGATGCTCCGCA GAGTG
Ins_HA-FP_frw	ccgtcagatccgctagcgtatccctatgacgtgcccgattatgccctaccggtcgccacca
Ins_HA-FP_rev	ggtggcgaccggtagggcataatcgggcacgtcatagggatacgctagcggatctgacgg

5.2.2. Site directed mutagenesis

C221S_frw	GCC TGG AAA GGT GGA ACT GGG GAC TCC AAG ATG GGA GGG
C221S_rev	GCC TGG AAA GGT GGA ACT GGG GAC TCC AAG ATG GGA GGG
C235S_frw	GGC TCA TCT CTT TTT GCC CAA TCT GAA GCA GTA GAT AAT GGG
C235S_rev	GGC TCA TCT CTT TTT GCC CAA TCT GAA GCA GTA GAT AAT GGG
C242S_frw	TGTGAAGCAGTAGATAATGGGTCTCAGCAGGTCCTGTGG
C242S_rev	CACAGGACCTGCTGAGACCCATTATCTACTGC
C293S_frw	AGTGACAAGGCGGTCCATTCTGGACCTGGC
C293S_rev	GCCAGGTCCAGAATGGACCGCCTTGTC
C335S rev	TGGGCAAACAACAGAGGCTGTACCAGAGCC
C335S frw	GGC TCT GGT ACA GCC TCT GTT GTT TGC CCA
C338S rev	CAG TAT ATC AGA AAC TGG GCT AAC AAC ACA GGC TGT ACC
C338S frw	GGT ACA GCC TGT GTT GTT AGC CCA GTT TCT GAT ATA CTG
C335S/C338S frw	GGT ACA GCC TCT GTT GTT AGC CCA GTT TCT
C335S/C338S rev	AGA AAC TGG GCT AAC AAC AGA GGC TGT ACC
BCAT1_K222A_frw	ggtggaactggggactgcgcgatgggagggaattacg
BCAT1_K222A_rev	cgtaattccctcccatcgcgcagtccccagttccac

6. Methods

6.1. Cell lines and culture conditions

U251MG, U87MG, LN229, and HEK293T were obtained from ATCC. 293FT were obtained from the clone repository facility (DKFZ, Rainer Will). U251MG, U87MG and MDA-MB-231 were cultured in DMEM with 1000 mg/ml glucose, 0.5 mM L-glutamine, 1x penicillin-streptomycin (P/S) and 10% fetal calf serum (FCS). Cell lines expressing the Tet-ON shRNA knockdown system were cultured with the same media compositions except that a Tet-free FCS (Takara, 631106) was used. LN229 and HEK293 were cultured in DMEM high glucose and 2mM L-glutamine, 1x P/S and 10% FCS. 293FT cells were grown as adherent cells in DMEM high glucose, supplemented with 10% FCS, 1X MEM non-essential amino acids, 1X Glutamax and 1 mM sodium pyruvate. 293FT adapted to grow in suspension were grown in CD293 media without FCS. Cell lines were maintained in an incubator at 37°C and 10% CO_2 for U251MG and U87MG and 5% CO_2 for LN229 and HEK293

6.2. α-KG FRET-sensor development

To measure intracellular fluctuations of α-KG under different conditions, a genetically encoded sensor based on FRET was constructed. The FRET sensor was established as described in (Lüddecke, Francois et al., 2017). Briefly, the protein PII from *Synechococcus elongatus* PCC 7942 was fused to the monomeric (m) cyan fluorescent protein mCerulean, and the yellow fluorescent protein mVenus. mCerulean was modified to create a circularly permuted version by connecting its native C- and N-terminus with a short flexible linker (GSGGTG) and was inserted between the amino acids 44 and 45 of the PII protein. The mVenus was linked to the C-terminus of the PII by a Strep-tag.

For the expression in mammalian cells, the sensor's cDNA was inserted into the mammalian expression vector pcDNA3.1 using the BamHI and HindIII restriction sites.

6.3. Time-lapse imaging for monitoring of α-KG levels using the FRET sensor

U87MG were seeded in chambered coverglasses (µ-slides, Ibidi) and transfected with 0.8 µg/mL plasmid DNA using the TransIT-LT1 reagent (Mirus). Fluorescence measurements were performed 48 h post-transfection at a Leica TCS-SP5 laser scanning confocal microscope using a 40x objective (HCX PL APO, NA 1.25, oil-immersion). To limit phototoxicity, resonant scanners and hybrid photon detectors (HyD) were used. Cells were excited with a UV diode (405 nm) and emission was detected at 450–490 nm (CFP) and 520–590 nm (FRET). Pictures were acquired every 60 sec. After a baseline of 5 min, media containing compounds or not were added and changes in fluorescence recorded for 15 min more. During imaging, cells were maintained at 37 °C and 5% CO_2. Image processing was performed with Fiji, ImageJ (http://fiji. sc/). After background subtraction and registration, single cells were segmented by threshold. For every cell, the mean intensity was measured for each channel at every time point. The FRET ratio was calculated by dividing the mean intensity of the acceptor (FRET) by the intensity of the donor (CFP). Ratios were normalized to baseline measurements.

6.4. BCAT1 constructs

BCAT1 cDNA obtained previously by Tönjes et al. 2013, was amplified by PCR and inserted into the mCerulean-C1 vector (Addgene) using the NheI and BamHI restriction sites, thus removing mCerulean (CFP). The undigested mCerulean-C1 (called CFP) was further on used as a control plasmid. BCAT1 was tagged with either an HA-tag (N-terminally) or a FLAG-tag (C-terminally). The tags were added by amplifying BCAT1 using primers containing the HA-tag sequence at the N-terminus or FLAG-tag signal at the C-terminus (see primer list). For lentivirus transduction, HA-BCAT1 or BCAT1-FLAG where inserted into the lentivirus delivery vector pLVX-puro using XhoI and XbaI or to the pLVX-hygro vector using the XhoI and XbaI BamHI restriction sites.

DNA sequences were verified by GATC (Eurofins Genomics) sequencing services using cycle sequencing on ABI 3730XL machines.

6.5. Site-directed mutagenesis of BCAT1 mutants

BCAT1 mutants SXXS (C335S and C338S) and K222A were created by site-directed mutagenesis using the QuikChange Lighting (# 210518, Aligent) or QuickChange II XL (#200521, Agilent) site-directed mutagenesis kits following the manufacturer protocol (see primer list).

DNA sequences were verified by GATC (Eurofins Genomics) sequencing services using cycle sequencing on ABI 3730XL machines.

6.6. Lentiviral Production

A 2nd generation lentiviral packaging system was used for lentiviral production with the packaging vector psPAX.2 (Addgene, #12260) and envelope vector pMD2.G (addgene, #12259). One day prior to transfection, 5 x 10^6 293T cells were seeded in 10 cm dishes. Medium was refreshed 2 h before transfection with 5 ml medium. Cells were transfected with 8 µg DNA, composed of 4 µg sgRNA vector, 2 µg packaging and 2 µg envelope vector. The DNA was mixed 3:1 with Polyethylenimine (PEI) in OptiMEM medium in a final volume of 250 µl. After an incubation of 15 min at room temperature the transfection mix was added to the cell dishes dropwise. 24 h after transfection, the medium was refreshed. Viral supernatant was collected 72 h post transfection and filtered using a 0.45 µm syringe filter. The solution was centrifuged at 1800 x g for 90 min at 4 °C. The pelleted virus was resuspended in 100 µl OptiMEM and stored at -80 °C.

6.7. Development of CRISPR/Cas9 KO cell lines

To create BCAT1 knockout (BCAT1-KO) cell lines, the CRISPR/Cas9 technology was used. Four different guide RNAs (sgRNAs) targeting exon 2 and 3 (two guides per exon) were designed using the online tool http://crispr.mit.edu/. The oligos coding for the sgRNAs were cloned into the lentiCRISPRv2 vector as described in Sanjana, Shalem, & Zhang, 2014 and Shalem et al., 2014.

Cas9 and sgRNA contained in the lentiCRISPRv2 vector were delivered to the cells by lentiviral transduction (as described above) followed by puromycin selection for two days. The sgRNA (guide #1 targeting Exon 3) exhibiting the best knockdown efficiency measured by a decrease in

total BCAT1 protein levels was used for subsequent experiments. U251MG, LN229 and U87MG were transduced with the lentiCRISPRv2-sgRNA#1 -exon3. Two days later, single clones created by serial dilution were seeded in 96-well plates. Single clones were allowed to grow and expand for 10 days in media containing puromycin. Eight clones were screened for efficiency of BCAT1 depletion by WB. The CRISPR/Cas9-induced INDEL (insertion-deletion) area was confirmed by sequencing of genomic DNA.

sgRNA oligos

Ex3g1_oligo1	caccgCACGGATCATATGCTGACGG
Ex3g1_oligo2	aaacCCGTCAGCATATGATCCGTGc
SgRNA CTRL sequence	GCGAGGTATTCGGCTCCGCG

6.8. Immunofluorescence

Cells were seeded in 12-well chambers µ-slides (ibidi) and grown for 24-48 h. Cells were washed with PBS and fixed with 4 % paraformaldehyde (PFA) for 10 min at room temperature (RT). After washing with PBS, cells were permeabilized with 0.2% triton X-100, 1% BSA in PBS for 20-30 min and blocked for 30 min in blocking buffer (3% BSA 0.02% Triton X-100 PBS) at RT. The primary antibody was diluted in blocking buffer and incubated on the samples overnight at 4°C in a humidified chamber. After washing 3 times with PBS, the secondary antibody, diluted 1:1000 in TBS, was added and incubated for 1-2 h, protected from the light at RT. The slides were then washed three times with PBS and mounted using Vectrashield mounting media with DAPI. Slides were allowed to dry at RT overnight before imaging. Pictures were acquired with a Leica TCS-SP5 or SP8 laser scanning confocal microscope.

6.9. Time-lapse imaging to assess EGFR endocytosis

U87MG cells were transfected with 1 µg/ml of EGFR-GFP (addgene, Carter and Sorkin 1998) or 0.5 µg/ml of mVenus (addgene) using TransIT-LT1 (mirus) and selected with neomycin (G418, 400 µg/ml) to enrich for cells expressing the constructs. $1x10^4$ EGFR-GFP or mVenus expressing cells were seeded in 8-chambers µ-slides (ibidi #80826) and allowed to attach for 24 h. Three to four hours before imaging, cells were washed with PBS and incubated in serum-free media.

Before treatments, cells were imaged for 7 min to determine the baseline; then hEGF (final concentration 100 ng/ml) or vehicle were added to the wells and acquisition was resumed for 90 min. Imaging was performed with a Leica TCS-SP5 laser scanning confocal microscope using a 40x objective (HCX PL APO, NA 1.25, oil-immersion), resonant scanners and hybrid photon detectors (HyD). The 488 nm argon laser line was used to excite GFP-EGFR. At all times during imaging, cells were kept in an incubation chamber with controlled temperature at 37°C and 5% CO_2. Two independent experiments were performed. At each experiment, at least 3-4 fields of view were imaged per condition. Images were processed with Fiji, ImageJ (http://fiji. sc/).

6.10. Click-iT™ EdU cell proliferation assay

Cells were seeded in 12- or 6-well plates and transfected with the indicated HA-BCAT1 variants. Twenty-four hours after transfection, 5-ethynyl-2´-deoxyuridine (EdU) was added to each well to a final concentration of 10 µM and incubated for 4-8 h. Cells were washed with PBS, detached with trypsin and fixed with 4% PFA for 15 min. Fixed cells were washed with 1% BSA/ PBS and permeabilized for 30 min. using 0.1% (v/v) Triton-X100 PBS. Click-iT detection was performed as indicated by the manufacturer using either Alexa-488 azide or Alexa647 pycolyl-azide. The latter was applied when Click-iT was used in combination with propidium iodide (PI) staining to quantify the proportion of cells in each cell cycle phase. Cytometric analysis was performed at a FACS Canto II (BD biosciences). Acquisition was stopped after 10 000 cells were measured. Data was further processed and analyzed using Flowjo software (Flowjo LLC, V10).

6.11. Transwell cell migration assay

The migration capacity of BCAT1-KO and NT glioblastoma cells was assessed using Costar Polycarbotate Membrane Transwell inserts (8 µm pores, Cat #3422, Corning). Cells were seeded in 6-well plates and starved in serum-free media overnight. Then, $1x10^4$ cells were transferred into pre-wet insert cups and allowed to migrate for 24 h. Media containing 10 % FCS or 50 ng/ml hEGF were used as chemoattractant. Migrated cells were fixed on the membrane using methanol, followed by hematoxylin staining and sequential dehydration in 80% and 100% ethanol. Per insert, 5 fields of view were imaged using a 20x objective in a Zeiss Axio Vert.A1. Migrated cells were counted by eye.

6.12. Nuclear fractionation

U251MG were grown in 15 cm dishes and allowed to reach confluency. After washing once in ice-cold PBS, cells were scraped into 1.5 ml Eppendorf tubes and centrifuged at 1000 xg for 5 min (3 200 rpm). The supernatant was removed, the pellet resuspended in 3 times the pellet volume (~900 µl) of extraction buffer (0.5x PBS, 50mmol/l MOPS pH 7,4, 1mMol/L MgCl2, 0.2% Triton X100) and incubated at 4°C for 10 min with gentle rotation. After centrifugation at 4 000 x g (6 500 rpm) for 5 min, the supernatant (cytoplasmic fraction) was stored and the pellet (nuclear fraction) was resuspended in Pierce IP-buffer containing protease inhibitor cocktail (Roche, mini EDTA-free). DNA was digested with 2 µl of Benzonase for 5-10 min at RT. Protein concentration was measured by the Pierce BCA assay before the samples were subjected to IP or SDS-PAGE.

6.13. Immunoprecipitation (IP) using an anti-BCAT1 antibody

350 µg of protein of the nuclear or cytoplasmic fractions was pre-cleared with 20 µl of Dynabead protein G (Invitrogen #10003D) and incubated with 12 µg of BCAT1 antibody (Gift from Myra Conway, Bristol) or rabbit IgG control for 3 h rotating at 4 °C. The Dynabeads were washed 2 times with PBS (0.02% Tween-20) and added to the protein-antibody complex. After 16 h of incubation a 4 °C with gentle rotation, the beads were washed 3 times with ice cold PBS before preparing them for Mass-Spectrometry analysis.

6.14. Mass-Spectrometry analysis

Mass-Spectrometry analysis of BCAT1's binding partners from nuclear and cytoplasmic fractions was performed in collaboration with Gianluca Sigismondo at the Krijgsveld lab (DKFZ). Beads were recovered on the magnet and sequentially washed three times with PBS-T, Native Washing buffer A (Tris HCl ph 7.6 50mM, EDTA 10mM, NaCl 75mM), Native washing buffer B (Native Washing buffer A with 125mM NaCl) and Native Washing buffer C (Native Washing buffer A with 175mM NaCl). Beads were then conditioned in 50mM ammonium bicarbonate (NH_4HCO_3). DTT was added to 7 mM final concentration and samples were subjected to disulphide bond reduction by heating at 55°C for 30min, followed by alkylation with iodoacetamide, 12 mM at RT for 40 min in the dark. The reaction was quenched with DTT and

proteins were trypsin-digested on-beads overnight at 37°C. Digested peptides were desalted with 5 µL of SP3 para-magnetic beads following a protocol previously described (Hughes C. S. et al. 2014; Rafiee et al. 2016; Hughes C. S. et al. 2019). Peptides were eluted in 0.1% trifluoroacetic acid (TFA) in H_2O and injected on an Q Exactive-HF (Thermo Scientific) coupled to a Thermo EASY LC 1200 UPLC system. Samples were loaded onto trap column (Acclaim PepMap100 C18 Nano-Trap 2 cm x 100 um x 5 um) with Buffer A (0.1% formic acid in water) and separated over a 50 cm analytical column (Acclaim PepMap RSLC, 75 um x 2 um) using a 105 min linear gradient from 3% to 40% Buffer B (0.1% formic acid, acetonitrile 80% in water). MS2 fragmentation was set to Higher-energy collisional dissociation (HCD).

RAW data were processed with Maxquant (1.5.2.8) (Cox and Mann, 2008) using default settings. MSMS spectra were searched against the *Homo sapiens* Uniprot database concatenated to a database containing protein sequences of contaminants. Enzyme specificity was set to trypsin/P, allowing a maximum of two missed cleavages. Cysteine carbamidomethylation was set as fixed modification, while methionine oxidation and protein N-terminal acetylation were used as variable modifications. Global false discovery rate for both protein and peptides was set to 1%. The match-between-runs option was enabled. Intensity-based quantification options (iBAQ and LFQ) were calculated. Data analysis was performed with Perseus software (1.5.3.0) (Tyanova et al, 2016). Upon filtering for contaminants and reverse, only proteins with at least one unique peptide were considered for further analysis. For the proteins identified, the ratio between the LFQ values in the target over the respective control was calculated and only proteins with LFQ ratio greater than 1.5 were used for table generation. Imputation was applied for proteins without an LFQ value in the IgG negative control were the LFQ ratio was set to 3 (in Log2) as highest value.

6.15. HA-BCAT1 overexpression and purification for *in vitro* biochemical assays

For overexpression and purification, HA-tagged BCAT1 was used. HA-BCAT1 variants (HA-BCAT1^{wt}, HA-BCAT1^{SXXS} and HA-BCAT1^{K222A}) were cloned into the lentiviral vector pLVX-puro as described above. 293FT cells were transduced by lentivirus with the pLVX-puro-HA-BCAT1 variants or empty vector and selected with puromycin for 48 h. Cells stably expressing HA-

BCAT1^{wt}, HA-BCAT1^{SXXS} or HA-BCAT1^{K222A} were adapted to grown in suspension by gradually decreasing the content of FCS in the media (10 %, 5%, 2 %) until complete removal. Suspension cells were then transferred into spinner flasks (Wheaton). After reaching a density of 1x10^6 /ml, cells were pelleted by centrifugation at 900 rpm at 4 °C, washed once with ice-cold PBS and frozen at – 80 °C. Cell pellets were lysed in Pierce IP buffer (with proteinase inhibitors cocktail, Roche) for 30 min at 4 °C with gentle rotation and cleared by centrifugation at 13 000 rpm for 20 min at 4 °C. Cleared proteins were incubated with anti-HA magnetic beads for 3 h at 4 °C with gentle rotation. Beads were then washed 3 times with 0.05% Tween-20 TBS (TBS-T) and 1 time with de-ionized water. The HA-BCAT1 variants were eluted with HA-peptide (200 µg/ml in PBS) for 30 min at 30 °C while shaking at 600 rpms. Eluted HA-BCAT1 was further concentrated using the Pierce concentration columns MWKO 10K. HA-BCAT1 purity was determined by SDS-PAGE and Coomassie staining, the concentration was estimated photometrically using a Nanodrop instrument.

6.16. Immunoprecipitation (IP) of BCAT1-FLAG using anti-FLAG magnetic beads

For investigation of BCAT1 redox binding partners, U251MG and LN229 cell lines overexpressing BCAT1-FLAG variants were subjected to immunoprecipitation using anti-FLAG magnetic beads. Immunoprecipitation was performed as described for HA-tag except that all washing steps were performed with the Pierce-IP buffer and the samples were eluted with FLAG-peptide (1.5 mg/ml) in PBS for 30 min at 30 °C, shaking (1400 rpm). Eluates were analyzed by WB.

6.17. Cell cycle synchronization

Cells were synchronized at G1/S using double thymidine block (2TB). Cells were seeded in 15 cm dishes. When the cells reached 60% confluency, 2.5 mM of thymidine was added and the cells incubated for 16 h. To release the cells from thymidine, cells were washed twice with serum-free media and incubated for 10 h in complete media (10% FCS) before treating for a second time with 2.5 mM thymidine. 16 h after the second block, cells stopped at G1/S were harvested. To obtain a population of S and G2, cells were released from the thymidine block and allowed to grow for 6 and 9 h, respectively. To synchronize the cells at mitosis, Nocodazole (50 ng/ml) was applied instead of the second thymidine block. Mitotic cells were collected by

shake off. Collected cells were placed on ice, spun for 5 min at 1000 rpm at 4°C and washed with 100 mM NEM PBS for 5 min. After another centrifugation, pellets were resuspended in lysis buffer (1% TritonX100, TBS) containing 10 mM NEM and protease inhibitors cocktail.

6.18. Cell lysate processing and protein quantification

Cells were lysed in the appropriate lysis buffer and incubated for 30 min on ice or rotating at 4°C. Insoluble material was cleared by centrifugation at 13 000 rpm for 15-20 min at 4°C. Protein content was quantified using the Pierce BCA assay following the manufacturer's instructions. The BSA standard and samples were measured in technical triplicates. The absorbance was measured at 560 nm using a Mithras LB 940 (Berthold) plate reader.

6.19. SDS-PAGE and Western blot

Cleared cell lysate or purified proteins were prepared in NuPAGE LDS Sample Buffer (4X) with NuPAGE reducing agent (10x). For non-reducing gels, the reducing agent was omitted. Before loading, the samples were heated at 70°C for 10 min. Proteins were separated by 4-12% Bis-Tris SDS-PAGE and transferred to a PVDF membrane. Membranes were blocked for 1-2 h in 5 % milk TBS-T (blocking solution) and incubated overnight at 4°C with the primary antibody in 1% milk TBS-T. After washing 3 times with TBS-T, membranes were incubated 1 h with HRP conjugated secondary antibody in 1% milk TBS-T. After another 3 washes, 1:1 mix of the ECL mixture was added and the chemilumiscence was measured using an ECL chemiluminescence imager (Chemostar V60+, INTAS).

6.20. *In vitro* Actin spin down assay

To study whether HA-BCAT1 binds to actin *in vitro*, the Actin-Binding Protein Spin-Down Biochemical Kit from Cytoskeleton, Inc. was used. The assay was performed according to the manufacturer's instructions using a Beckman Airfuge with Ultraclear tubes (Beckman, Cat. # 344718). Before starting, purified HA-BCAT1 was cleared 30 min at 120 000 rpm to remove any insoluble material. Briefly, actin was reconstituted to 1 mg/ml in general actin Buffer (5 mM Tris-HCl pH 8.0 and 0.2 mM $CaCl_2$) and allowed to polymerize (F-actin) for 1h at RT after addition of 10X actin polymerization buffer (100 mM Tris pH 7.5, 500 mM KCl, 20 mM MgCl2,

and 10 mM ATP). 200 nM of HA-BCAT1 was mixed with F-actin to a final volume of 50 µl in F-actin buffer (1:100 Actin polymerization buffer and general actin buffer). 2 µM BSA and 2 µM α-actinin (provided in the kit) were used as a negative and positive control, respectively. For "method 1", all samples were centrifuged for 1 h at 150,000 x g in a Beckman Airfuge. For "method 3", samples were spun at 14 000 x g for 1h at 24°C. Supernatants (unbound fraction) were separated and the pellets (F-actin bound) were resuspended in milli-Q water. Samples were analyzed by SDS-PAGE and Coomassie staining and/or Western blot.

6.21. *In vitro* Actin de-/polymerization assays

To assess the effects of HA-BCAT1 on actin assembly and disassembly, the Actin Polymerization Biochemical Kit (BK003, fluorescence format) from Cytoskeleton, Inc. was used. Prior to start, 5 µM of purified HA-BCAT1 (see above) was cleared for 30 min at 120 000 rpm to remove any insoluble material.

For the polymerization assay, G-actin stock (0.4 mg/ml) was prepared as specified by the manufacturers: Pyrene actin was resuspended in G-actin buffer and allowed to completely depolymerize on ice for 1 h. F-actin was precipitated at 14 000 rpm at 4°C for 1 h and the supernatant containing G-actin was collected. 200 µl of G-actin was loaded into a 96 well plate. Baseline fluorescence was recoded for 3 min, then 20 µl of the different HA-BCAT1 variants were added, mixed by shaking for 5 sec and measurements were renewed for 20 more min. 20 µl of 10X actin polymerization buffer was added, mixed for 5 sec and fluorescence was recoded for 1 h.

For the depolymerization assay, pyrene-actin was allowed to polymerize in actin polymerization buffer for 1 h at RT. F-actin was then diluted 4x in G-actin buffer (final 1.2 µM F-actin) before loading into a 96-well plate (100 µl per well). After recording the baseline fluorescence for 3 min, 10 µl of HA-BCAT1 variants (final concentration 500 nM), 20 mM H_2O_2 or vehicle (PBS) were added to each well, mixed for 5 sec and fluorescence measurements were continued for 60-90 min.

Measurements were performed using the GloMax® Discover (Promega) using the UV 365 nm excitation filter and a 415-445 nm emission filter. Samples were loaded in technical triplicates.

Wells with buffer only were used as blank. After blank subtraction, the change in fluorescence was calculated as indicated by the company's protocol with the formula: $(T_n-T_0)+1$, where T_0 is the baseline fluorescence measured before addition of HA-BCAT1.

6.22. Determination of ROS levels

To measure intracellular levels of ROS, the DCFDA Cellular ROS Detection Assay Kit (Abcam) was used as described by the manufacturer. Briefly, cells were seeded in black 96-well plates and allowed to reach 80 % confluency. Cells were washed 2 times with DCFDA washing buffer and stained for 45 min with 20 µM of DCFDA in the dark (in the cell culture incubator at 37°C 5-10% CO_2). The cells were then washed once with DCFDA washing buffer and fresh media was added. The baseline fluorescence was determined and the change in fluorescence after addition of treatments (H_2O_2) was recorded for 25 min. Measurements were performed in a plate reader (GloMax® Discover, Promega). The cells were kept at 37°C during all measurements. To calculate the change in ROS in response to H_2O_2, the recorings of the blank (unstained) sample were subtracted and the fluorescence at each time point was normalized to the baseline.

6.23. Metaphase spreads

Mitotic cells were detached of the cell culture dish using PBS and gently pelleted at 1 000 rpm for 1 min. Cell pellets were washed twice with PBS at RT and incubated in hypotonic swelling buffer (0.56% KCl) for 6 min at 37°C. Cells were then pelleted, and fixed with ice-cold 3 parts methanol and 1 part glacial acetic acid. Fixed cells were either dropped on pre-cleaned glass slides or stored at -20 °C. For microscopic analysis mitotic spreads were sealed with Vectrashield mounting media with DAPI.

6.24. Statistical analysis

Statistical significance was calculated for experiments for which at least 3 independent experiments were performed. Data are presented as mean ± SEM. P-values are indicated with *p<0.05, **p<0.01, ***p<0.001. The statistical significance of differences was determined using the unpaired, two-tailed Student's *t* test. For the rescue Click-iT experiments, a paired t test

was used. Statistical analyses were carried out using GraphPad Prism 6.01 (San Diego, CA), and a p-value < 0.05 was considered statistically significant.

7. Supplementary figures

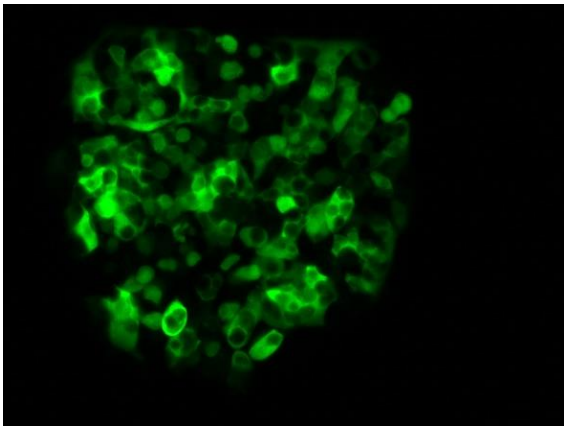

Figure S 1. HEK293 do not express GFP-BCAT1 in the nucleus. HEK293 cells were seeded in 6 well plates and transfected with 0.5 µg/ml of pDNA using TransIT-LT1 transfection reagent. Cells were imaged 48 h after transfection using an inverted fluorescent microscope

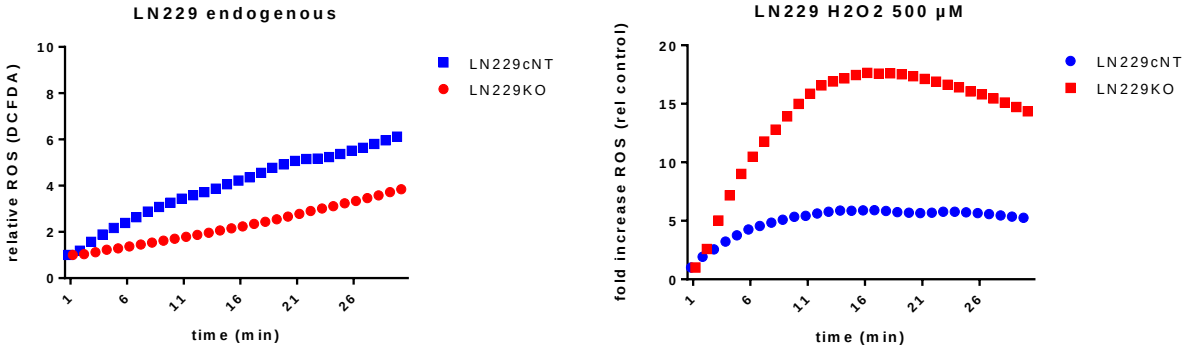

Figure S 2. Intracellular levels of ROS in LN229. Oxidation of DCFDA was monitored before and after addition of H_2O_2 for a period of 25 minutes. After blank subtraction, change in ROS was calculated by dividing the emitted fluorescence at the time measured by the initial fluorescence (T0). A) endogenous ROS production. B) ROS production in response to H_2O_2 500 µM. Fluorescence intensity emitted by treated cells was normalized to the fluorescence of untreated cells.

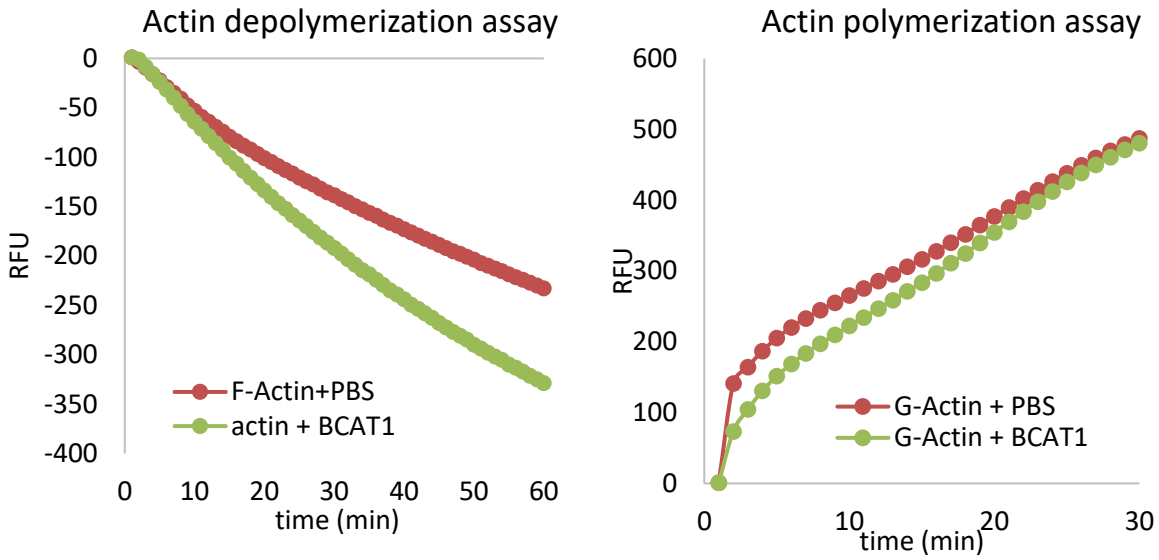

Figure S 3. Effects of HA-BCAT1 on actin dynamics evaluated using the Actin Polymerization Biochem Kit (cytoskeleton, Inc. #BK003).

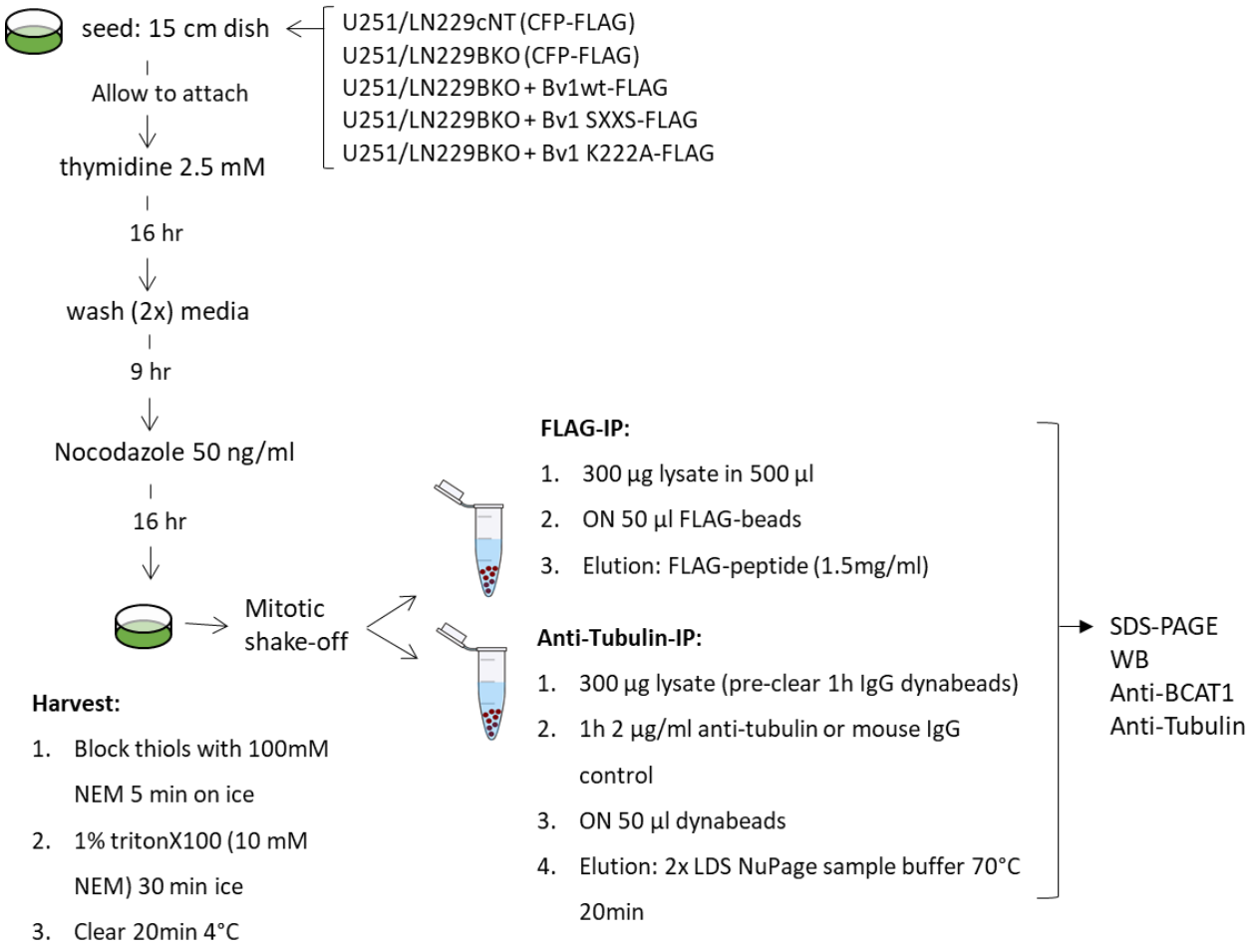

Figure S 4. Protocol for synchronization of mitotic cells and co-immunoprecipitation (co-IP) of BCAT1 and tubulin. U251 or LN229 cNT or BCAT1-KO (BKO) were seeded in 15 cm dishes and synchronized using thymidine 2.5 mM for 16 h. After washing 2 times with PBS, cells were released for 9 h and then arrested in mitosis using 50 ng/ml nocodazole for 16 h. Mitotic cells were harvested by shake-off, followed by blockade of free thiols by incubating with 100 mM NEM for 5 min on ice. Lysis was performed in the presence of NEM for 30 min on ice

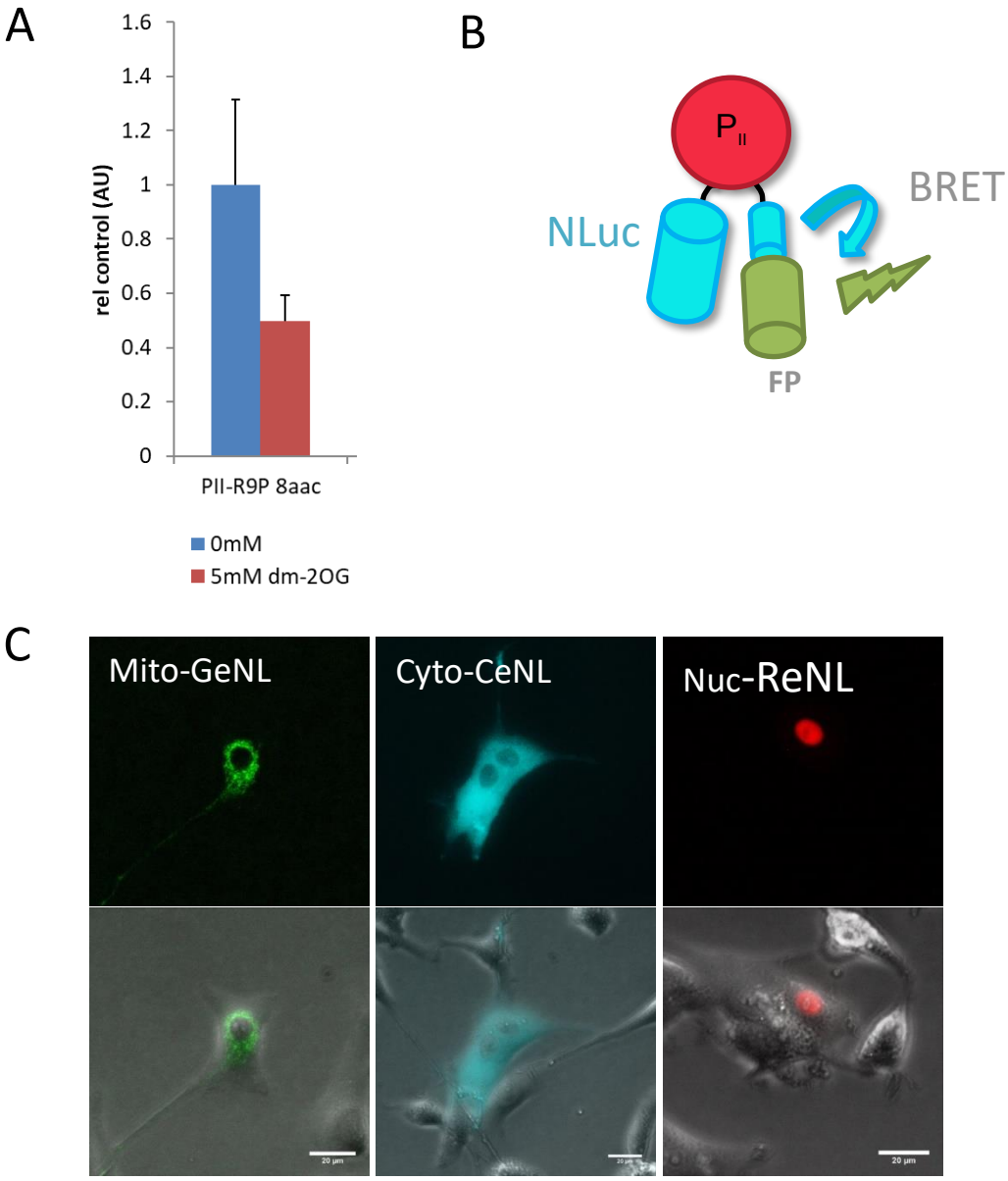

Figure S 5. Improvement of genetically encoded α-KG sensors using NanoLuc (NL) technology. The BRET sensor was expressed in U251 cells, and changes in bioluminescence was monitored after addition of dm-α-KG. In response to 5 mM of dm-α-KG the emitted signal was reduced by 50 %. Compared to the FRET sensor which allow showed a change in signal of 5 % after the same treatments (see section 3.2), this represent a significant improvement of the dynamic range. B) multicolor BRET sensor are created by combining the PII α-KG-binding protein with a NanoLuc® luciferase donor and a acceptor fluorescent protein (FP). Using different fluorescent proteins and C) signaling peptides (SP) to different subcellular compartments, these improved BRET sensors could allow the study of fluctuations of α-KG in living cells. MitoGeNL: Mitochondria SP + green FP, Cyto-CeNL: no SP + Cerulean FP, Nuc-CeNL: Nuclear SP + Red FP

8. Supplementary tables

The candidate binding partners of BCAT1 identified IP-MS were classified by Ingenuity Pathway Analysis (IPA) in different categories. Here are listed in alphabetical order the proteins grouped into the three most significant categories:

Table S 1. Top molecular and cellular function: Cell cycle

Gene Symbol	Entrez Gene Name
AURKA	aurora kinase A
BCAT1	branched chain amino acid transaminase 1
CDC20	cell division cycle 20
CDC42	cell division cycle 42
CDH13	cadherin 13
CDK1	cyclin dependent kinase 1
CDK13	cyclin dependent kinase 13
CDK5RAP3	CDK5 regulatory subunit associated protein 3
CLASP1	cytoplasmic linker associated protein 1
CLASP2	cytoplasmic linker associated protein 2
CLK3	CDC like kinase 3
CSE1L	chromosome segregation 1 like
CSNK1A1	casein kinase 1 alpha 1
CUL1	cullin 1
DARS	aspartyl-tRNA synthetase
DDB1	damage specific DNA binding protein 1
DEK	DEK proto-oncogene
EIF3M	eukaryotic translation initiation factor 3 subunit M
EIF4E	eukaryotic translation initiation factor 4E
EWSR1	EWS RNA binding protein 1
HMGA2	high mobility group AT-hook 2
INTS3	integrator complex subunit 3
IPO5	importin 5
KIF18B	kinesin family member 18B
KIF2C	kinesin family member 2C
KMT2A	lysine methyltransferase 2A
LYN	LYN proto-oncogene, Src family tyrosine kinase
MAP1S	microtubule associated protein 1S
MIB1	mindbomb E3 ubiquitin protein ligase 1
MSH2	mutS homolog 2
NBN	nibrin
NUMB	NUMB, endocytic adaptor protein

NUSAP1	nucleolar and spindle associated protein 1
ORC3	origin recognition complex subunit 3
PRPF4	pre-mRNA processing factor 4
PRR11	proline rich 11
RB1CC1	RB1 inducible coiled-coil 1
RBBP6	RB binding protein 6, ubiquitin ligase
RBM5	RNA binding motif protein 5
SMARCA1	SWI/SNF related, matrix associated, actin dependent regulator of chromatin, subfamily a, member 1
SMC1A	structural maintenance of chromosomes 1A
SMC5	structural maintenance of chromosomes 5
THOC1	THO complex 1
TUBA1A	tubulin alpha 1a
VPS18	VPS18, CORVET/HOPS core subunit
XPO1	exportin 1
XRCC1	X-ray repair cross complementing 1

Table S 2. Top molecular and cellular function: Cellular assembly and Organization

Gene Symbol	Entrez Gene Name
ACTR3	actin related protein 3
AURKA	aurora kinase A
BMP2K	BMP2 inducible kinase
CDC42	cell division cycle 42
CDH13	cadherin 13
CDK1	cyclin dependent kinase 1
CDK5RAP3	CDK5 regulatory subunit associated protein 3
CEP350	centrosomal protein 350
CLASP1	cytoplasmic linker associated protein 1
CLASP2	cytoplasmic linker associated protein 2
CSE1L	chromosome segregation 1 like
CSNK1A1	casein kinase 1 alpha 1
CTNNA1	catenin alpha 1
CUL1	cullin 1
DDB1	damage specific DNA binding protein 1
DDX31	DEAD-box helicase 31
DSP	desmoplakin
EIF2A	eukaryotic translation initiation factor 2A
EIF4E	eukaryotic translation initiation factor 4E
EWSR1	EWS RNA binding protein 1
EZR	ezrin

GNB1	G protein subunit beta 1
HIP1	huntingtin interacting protein 1
HMGA2	high mobility group AT-hook 2
ITPR1	inositol 1,4,5-trisphosphate receptor type 1
JUP	junction plakoglobin
KHSRP	KH-type splicing regulatory protein
KIF18B	kinesin family member 18B
KIF2C	kinesin family member 2C
MAP1S	microtubule associated protein 1S
MAP2	microtubule associated protein 2
MICAL2	microtubule associated monooxygenase, calponin and LIM domain containing 2
MRPL14	mitochondrial ribosomal protein L14
MSH2	mutS homolog 2
NBN	nibrin
NUSAP1	nucleolar and spindle associated protein 1
PALLD	palladin, cytoskeletal associated protein
PEX14	peroxisomal biogenesis factor 14
PHIP	pleckstrin homology domain interacting protein
PIK3C2A	phosphatidylinositol-4-phosphate 3-kinase catalytic subunit type 2 alpha
RAB13	RAB13, member RAS oncogene family
RAB1A	RAB1A, member RAS oncogene family
RAB1B	RAB1B, member RAS oncogene family
RBBP4	RB binding protein 4, chromatin remodeling factor
RRBP1	ribosome binding protein 1
SMC1A	structural maintenance of chromosomes 1A
SMC5	structural maintenance of chromosomes 5
TERF2	telomeric repeat binding factor 2
TOE1	target of EGR1, exonuclease
TUBA1A	tubulin alpha 1a
TUBGCP2	tubulin gamma complex associated protein 2
VAPB	VAMP associated protein B and C
VPS18	VPS18 core subunit of CORVET and HOPS complexes
XPO1	exportin 1

Table S 3. Top canonical pathway: Clathrin-mediaded Endocytosis Signaling

Gene Symbol	Entrez Gene Name
ACTA1	actin alpha 1, skeletal muscle
ACTA2	actin alpha 2, smooth muscle
ACTC1	actin alpha cardiac muscle 1
ACTG2	actin gamma 2, smooth muscle
ACTR3	actin related protein 3
AP2A1	adaptor related protein complex 2 subunit alpha 1
AP2A2	adaptor related protein complex 2 subunit alpha 2
AP2B1	adaptor related protein complex 2 subunit beta 1
AP2M1	adaptor related protein complex 2 subunit mu 1
AP3M1	adaptor related protein complex 3 subunit mu 1
CDC42	cell division cycle 42
CLTA	clathrin light chain A
CLTB	clathrin light chain B
CLTC	clathrin heavy chain
HIP1	huntingtin interacting protein 1
MYO1E	myosin IE
NUMB	NUMB endocytic adaptor protein
PIK3C2A	phosphatidylinositol-4-phosphate 3-kinase catalytic subunit type 2 alpha
PON1	paraoxonase 1
RAB5C	RAB5C, member RAS oncogene family
SH3BP4	SH3 domain binding protein 4
SYNJ1	synaptojanin 1

9. Publication

PII Protein-Derived FRET Sensors for Quantification and Live-Cell Imaging of 2-Oxoglutarate'

Lüddecke Jan*, **Francois Liliana*,** Spät Philipp, Watzer Björn, ChilczukTomasz, Poschet Gernot, Hell Rüdiger, Radlwimmer Bernhard, Forchhammer Karl.

*these authors contributed equally to this work

Abstract: The citric acid cycle intermediate 2-oxoglutarate (2-OG, a.k.a. alpha-ketoglutarate) links the carbon and nitrogen metabolic pathways and can provide information on the metabolic status of cells. In recent years, it has become exceedingly clear that 2-OG also acts as a master regulator of diverse biologic processes in all domains of life. Consequently, there is a great demand for time-resolved data on 2-OG fluctuations that can't be adequately addressed using established methods like mass spectrometry-based metabolomics analysis. Therefore, we set out to develop a novel intramolecular 2-OG FRET sensor based on the signal transduction protein PII from Synechococcus elongatus PCC 7942. We created two variants of the sensor, with a dynamic range for 2-OG from 0.1 µM to 0.1 mM or from 10 µM to 10 mM. As proof of concept, we applied the sensors to determine in situ glutamine:2-oxoglutarate aminotransferase (GOGAT) activity in Synechococcus elongatus PCC 7942 cells and measured 2-OG concentrations in cell extracts from Escherichia coli in vitro. Finally, we could show the sensors' functionality in living human cell lines, demonstrating their potential in the context of mechanistic studies and drug screening.

Scientific Reports, 7(1), p. 1437. doi: 10.1038/s41598-017-01440-w.

10. References

Alberts, B. *et al.* (2002) 'How Cells Regulate Their Cytoskeletal Filaments'. Garland Science. Available at: https://www.ncbi.nlm.nih.gov/books/NBK26809/ (Accessed: 24 January 2019).

Amin, S., Yang, P. and Li, Z. (2019) 'Pyruvate kinase M2: A multifarious enzyme in non-canonical localization to promote cancer progression', *Biochimica et Biophysica Acta (BBA) - Reviews on Cancer*. Elsevier, 1871(2), pp. 331–341. doi: 10.1016/J.BBCAN.2019.02.003.

An, Z. *et al.* (2018) 'Epidermal growth factor receptor and EGFRvIII in glioblastoma: Signaling pathways and targeted therapies', *Oncogene*. Nature Publishing Group, pp. 1561–1575. doi: 10.1038/s41388-017-0045-7.

Anitei, M. and Hoflack, B. (2012) 'Bridging membrane and cytoskeleton dynamics in the secretory and endocytic pathways', *Nature Cell Biology*. Nature Publishing Group, 14(1), pp. 11–19. doi: 10.1038/ncb2409.

Arts, R., Aper, S. J. A. and Merkx, M. (2017) 'Engineering BRET-Sensor Proteins.', *Methods in enzymology*, 589, pp. 87–114. doi: 10.1016/bs.mie.2017.01.010.

Bae, G. U. *et al.* (1999) 'Hydrogen peroxide activates p70(S6k) signaling pathway.', *The Journal of biological chemistry*. American Society for Biochemistry and Molecular Biology, 274(46), pp. 32596–602. doi: 10.1074/jbc.274.46.32596.

Bae, Y. S. *et al.* (1997) 'Epidermal growth factor (EGF)-induced generation of hydrogen peroxide. Role in EGF receptor-mediated tyrosine phosphorylation.', *The Journal of biological chemistry*. American Society for Biochemistry and Molecular Biology, 272(1), pp. 217–21. doi: 10.1074/JBC.272.1.217.

Bae, Y. S. *et al.* (2011) 'Regulation of reactive oxygen species generation in cell signaling', *Molecules and Cells*, 32(6), pp. 491–509. doi: 10.1007/s10059-011-0276-3.

Bakayan, A. *et al.* (2011) 'Red fluorescent protein-aequorin fusions as improved bioluminescent Ca2+ reporters in single cells and mice', *PLoS ONE*, 6(5). doi: 10.1371/journal.pone.0019520.

Ben-Yosef, T. *et al.* (1998) 'Involvement of Myc targets in c-myc and N-myc induced human tumors', *Oncogene*. doi: 10.1038/sj.onc.1201939.

Benvenisty, N. *et al.* (1992) 'An embryonically expressed gene is a target for c-Myc regulation via the c-Myc-binding sequence.', *Genes & Development*, 6(12b), pp. 2513–2523. doi: 10.1101/gad.6.12b.2513.

Bezanilla, M. *et al.* (2015) 'Cytoskeletal dynamics: a view from the membrane.', *The Journal of cell biology*. Rockefeller University Press, 209(3), pp. 329–37. doi: 10.1083/jcb.201502062.

Blaschke, K. *et al.* (2013) 'Vitamin C induces Tet-dependent DNA demethylation and a blastocyst-like state in ES cells', *Nature*, 500(7461), pp. 222–226. doi: 10.1038/nature12362.

Boukouris, A. E., Zervopoulos, S. D. and Michelakis, E. D. (2016) 'Metabolic Enzymes Moonlighting in the Nucleus: Metabolic Regulation of Gene Transcription.', *Trends in biochemical sciences*, 41(8), pp. 712–30. doi: 10.1016/j.tibs.2016.05.013.

Bradley, S. V. *et al.* (2007) 'Huntingtin Interacting Protein 1 Is a Novel Brain Tumor Marker that Associates with Epidermal Growth Factor Receptor', *Cancer Research*, 67(8), pp. 3609–3615. doi: 10.1158/0008-5472.CAN-06-4803.

Bradley, S. V *et al.* (2007) 'Huntingtin Interacting Protein 1 Is a Novel Brain Tumor Marker that Associates with Epidermal Growth Factor Receptor'. doi: 10.1158/0008-5472.CAN-06-4803.

Brodsky, F. M. *et al.* (2015) 'Unconventional Functions for Clathrin, ESCRTs, and Other Endocytic Regulators in the Cytoskeleton, Cell Cycle, Nucleus, and Beyond: Links to Human Disease', *Cold Spring Harbor Perspectives in Biology*, pp. 1–16. Available at: https://cshperspectives.cshlp.org/content/6/9/a017004.full.pdf.

Butera, G. *et al.* (2019) 'Regulation of Autophagy by Nuclear GAPDH and Its Aggregates in Cancer and Neurodegenerative Disorders', *International Journal of Molecular Sciences*. Multidisciplinary Digital Publishing Institute, 20(9), p. 2062. doi: 10.3390/ijms20092062.

Byrne, D. P. *et al.* (2019) 'An evolutionary-conserved redox regulatory mechanism in human Ser/Thr protein kinases', *bioRxiv*. doi: 10.1101/571844.

Campion, C. G. *et al.* (2018) 'COMMD5/HCaRG Hooks Endosomes on Cytoskeleton and Coordinates EGFR Trafficking', *Cell Reports*, 24(3), pp. 670-684.e7. doi: 10.1016/j.celrep.2018.06.056.

Carter, R. E. and Sorkin, A. (1998) 'Endocytosis of functional epidermal growth factor receptor-green fluorescent protein chimera', *Journal of Biological Chemistry*, 273(52), pp. 35000–35007. doi: 10.1074/jbc.273.52.35000.

Cascella, B. and Mirica, L. M. (2012) 'Kinetic analysis of iron-dependent histone demethylases: a-Ketoglutarate substrate inhibition and potential relevance to the regulation of histone demethylation in cancer cells', *Biochemistry*, 51(44), pp. 8699–8701. doi: 10.1021/bi3012466.

Catarzi, S. *et al.* (2005) 'Redox regulation of platelet-derived-growth-factor-receptor: Role of NADPH-oxidase and c-Src tyrosine kinase', *Biochimica et Biophysica Acta (BBA) - Molecular Cell Research*, 1745(2), pp. 166–175. doi: 10.1016/j.bbamcr.2005.03.004.

Cheng, J., Grassart, A. and Drubin, D. G. (2012) 'Myosin 1E coordinates actin assembly and cargo trafficking during clathrin-mediated endocytosis', *Molecular Biology of the Cell*, 23(15), pp. 2891–2904. doi: 10.1091/mbc.E11-04-0383.

Chesnelong, C. *et al.* (2014) 'Lactate dehydrogenase A silencing in IDH mutant gliomas', *Neuro-Oncology*. doi: 10.1093/neuonc/not243.

Coles, S. J., Hancock, J. T. and Conway, M. E. (2012) 'Differential redox potential between the human cytosolic and mitochondrial branched-chain aminotransferase.', *Acta biochimica et biophysica Sinica*, 44(2), pp. 172–6. doi: 10.1093/abbs/gmr103.

Conway, M. E. *et al.* (2002) 'Identification of a peroxide-sensitive redox switch at the CXXC motif in the human mitochondrial branched chain aminotransferase', *Biochemistry*, 41(29), pp. 9070–9078. doi: 10.1021/bi020200i.

Conway, M. E. *et al.* (2008) 'Regulatory control of human cytosolic branched-chain aminotransferase by oxidation and S-glutathionylation and its interactions with redox sensitive neuronal proteins.', *Biochemistry*. American Chemical Society, 47(19), pp. 5465–79. doi:

10.1021/bi800303h.

Conway, M. E., Poole, L. B. and Hutson, S. M. (2004) 'Roles for cysteine residues in the regulatory CXXC motif of human mitochondrial branched chain aminotransferase enzyme', *Biochemistry*. American Chemical Society, 43(23), pp. 7356–7364. doi: 10.1021/bi0498050.

Cremers, C. M. and Jakob, U. (2013) 'Oxidant sensing by reversible disulfide bond formation', *Journal of Biological Chemistry*. American Society for Biochemistry and Molecular Biology, pp. 26489–26496. doi: 10.1074/jbc.R113.462929.

Cumming, R. C. *et al.* (2004) 'Protein disulfide bond formation in the cytoplasm during oxidative stress', *Journal of Biological Chemistry*. American Society for Biochemistry and Molecular Biology, 279(21), pp. 21749–21758. doi: 10.1074/jbc.M312267200.

D'Angiolella, V., Santarpia, C. and Grieco, D. (2007) 'Oxidative Stress Overrides the Spindle Checkpoint', *Cell Cycle*. Taylor & Francis, 6(5), pp. 576–579. doi: 10.4161/cc.6.5.3934.

Dalle-Donne, I. *et al.* (2007) 'S-glutathionylation in protein redox regulation.', *Free radical biology & medicine*, 43(6), pp. 883–98. doi: 10.1016/j.freeradbiomed.2007.06.014.

DalleDonne, I., Milzani, A. and Colombo, R. (1995) 'H2O2-treated actin: assembly and polymer interactions with cross-linking proteins', *Biophysical Journal*. Elsevier, 69(6), pp. 2710–2719. doi: 10.1016/S0006-3495(95)80142-6.

Dang, L. *et al.* (2009) 'Cancer-associated IDH1 mutation produce 2-hydroxyglutarate', 462(7274), pp. 1–18. doi: 10.1038/nature08617.Cancer-associated.

Davoodi, J. *et al.* (1998) 'Overexpression and characterization of the human mitochondrial and cytosolic branched-chain aminotransferases', *Journal of Biological Chemistry*, 273(9), pp. 4982–4989. doi: 10.1074/jbc.273.9.4982.

DE, A. *et al.* (2013) 'Evolution of BRET Biosensors from Live Cell to Tissue-Scale In vivo Imaging', *Frontiers in Endocrinology*, 4, p. 131. doi: 10.3389/fendo.2013.00131.

Delatte, B. *et al.* (2015) 'Genome-wide hydroxymethylcytosine pattern changes in response to oxidative stress', *Scientific Reports*. Nature Publishing Group, 5(December 2014), pp. 1–10. doi:

10.1038/srep12714.

DeNicola, G. M. *et al.* (2011) 'Oncogene-induced Nrf2 transcription promotes ROS detoxification and tumorigenesis', *Nature*. Nature Publishing Group, 475(7354), pp. 106–109. doi: 10.1038/nature10189.

Dominguez-Brauer, C. *et al.* (2015) 'Targeting Mitosis in Cancer: Emerging Strategies', *Molecular Cell*, pp. 524–536. doi: 10.1016/j.molcel.2015.11.006.

Fehr, M. *et al.* (2003) 'In vivo imaging of the dynamics of glucose uptake in the cytosol of COS-7 cells by fluorescent nanosensors.', *The Journal of biological chemistry*, 278(21), pp. 19127–33. doi: 10.1074/jbc.M301333200.

Fletcher, D. A. and Mullins, R. D. (2010) 'Cell mechanics and the cytoskeleton', *Nature*, 463(7280), pp. 485–492. doi: 10.1038/nature08908.

Fomenko, D. E. and Gladyshev, V. N. (2003) 'Identity and functions of CxxC-derived motifs', *Biochemistry*. American Chemical Society, 42(38), pp. 11214–11225. doi: 10.1021/bi034459s.

Frémont, S., Romet-Lemonne, G., *et al.* (2017) 'Emerging roles of MICAL family proteins – from actin oxidation to membrane trafficking during cytokinesis', *Journal of Cell Science*, 130(9), pp. 1509–1517. doi: 10.1242/jcs.202028.

Frémont, S., Hammich, H., *et al.* (2017) 'Oxidation of F-actin controls the terminal steps of cytokinesis.', *Nature communications*, 8, p. 14528. doi: 10.1038/ncomms14528.

Frémont, S. and Echard, A. (2018) 'Membrane Traffic in the Late Steps of Cytokinesis', *Current Biology*, pp. R458–R470. doi: 10.1016/j.cub.2018.01.019.

Gadde, S. and Heald, R. (2004) 'Mechanisms and Molecules of the Mitotic Spindle', *Current Biology*. Cell Press, 14(18), pp. R797–R805. doi: 10.1016/J.CUB.2004.09.021.

Galeffi, F. and Turner, D. A. (2012) 'Exploiting metabolic differences in glioma therapy.', *Current drug discovery technologies*, 9(4), pp. 280–93. Available at: http://www.pubmedcentral.nih.gov/articlerender.fcgi?artid=3638785&tool=pmcentrez&rendertype=abstract (Accessed: 1 October 2015).

Gerien, K. S. and Wu, J. Q. (2018) 'Molecular mechanisms of contractile-ring constriction and membrane trafficking in cytokinesis', *Biophysical Reviews*, pp. 1649–1666. doi: 10.1007/s12551-018-0479-3.

Ghezzi, P. (2013) 'Protein glutathionylation in health and disease', *Biochimica et Biophysica Acta (BBA) - General Subjects*. Elsevier, 1830(5), pp. 3165–3172. doi: 10.1016/J.BBAGEN.2013.02.009.

Goto, M. *et al.* (2005) 'Structural determinants for branched-chain aminotransferase isozyme-specific inhibition by the anticonvulsant drug gabapentin', *Journal of Biological Chemistry*, 280(44), pp. 37246–37256. doi: 10.1074/jbc.M506486200.

Goto, M., Shinno, H. and Ichihara, A. (1977) 'Isozyme patterns of branched-chain amino acid transaminase in human tissues and tumors', *Gann, The Japanese Journal of Cancer Research*, 68(5), pp. 663–667.

Goyet, E. *et al.* (2016) 'Fast and high resolution single-cell BRET imaging', *Scientific Reports*, 6(1), p. 28231. doi: 10.1038/srep28231.

Groitl, B. and Jakob, U. (2014) 'Thiol-based redox switches', *Biochimica et Biophysica Acta - Proteins and Proteomics*. Elsevier B.V., 1844(8), pp. 1335–1343. doi: 10.1016/j.bbapap.2014.03.007.

Gu, Z. *et al.* (2019) 'Loss of EZH2 Reprograms BCAA Metabolism to Drive Leukemic Transformation', *Cancer Discovery*. American Association for Cancer Research, 9(9), pp. 1228–1247. doi: 10.1158/2159-8290.CD-19-0152.

Guertin, D. A. and Sabatini, D. M. (2007) 'Defining the Role of mTOR in Cancer', *Cancer Cell*. doi: 10.1016/j.ccr.2007.05.008.

Hattori, A. *et al.* (2017) 'Cancer progression by reprogrammed BCAA metabolism in myeloid leukaemia', *Nature*. Nature Publishing Group, 545(7655), pp. 500–504. doi: 10.1038/nature22314.

Heberle, A. M. *et al.* (2015) 'Molecular mechanisms of mTOR regulation by stress', *Molecular*

and Cellular Oncology, 2(2). doi: 10.4161/23723548.2014.970489.

Henriques, A. C. *et al.* (2019) 'Mitosis inhibitors in anticancer therapy: When blocking the exit becomes a solution', *Cancer Letters*. Elsevier, 440–441, pp. 64–81. Available at: https://www.sciencedirect.com/science/article/pii/S0304383518306116 (Accessed: 12 August 2019).

Hindy, M. E. L. and Conway, M. E. (2019) 'Redox-regulated, targeted affinity isolation of nadh-dependent protein interactions with the branched chain aminotransferase proteins', in *Methods in Molecular Biology*, pp. 151–163. doi: 10.1007/978-1-4939-9463-2_13.

El Hindy, M. *et al.* (2014) 'The branched-chain aminotransferase proteins: novel redox chaperones for protein disulfide isomerase--implications in Alzheimer's disease.', *Antioxidants & redox signaling*, 20(16), pp. 2497–513. doi: 10.1089/ars.2012.4869.

Hou, B.-H. *et al.* (2011) 'Optical sensors for monitoring dynamic changes of intracellular metabolite levels in mammalian cells.', *Nature protocols*. Nature Publishing Group, a division of Macmillan Publishers Limited. All Rights Reserved., 6(11), pp. 1818–33. doi: 10.1038/nprot.2011.392.

Huang, P. H., Xu, A. M. and White, F. M. (2009) 'Oncogenic EGFR signaling networks in glioma.', *Science signaling*. American Association for the Advancement of Science, 2(87), p. re6. doi: 10.1126/scisignal.287re6.

Hull, J. and Patel, V. (2015) 'New insights into the role of the branched-chain aminotransferase proteins in the human brain', *Journal of neuroscience …*. doi: 10.1002/jnr.23558.

Hung, R.-J., Pak, C. W. and Terman, J. R. (2011) 'Direct Redox Regulation of F-Actin Assembly and Disassembly by Mical', *Science*, 334(6063), pp. 1710–1713. doi: 10.1126/science.1211956.

Hutson, S. M., Fenstermacher, D. and Mahar, C. (1988) 'Role of mitochondrial transamination in branched chain amino acid metabolism', *Journal of Biological Chemistry*, 263(8), pp. 3618–3625.

Hutson, S. M., Sweatt, A. J. and Lanoue, K. F. (2005) 'Branched-chain [corrected] amino acid

metabolism: implications for establishing safe intakes.', *The Journal of nutrition*. doi: 135/6/1557S [pii].

Islam, M. M. *et al.* (2010) 'Branched-chain amino acid metabolon: interaction of glutamate dehydrogenase with the mitochondrial branched-chain aminotransferase (BCATm).', *The Journal of biological chemistry*, 285(1), pp. 265–76. doi: 10.1074/jbc.M109.048777.

Iwaya, K. *et al.* (2007) 'Correlation between liver metastasis of the colocalization of actin-related protein 2 and 3 complex and WAVE2 in colorectal carcinoma', *Cancer Science*, 98(7), pp. 992–999. doi: 10.1111/j.1349-7006.2007.00488.x.

Izquierdo-Garcia, J. L. *et al.* (2015) 'Metabolic Reprogramming in Mutant IDH1 Glioma Cells', *PLOS ONE*. doi: 10.1371/journal.pone.0118781.

Janke, C. and Chloë Bulinski, J. (2011) 'Post-translational regulation of the microtubule cytoskeleton: mechanisms and functions', *Nature Reviews Molecular Cell Biology*. Nature Publishing Group, 12(12), pp. 773–786. doi: 10.1038/nrm3227.

Jeffery, C. J. (1999) 'Moonlighting proteins', *Trends in Biochemical Sciences*, 24(1), pp. 8–11. doi: 10.1016/S0968-0004(98)01335-8.

Jeffery, C. J. (2016) 'Protein species and moonlighting proteins: Very small changes in a protein's covalent structure can change its biochemical function', *Journal of Proteomics*. Elsevier, 134, pp. 19–24. doi: 10.1016/J.JPROT.2015.10.003.

Jiang, F. *et al.* (2014) 'NADPH oxidase-dependent redox signaling in TGF-β-mediated fibrotic responses', *Redox Biology*, 2, pp. 267–272. doi: 10.1016/j.redox.2014.01.012.

Kaksonen, M., Toret, C. P. and Drubin, D. G. (2006) 'Harnessing actin dynamics for clathrin-mediated endocytosis.', *Nature reviews. Molecular cell biology*, 7(6), pp. 404–14. doi: 10.1038/nrm1940.

Katayama, H. and Sen, S. (2010) 'Aurora kinase inhibitors as anticancer molecules', *BBA - Gene Regulatory Mechanisms*, 1799, pp. 829–839. doi: 10.1016/j.bbagrm.2010.09.004.

Kelly, B. T. *et al.* (2014) 'AP2 controls clathrin polymerization with a membrane-activated

switch', *Science*, 345(6195), pp. 459–463. doi: 10.1126/science.1254836.

Kingsbury, J. M., Sen, N. D. and Cardenas, M. E. (2015) 'Branched-Chain Aminotransferases Control TORC1 Signaling in Saccharomyces cerevisiae', *PLOS Genetics*. Edited by G. P. Copenhaver. Public Library of Science, 11(12), p. e1005714. doi: 10.1371/journal.pgen.1005714.

Kispal, G. *et al.* (1996) 'Mitochondrial and cytosolic branched-chain amino acid transaminases from yeast, homologs of the myc oncogene-regulated Eca39 protein', *Journal of Biological Chemistry*. American Society for Biochemistry and Molecular Biology, 271(40), pp. 24458–24464. doi: 10.1074/jbc.271.40.24458.

Kreuz, S. and Fischle, W. (2016) 'Oxidative stress signaling to chromatin in health and disease', *Epigenomics*, 8(6), pp. 843–862. doi: 10.2217/epi-2016-0002.

Lamadema, N., Burr, S. and Brewer, A. C. (2019) 'Dynamic regulation of epigenetic demethylation by oxygen availability and cellular redox', *Free Radical Biology and Medicine*. Elsevier B.V., 131(September 2018), pp. 282–298. doi: 10.1016/j.freeradbiomed.2018.12.009.

Laplante, M. and Sabatini, D. M. (2009) 'mTOR signaling at a glance.', *Journal of cell science*. The Company of Biologists Ltd, 122(Pt 20), pp. 3589–94. doi: 10.1242/jcs.051011.

Lee, G. *et al.* (2016) 'Oxidative Dimerization of PHD2 is Responsible for its Inactivation and Contributes to Metabolic Reprogramming via HIF-1α Activation', *Scientific Reports*. Nature Publishing Group, 6(1), p. 18928. doi: 10.1038/srep18928.

Lennicke, C. *et al.* (2015) 'Hydrogen peroxide - Production, fate and role in redox signaling of tumor cells', *Cell Communication and Signaling*. BioMed Central, p. 39. doi: 10.1186/s12964-015-0118-6.

Li, D. *et al.* (2017) 'Knockdown of HIP1 expression promotes ligand-induced endocytosis of EGFR in HeLa cells', *Oncology Reports*. Spandidos Publications, 38(6), p. 3387. doi: 10.3892/OR.2017.6025.

Lim, J. M. *et al.* (2015) 'Control of the pericentrosomal H2O2 level by peroxiredoxin I is critical for mitotic progression', *Journal of Cell Biology*, 210(1), pp. 23–33. doi: 10.1083/jcb.201412068.

Liou, G. Y. and Storz, P. (2010) 'Reactive oxygen species in cancer', *Free Radical Research*, pp. 479–496. doi: 10.3109/10715761003667554.

Lladó, A. *et al.* (2008) 'Protein Kinase C and Calmodulin Regulate Epidermal Growth Factor Receptor Recycling from Early Endosomes through Arp2/3 Complex and Cortactin', *Molecular Biology of the Cell*, 19, pp. 17–29. doi: 10.1091/mbc.E07-05-0411.

Long, H. K., Blackledge, N. P. and Klose, R. J. (2013) 'ZF-CxxC domain-containing proteins, CpG islands and the chromatin connection.', *Biochemical Society transactions*. Portland Press Limited, 41(3), pp. 727–40. doi: 10.1042/BST20130028.

López-Grueso, M. J. *et al.* (2019) 'Thioredoxin and glutaredoxin regulate metabolism through different multiplex thiol switches', *Redox Biology*. Elsevier, 21, p. 101049. doi: 10.1016/j.redox.2018.11.007.

Louis, D. N. *et al.* (2016) 'The 2016 World Health Organization Classification of Tumors of the Central Nervous System: a summary', *Acta Neuropathologica*. Springer Berlin Heidelberg, 131(6), pp. 803–820. doi: 10.1007/s00401-016-1545-1.

Lüddecke, J. *et al.* (2017) 'PII Protein-Derived FRET Sensors for Quantification and Live-Cell Imaging of 2-Oxoglutarate', *Scientific Reports*, 7(1), p. 1437. doi: 10.1038/s41598-017-01440-w.

Lüders, Jens (2016) 'The microtubule cytoskeleton: Organisation, function and role in disease', in *The Microtubule Cytoskeleton: Organisation, Function and Role in Disease*, pp. 1–189. doi: 10.1007/978-3-7091-1903-7.

Lüders, Jan (2016) 'The Microtubule Cytoskeleton', in *The Microtubule Cytoskeleton*. doi: 10.1007/978-3-7091-1903-7.

Lundquist, M. R. *et al.* (2014) 'Redox Modification of Nuclear Actin by MICAL-2 Regulates SRF Signaling', *Cell*, 156, pp. 563–576. doi: 10.1016/j.cell.2013.12.035.

Luo, W. *et al.* (2011) 'Pyruvate Kinase M2 Is a PHD3-Stimulated Coactivator for Hypoxia-Inducible Factor 1', *Cell*. Cell Press, 145(5), pp. 732–744. doi: 10.1016/J.CELL.2011.03.054.

Ma, Y. *et al.* (2016) 'Chiral Antioxidant-based Gold Nanoclusters Reprogram DNA Epigenetic

Patterns', *Scientific Reports*. Nature Publishing Group, 6(September), pp. 1–12. doi: 10.1038/srep33436.

Mannino, M. *et al.* (2014) 'Differential sensitivity of Glioma stem cells to Aurora kinase A inhibitors: Implications for stem cell mitosis and centrosome dynamics', *Stem Cell Research*. Elsevier, 13(1), pp. 135–143. doi: 10.1016/j.scr.2014.05.001.

Mayers, J. R. *et al.* (2016) 'Tissue of origin dictates branched-chain amino acid metabolism in mutant Kras-driven cancers', *Science*, 353(6304), pp. 1161–1165. doi: 10.1126/science.aaf5171.

Min, K.-W., Lee, S.-H. and Baek, S. J. (2016) 'Moonlighting proteins in cancer.', *Cancer letters*, 370(1), pp. 108–16. doi: 10.1016/j.canlet.2015.09.022.

Monaghan, R. M. *et al.* (2015) 'A nuclear role for the respiratory enzyme CLK-1 in regulating mitochondrial stress responses and longevity.', *Nature cell biology*, 17(6), pp. 782–92. doi: 10.1038/ncb3170.

Monaghan, R. M. and Whitmarsh, A. J. (2015) 'Mitochondrial Proteins Moonlighting in the Nucleus', *Trends in Biochemical Sciences*. Elsevier Current Trends, pp. 728–735. doi: 10.1016/j.tibs.2015.10.003.

Mosesson, Y., Mills, G. B. and Yarden, Y. (2008) 'Derailed endocytosis: An emerging feature of cancer', *Nature Reviews Cancer*, 8(11), pp. 835–850. doi: 10.1038/nrc2521.

Neumann, C. A., Cao, J. and Manevich, Y. (2009) 'Peroxiredoxin 1 and its role in cell signaling', *Cell Cycle*, 8(24), pp. 4072–4078. doi: 10.4161/cc.8.24.10242.

Niu, Y. *et al.* (2015) 'Oxidative stress alters global histone modification and DNA methylation', *Free Radical Biology and Medicine*. Elsevier, 82, pp. 22–28. doi: 10.1016/j.freeradbiomed.2015.01.028.

Niwa, O. *et al.* (1990) 'A cDNA clone overexpressed and amplified in a mouse teratocarcinoma line', *Nucleic Acids Research*, 18(22), pp. 6709–6709. doi: 10.1093/nar/18.22.6709.

Oakley, B. R., Paolillo, V. and Zheng, Y. (2015) 'γ-Tubulin complexes in microtubule nucleation and beyond', *Molecular Biology of the Cell*. Edited by D. G. Drubin, 26(17), pp. 2957–2962. doi:

10.1091/mbc.E14-11-1514.

Oka, S. *et al.* (2017) 'Thioredoxin-1 maintains mechanistic target of rapamycin (mTOR) function during oxidative stress in cardiomyocytes', *Journal of Biological Chemistry*, 292(46), pp. 18988–19000. doi: 10.1074/jbc.M117.807735.

Pan, Y. *et al.* (2007) 'Multiple Factors Affecting Cellular Redox Status and Energy Metabolism Modulate Hypoxia-Inducible Factor Prolyl Hydroxylase Activity In Vivo and In Vitro', *Molecular and Cellular Biology*. doi: 10.1128/mcb.01223-06.

Parker, A. L., Kavallaris, M. and McCarroll, J. A. (2014) 'Microtubules and Their Role in Cellular Stress in Cancer', *Frontiers in Oncology*. Frontiers, 4, p. 153. doi: 10.3389/fonc.2014.00153.

Parker, N. R. *et al.* (2015) 'Molecular Heterogeneity in Glioblastoma: Potential Clinical Implications', *Frontiers in Oncology*. Frontiers, 5, p. 55. doi: 10.3389/fonc.2015.00055.

Parsons, D. W. *et al.* (2008) 'An integrated genomic analysis of human glioblastoma multiforme', *Science*, 321(5897), pp. 1807–1812. doi: 10.1126/science.1164382.

Pastor, W. A., Aravind, L. and Rao, A. (2013) 'TETonic shift: Biological roles of TET proteins in DNA demethylation and transcription', *Nature Reviews Molecular Cell Biology*. Nature Publishing Group, 14(6), pp. 341–356. doi: 10.1038/nrm3589.

Pastore, A. and Piemonte, F. (2012) 'S-Glutathionylation signaling in cell biology: Progress and prospects', *European Journal of Pharmaceutical Sciences*. Elsevier B.V., 46(5), pp. 279–292. doi: 10.1016/j.ejps.2012.03.010.

Patterson, J. C., Joughin, B. A., van de Kooij, B., *et al.* (2019) 'ROS and Oxidative Stress Are Elevated in Mitosis during Asynchronous Cell Cycle Progression and Are Exacerbated by Mitotic Arrest', *Cell Systems*. Elsevier Inc., 8(2), pp. 163-167.e2. doi: 10.1016/j.cels.2019.01.005.

Patterson, J. C., Joughin, B. A., Prota, A. E., *et al.* (2019) 'VISAGE Reveals a Targetable Mitotic Spindle Vulnerability in Cancer Cells', *Cell Systems*. Cell Press, 9(1), pp. 74-92.e8. doi: 10.1016/j.cels.2019.05.009.

Paulsen, C. E. *et al.* (2012) 'Peroxide-dependent sulfenylation of the EGFR catalytic site

enhances kinase activity', *Nature Chemical Biology*. Nature Publishing Group, 8(1), pp. 57–64. doi: 10.1038/nchembio.736.

Pavitt, G. D. (2018) 'Regulation of translation initiation factor eIF2B at the hub of the integrated stress response', *Wiley Interdisciplinary Reviews: RNA*. John Wiley & Sons, Ltd, 9(6), pp. 1–22. doi: 10.1002/wrna.1491.

Pike, R. *et al.* (2018) 'KIF22 coordinates CAR and EGFR dynamics to promote cancer cell proliferation.', *Science signaling*. American Association for the Advancement of Science, 11(515), p. eaaq1060. doi: 10.1126/scisignal.aaq1060.

Pollard, T. D. and O'Shaughnessy, B. (2019) 'Molecular Mechanism of Cytokinesis', *Annual Review of Biochemistry*. Annual Reviews, 88(1), p. annurev-biochem-062917-012530. doi: 10.1146/annurev-biochem-062917-012530.

Qvit, N. *et al.* (2016) 'Glyceraldehyde-3-Phosphate Dehydrogenase (GAPDH) Protein-Protein Interaction Inhibitor Reveals a Non-catalytic Role for GAPDH Oligomerization in Cell Death.', *The Journal of biological chemistry*, 291(26), pp. 13608–21. doi: 10.1074/jbc.M115.711630.

Raffel, S. *et al.* (2017) 'BCAT1 restricts αkG levels in AML stem cells leading to IDHmut-like DNA hypermethylation', *Nature*. Nature Publishing Group, 551(7680), pp. 384–388. doi: 10.1038/nature24294.

Rudolph, J. (2005) 'Redox Regulation of the Cdc25 Phosphatases', *Antioxidants & Redox Signaling*. Mary Ann Liebert, Inc. 2 Madison Avenue Larchmont, NY 10538 USA , 7(5–6), pp. 761–767. doi: 10.1089/ars.2005.7.761.

Salazar-Ramiro, A. *et al.* (2016) 'Role of redox status in development of Glioblastoma', *Frontiers in Immunology*. Frontiers, p. 156. doi: 10.3389/fimmu.2016.00156.

Saleem, H. *et al.* (2019) 'The TICking clock of EGFR therapy resistance in glioblastoma: Target Independence or target Compensation', *Drug Resistance Updates*, 43, pp. 29–37. doi: 10.1016/j.drup.2019.04.002.

San Martín, A. *et al.* (2013) 'A genetically encoded FRET lactate sensor and its use to detect the

Warburg effect in single cancer cells.', *PloS one*. Public Library of Science, 8(2), p. e57712. doi: 10.1371/journal.pone.0057712.

Sanjana, N. E., Shalem, O. and Zhang, F. (2014) 'Improved vectors and genome-wide libraries for CRISPR screening', *Nature Methods*, 11(8), pp. 783–784. doi: 10.1038/nmeth.3047.

Sarsour, E. H. *et al.* (2009) 'Redox Control of the Cell Cycle in Health and Disease', *Antioxidants & Redox Signaling*. Mary Ann Liebert, Inc. 140 Huguenot Street, 3rd Floor New Rochelle, NY 10801 USA, 11(12), pp. 2985–3011. doi: 10.1089/ars.2009.2513.

Schatten, H. (2015) 'The cytoskeleton in health and disease', in *The Cytoskeleton in Health and Disease*, pp. 1–391. doi: 10.1007/978-1-4939-2904-7.

Schuldiner, O. *et al.* (1996) 'ECA39, a conserved gene regulated by c-Myc in mice, is involved in G1/S cell cycle regulation in yeast', *Proceedings of the National Academy of Sciences of the United States of America*, 93, pp. 7143–7148. Available at: http://www.pnas.org/content/pnas/93/14/7143.full.pdf (Accessed: 12 March 2018).

Shalem, O. *et al.* (2014) 'Genome-Scale CRISPR-Cas9 Knockout Screening in Human Cells', *Science*, 343(6166), pp. 84–87. doi: 10.1126/science.1247005.

Sies, H. (2017) 'Hydrogen peroxide as a central redox signaling molecule in physiological oxidative stress: Oxidative eustress', *Redox Biology*, pp. 613–619. doi: 10.1016/j.redox.2016.12.035.

Sigismund, S. *et al.* (2008) 'Clathrin-Mediated Internalization Is Essential for Sustained EGFR Signaling but Dispensable for Degradation', *Developmental Cell*. Cell Press, 15(2), pp. 209–219. doi: 10.1016/J.DEVCEL.2008.06.012.

Silva, L. S. *et al.* (2017) 'Branched-chain ketoacids secreted by glioblastoma cells via MCT 1 modulate macrophage phenotype', *EMBO reports*, 18(12), pp. 2172–2185. doi: 10.15252/embr.201744154.

Singh, S. *et al.* (2018) 'The reduced activity of PP-1α under redox stress condition is a consequence of GSH-mediated transient disulfide formation', *Scientific Reports*. Nature

Publishing Group, 8(1), p. 17711. doi: 10.1038/s41598-018-36267-6.

Sirover, M. A. (2018) 'Pleiotropic effects of moonlighting glyceraldehyde-3-phosphate dehydrogenase (GAPDH) in cancer progression, invasiveness, and metastases', *Cancer and Metastasis Reviews*. Cancer and Metastasis Reviews, 37(4), pp. 665–676. doi: 10.1007/s10555-018-9764-7.

Sobotta, M. C. *et al.* (2014) 'Peroxiredoxin-2 and STAT3 form a redox relay for H2O2 signaling.', *Nature chemical biology*, 11(november), pp. 1–16. doi: 10.1038/nchembio.1695.

Sorkin, A. and von Zastrow, M. (2009) 'Endocytosis and signalling: intertwining molecular networks', *Nature Publishing Group*, 10. doi: 10.1038/nrm2748.

Stöcker, S. *et al.* (2017) 'A role for 2-Cys peroxiredoxins in facilitating cytosolic protein thiol oxidation', *Nature Chemical Biology*, (december). doi: 10.1038/nchembio.2536.

Sturm, D., Bender, S., Jones, D. T. W. W., *et al.* (2014) 'Paediatric and adult glioblastoma: Multiform (epi)genomic culprits emerge', *Nature Reviews Cancer*. Nature Publishing Group, 14(2), pp. 92–107. doi: 10.1038/nrc3655.

Sturm, D., Bender, S., Jones, D. T. W., *et al.* (2014) 'Paediatric and adult glioblastoma: mutiform (epi)genomic culprits emerge', *Nature reviews Cancer*, 14(2), pp. 92–107. doi: 10.1038/nrc3655.Paediatric.

Sullivan, L. B. and Chandel, N. S. (2014) 'Mitochondrial reactive oxygen species and cancer', *Cancer and Metabolism*, 2(1), pp. 1–12. doi: 10.1186/2049-3002-2-17.

Suzuki, K. *et al.* (2016) 'Five colour variants of bright luminescent protein for real-time multicolour bioimaging.', *Nature communications*. Nature Publishing Group, 7, p. 13718. doi: 10.1038/ncomms13718.

Sweatt, A. J. *et al.* (2004) 'Branched-chain amino acid catabolism: unique segregation of pathway enzymes in organ systems and peripheral nerves', *American Journal of Physiology-Endocrinology and Metabolism*. American Physiological Society, 286(1), pp. E64–E76. doi: 10.1152/ajpendo.00276.2003.

Thewes, V. *et al.* (2017) 'The branched-chain amino acid transaminase 1 sustains growth of antiestrogen-resistant and ERα-negative breast cancer', *Oncogene*, 36(29), pp. 4124–4134. doi: 10.1038/onc.2017.32.

Thu Truong, A. H. *et al.* (2016) 'Molecular Basis for Redox Activation of Epidermal Growth Factor Receptor Kinase Cell Chemical Biology Article Molecular Basis for Redox Activation of Epidermal Growth Factor Receptor Kinase', *Cell Chemical Biology*. Elsevier Ltd, 23, pp. 1–12. doi: 10.1016/j.chembiol.2016.05.017.

Toedt, G. *et al.* (2011) 'Molecular signatures classify astrocytic gliomas by IDH1 mutation status', *International Journal of Cancer*. doi: 10.1002/ijc.25448.

Tomas, A., Futter, C. E. and Eden, E. R. (2014) 'EGF receptor trafficking: consequences for signaling and cancer', *Trends in Cell Biology*. Elsevier Current Trends, 24(1), pp. 26–34. doi: 10.1016/J.TCB.2013.11.002.

Tönjes, M. *et al.* (2013) 'BCAT1 promotes cell proliferation through amino acid catabolism in gliomas carrying wild-type IDH1', *Nature Medicine*, 19(7), pp. 0–1. doi: 10.1038/nm.3217.

Truitt, M. L. *et al.* (2015) 'Differential Requirements for eIF4E Dose in Normal Development and Cancer', *Cell*. Elsevier Inc., 162(1), pp. 59–71. doi: 10.1016/j.cell.2015.05.049.

Truong, T. H. and Carroll, K. S. (2012) 'Redox regulation of epidermal growth factor receptor signaling through cysteine oxidation', *Biochemistry*. American Chemical Society, 51(50), pp. 9954–9965. doi: 10.1021/bi301441e.

Truong, T. H. and Carroll, K. S. (2013) 'Redox regulation of protein kinases', *Critical Reviews in Biochemistry and Molecular Biology*, 48(4), pp. 332–356. doi: 10.3109/10409238.2013.790873.

Tsai, M. Y. M.-Y. *et al.* (2006) 'A mitotic lamin B matrix induced by RanGTP required for spindle assembly', *Science*, 311(5769), pp. 1887–1893. doi: 10.1126/science.1122771.

Turcan, S. *et al.* (2012) 'IDH1 mutation is sufficient to establish the glioma hypermethylation phenotype', *Nature*, 483(7390), pp. 479–483. doi: 10.1038/nature10866.IDH1.

Vader, G. and Lens, S. M. A. (2008) 'The Aurora kinase family in cell division and cancer',

Biochimica et Biophysica Acta (BBA) - Reviews on Cancer. Elsevier, 1786(1), pp. 60–72. doi: 10.1016/J.BBCAN.2008.07.003.

Wang, Y. *et al.* (2019) 'Branched-Chain Amino Acid Metabolic Reprogramming Orchestrates Drug Resistance to EGFR Tyrosine Kinase Inhibitors', *Cell Reports*. Cell Press, 28(2), pp. 512-525.e6. doi: 10.1016/j.celrep.2019.06.026.

Wang, Z.-Q. *et al.* (2015a) 'BCAT1 expression associates with ovarian cancer progression: possible implications in altered disease metabolism', *Oncotarget*. doi: 10.18632/oncotarget.5159.

Wang, Z.-Q. *et al.* (2015b) 'BCAT1 expression associates with ovarian cancer progression: possible implications in altered disease metabolism', *Oncotarget*. Impact Journals, pp. 31522–31543. Available at: http://www.impactjournals.com/oncotarget/index.php?journal=oncotarget&page=article&op=view&path%5B%5D=5159&path%5B%5D=13877 (Accessed: 2 March 2016).

Weller, M. *et al.* (2017) 'European Association for Neuro-Oncology (EANO) guideline on the diagnosis and treatment of adult astrocytic and oligodendroglial gliomas', *The Lancet Oncology*. Elsevier, 18(6), pp. e315–e329. doi: 10.1016/S1470-2045(17)30194-8.

De Wever, V. *et al.* (2014) 'The human mitotic kinesin KIF18A binds protein phosphatase 1 (PP1) through a highly conserved docking motif', *Biochemical and Biophysical Research Communications*. Academic Press, 453(3), pp. 432–437. doi: 10.1016/J.BBRC.2014.09.105.

Willems, E. *et al.* (2017) 'The Unexpected Roles of Aurora A Kinase in Gliobastoma Recurrences', *Targeted Oncology*. Springer International Publishing, 12(1), pp. 11–18. doi: 10.1007/s11523-016-0457-2.

Willems, E. *et al.* (2018) 'The functional diversity of Aurora kinases: A comprehensive review', *Cell Division*. BioMed Central, 13, p. 7. doi: 10.1186/s13008-018-0040-6.

Willems, E. *et al.* (2019) 'Aurora A plays a dual role in migration and survival of human glioblastoma cells according to the CXCL12 concentration', *Oncogene*. Nature Publishing Group,

38(1), pp. 73–87. doi: 10.1038/s41388-018-0437-3.

Wilson, L., Panda, D. and Jordan, M. A. (1999) 'Modulation of microtubule dynamics by drugs: a paradigm for the actions of cellular regulators.', *Cell structure and function*, 24(5), pp. 329–35. Available at: http://www.ncbi.nlm.nih.gov/pubmed/15216890 (Accessed: 28 August 2019).

Woo, H. A. *et al.* (2010) 'Inactivation of Peroxiredoxin I by Phosphorylation Allows Localized H2O2 Accumulation for Cell Signaling', *Cell*. Elsevier Ltd, 140(4), pp. 517–528. doi: 10.1016/j.cell.2010.01.009.

Woolner, S. *et al.* (2008) 'Myosin-10 and actin filaments are essential for mitotic spindle function', *Journal of Cell Biology*. Rockefeller University Press, 182(1), pp. 77–88. doi: 10.1083/jcb.200804062.

Xu, M. *et al.* (2016) 'BCAT1 promotes tumor cell migration and invasion in hepatocellular carcinoma.', *Oncology letters*. Spandidos Publications, 12(4), pp. 2648–2656. doi: 10.3892/ol.2016.4969.

Yang, J. *et al.* (2016) 'Coupling optogenetic stimulation with NanoLuc-based luminescence (BRET) Ca++ sensing', *Nature Communications*. Nature Publishing Group, 7, p. 13268. doi: 10.1038/ncomms13268.

Yang, W. *et al.* (2011) 'Nuclear PKM2 regulates β-catenin transactivation upon EGFR activation', *Nature*. Nature Publishing Group, 480(7375), pp. 118–122. doi: 10.1038/nature10598.

Yang, W., Zheng, Y., *et al.* (2012) 'ERK1/2-dependent phosphorylation and nuclear translocation of PKM2 promotes the Warburg effect', *Nature Cell Biology*. Nature Publishing Group, 14(12), pp. 1295–1304. doi: 10.1038/ncb2629.

Yang, W., Xia, Y., Hawke, D., Li, X., Liang, J., Xing, D., Aldape, K., Hunter, T., Alfred Yung, W. K., *et al.* (2012) 'PKM2 phosphorylates histone H3 and promotes gene transcription and tumorigenesis', *Cell*. Elsevier, 150(4), pp. 685–696. doi: 10.1016/j.cell.2012.07.018.

Yang, W., Xia, Y., Hawke, D., Li, X., Liang, J., Xing, D., Aldape, K., Hunter, T., Alfred Yung, W. K., *et al.* (2012) 'PKM2 Phosphorylates Histone H3 and Promotes Gene Transcription and

Tumorigenesis', *Cell*. Cell Press, 150(4), pp. 685–696. doi: 10.1016/J.CELL.2012.07.018.

Yang, X. and Lin, Y. (2018) 'Functions of nuclear actin-binding proteins in human cancer.', *Oncology letters*. Spandidos Publications, 15(3), pp. 2743–2748. doi: 10.3892/ol.2017.7658.

Yang, Z.-L. *et al.* (2013) 'CFL1 and Arp3 are Biomarkers for Metastasis and Poor Prognosis of Squamous Cell/Adenosquamous Carcinomas and Adenocarcinomas of Gallbladder', *Cancer Investigation*. Taylor & Francis, 31(2), pp. 132–139. doi: 10.3109/07357907.2012.756113.

Yennawar, N. *et al.* (2001) 'The structure of human mitochondrial branched-chain aminotransferase.', *Acta crystallographica. Section D, Biological crystallography*, 57(Pt 4), pp. 506–15. Available at: http://www.ncbi.nlm.nih.gov/pubmed/11264579 (Accessed: 5 October 2018).

Yennawar, N. H. *et al.* (2006) 'Human Mitochondrial Branched Chain Aminotransferase Isozyme', *Journal of Biological Chemistry*. American Society for Biochemistry and Molecular Biology, 281(51), pp. 39660–39671. doi: 10.1074/jbc.m607552200.

Yoshida, S. *et al.* (2011) 'Redox regulates mammalian target of rapamycin complex 1 (mTORC1) activity by modulating the TSC1/TSC2-Rheb GTPase pathway.' American Society for Biochemistry and Molecular Biology, 286(37). doi: 10.1074/jbc.M111.238014.

Yoshikawa, R. *et al.* (2006) 'ECA39 is a novel distant metastasis-related biomarker in colorectal cancer', *World Journal of Gastroenterology*. doi: 10.3748/wjg.v12.i36.5884.

Yun, J. *et al.* (2012) 'Interactions between epigenetics and metabolism in cancers.', *Frontiers in oncology*, 2(November), p. 163. doi: 10.3389/fonc.2012.00163.

Zhang, D. *et al.* (2017) 'Phosphoglycerate mutase 1 promotes cancer cell migration independent of its metabolic activity', *Oncogene*. Nature Publishing Group, 36(20), pp. 2900–2909. doi: 10.1038/onc.2016.446.

Zhang, J. *et al.* (2016) 'ROS and ROS-Mediated Cellular Signaling', *Oxidative Medicine and Cellular Longevity*, pp. 1–18. doi: 10.1155/2016/4350965.

Zhang, L. and Han, J. (2017) 'Branched-chain amino acid transaminase 1 (BCAT1) promotes the

growth of breast cancer cells through improving mTOR-mediated mitochondrial biogenesis and function', *Biochemical and Biophysical Research Communications*. Elsevier Ltd, 486(2), pp. 224–231. doi: 10.1016/j.bbrc.2017.02.101.

Zhao, Y. *et al.* (2015) 'SoNar, a Highly Responsive NAD+/NADH Sensor, Allows High-Throughput Metabolic Screening of Anti-tumor Agents.', *Cell metabolism*, 21(5), pp. 777–89. doi: 10.1016/j.cmet.2015.04.009.

Zheng, H.-C. *et al.* (no date) 'Arp2/3 overexpression contributed to pathogenesis, growth and invasion of gastric carcinoma.', *Anticancer research*, 28(4B), pp. 2225–32. Available at: http://www.ncbi.nlm.nih.gov/pubmed/18751399 (Accessed: 4 October 2019).

Zheng, Y. H. *et al.* (2016) 'BCAT1, a key prognostic predictor of hepatocellular carcinoma, promotes cell proliferation and induces chemoresistance to cisplatin', *Liver International*, 36(12), pp. 1836–1847. doi: 10.1111/liv.13178.

Zhou, W. *et al.* (2013) 'Over-expression of BCAT1, a c-Myc target gene, induces cell proliferation, migration and invasion in nasopharyngeal carcinoma', *Molecular Cancer*. doi: 10.1186/1476-4598-12-53.

11. Acknowledgements

The work presented in this PhD thesis would not have been possible to do without the support and guidance provided by many people, to whom I express my gratitude:

Dr. Bernhard Radlwimmer for the direct supervision of my PhD work, for giving me the opportunity to develop my project and for all the ongoing support.

Prof. Dr. Peter Lichter for providing me the opportunity to be part of his division and for all his helpful input throughout my PhD.

Prof. Dr. Thomas Höfer for being my first evaluator of my PhD defense examination committee.

Prof. Dr. Stefan Frings for his willingness to evaluate my PhD thesis and his contribution as a member of my examination committee.

PD. Dr. Tobias Dick for his willingness to evaluate my PhD thesis, his contribution as member of my examination committee and for useful advice on redox aspects of my work.

Dr. Jan Lüddecke and Prof. Dr. Karl Forchhammer for their collaboration and work performed on the α-KG-FRET sensor that led to a publication in Scientific Reports in 2017.

Dr. Gianluca Sigismondo for a great collaboration and advice regarding Mass-Spectrometry experiments.

Dr. Felix Bestvater, Damir Krunic and Manuela Bromm of the light microscopy facility who were super helpful in all microscopy-related experiments.

Dr. Matthias Plessner and Prof. Dr. Robert Grosse, for a great work in identifying mitotic defects by live-cell imaging of glioblastoma cells.

To all the members from the B06x division for providing a great working atmosphere.

Magdalena Schlotter for her excellent technical support during my last stage of my PhD, but also for her always energetic and playful presence in the lab. Thank you as well for teaching me some funny german words.
Jasmin Mangei and Laura Llaó for spending great times also outside the lab, having dinner and going to sports.
Theresa Schmidt, Pavle Boskovic and Anne Jenseit, which work has also contributed significantly to understand more about novel roles of BCAT1.

Manasi that was been next to me since my first steps in DKFZ and helping with the metaphase spreads.

Dwain, who's endless support has been essential for accomplishing my PhD.

To all my friends in Mexico and around the world. Gracias a mis chicas, que representan un gran pilar en mi vida y que están siempre presentes. Melimolas, gracias por todo tu apoyo.

A mi familia y a mis Papás que me an apoyado en todos momentos y que siempre me han motivado a seguir mis sueños.